1 Phase behavior of rod-like viruses and virus/sphere mixtures

Zvonimir Dogic[(1)] *and Seth Fraden*[(2)]

[(1)] Rowland Institute at Harvard
Harvard University
Cambridge, 02142 Massachusetts, USA
[(2)] Complex Fluids Group, Department of Physics
Brandeis University
Waltham, 02454 Massachusetts, USA

1.1 Introduction

The reasons physicists give for studying colloids are varied. Our initial motivation was that colloids can serve as model experimental systems to study simple fluids because with careful preparation, colloids approximate hard particles. Numerous studies have investigated the phase behavior, structure, and macroscopic viscoelastic properties of suspensions of spherical colloids (Poon and Pusey 1995). Far less studied have been colloids of anisotropic shape, in spite of their long recognized similarity to liquid crystals. Counterintuitively, hard rod fluids are theoretically simpler systems to understand than hard spheres (Forsyth et al. 1978). This surprising fact was first recognized by Onsager who realized that the isotropic - nematic (I-N) transition in the rodlike colloid Tobacco Mosaic Virus (TMV) occurred at such low concentrations that only two-body interactions were necessary in order to quantitatively explain the I-N phase transition (Onsager 1949). In fact, in the limit of long thin rods Onsager's theory becomes exact. This in contrast to the theory of phase transitions of hard spheres, for which no exact results exist (in three dimensions).

For some years the Complex Fluids Group at Brandeis has studied the liquid crystalline behavior of suspensions of TMV (Fraden et al. 1985; Hurd et al. 1985; Wen and Meyer 1987; Oldenbourg et al. 1988; Fraden et al. 1989; Meyer 1990; Fraden et al. 1993; Wang et al. 1994; Fraden 1995; Adams and Fraden 1998) and filamentous phage *fd* (Tang and Fraden 1993; Tang and Fraden 1995; Fraden 1995; Tang and Fraden 1996; Dogic and Fraden 1997; Adams et al. 1998; Dogic et al. 2000; Dogic and Fraden 2001; Grelet and Fraden 2003; Dogic 2003; Purdy et al. 2003; Purdy and Fraden 2004b; Purdy and Fraden 2004a; Purdy et al. 2004). TMV is a beautiful colloidal rod (Kreibig and Wetter 1980; Wetter 1985). It is completely rigid and forms isotropic, nematic, smectic and colloidal crystalline phases. However, TMV is difficult to work with. One must cultivate tobacco plants, infect them with virus, harvest the crop, extract the virus - which takes months - plus all this must be done with care

Phase Behavior of Rod-Like Viruses and Virus–Sphere Mixtures, Z. Dogic and S. Fraden,
Chapter 1, in Soft Matter, Volume 2: Complex Colloidal Suspensions (eds G. Gompper and M. Schick),
Wiley-VCH Verlag GmbH & Co. KGaA, Weinheim, Germany (2006).
ISBN: 978-3-527-31369-3, DOI: 10.1002/9783527617067.ch1.

to preserve the monodispersity of the virus. Physics graduate students rebel at the thought of producing enough virus for a PhD thesis. Without an abundant source of TMV, studies of its phase behavior are impractical.

So our laboratory switched from TMV to the semi-flexible bacteriophage *fd*, which also forms several liquid crystalline phases: isotropic, cholesteric and smectic, but not a colloidal crystals. Because *fd* infects bacteria, growing *fd* is relatively quick and easy. Furthermore, genetic engineering of *fd* is well established and we have produced mutants of varying length and charge.

This chapter describes the phase behavior of *fd* suspensions. First, we present our results on *fd* alone. The results obtained up to 1995 are summarized in another review article (Fraden 1995). While theory and experiment are in agreement for the isotropic - cholesteric phase transition for suspensions with high salt concentrations used to screen long-range electrostatic repulsion, theoretical explanations of all other phases fail. We see a quantitative discrepancy between theory and experiment for the nematic phase at low ionic strength, and multiple quantitative and qualitative breakdowns of the theory of the smectic phase. And we have not even a clue of why a cholesteric phase is observed in *fd*, but a nematic in a closely related species, pf1, which has a nearly identical atomic structure (Grelet and Fraden 2003). Second, we present results on mixtures of the viral rods with spherical colloids or spherical polymers. Some of the phase behavior, such as depletion induced phase separation, was as anticipated. But an astounding array of unexpected results was also observed. A laundry list includes microphase separation of rods and spheres into columnar, cubic, and lamellar structure; isolated colloidal membranes consisting of a sheet of rods and stabilized via protrusion forces; and a quasi two dimensional smectic phase that exists on the isotropic - nematic interface that plays a key role in phase separation kinetics. While originally we were motivated to study virus suspensions because they are model systems of simple fluids, now we are motivated by a spirit of exploration driven by the expectation that more unexpected results will follow the ones described below.

1.2 Entropy driven ordering within the second virial approximation

In the first part of the paper we briefly review the theoretical work describing liquid crystalline phase transitions in colloidal rods. This part of the review is not meant to be exhaustive. For more detailed theoretical accounts the reader is referred to recent review articles and the original article by Onsager (Stephen and Straley 1974; Odijk 1986; Vroege and Lekkerkerker 1992; Onsager 1949).

The majority of studies of the ordering transitions in hard particle fluids belongs to a class of theories called Density Functional Theories (DFT) (Hansen and McDonald 1986). The simplest version of DFT takes into account the interactions between particles at the level of second virial approximation. The free energy of a hard particle fluid is then,

$$\frac{F}{k_b T} = \int_V d\mathbf{r}\rho(\mathbf{r})\ln(\rho(\mathbf{r})) - \frac{1}{2}\int_V d\mathbf{r_1}\int_V d\mathbf{r_2}\rho(\mathbf{r_1})\rho(\mathbf{r_2})\beta(\mathbf{r_1},\mathbf{r_2}) \tag{1.1}$$

where $\beta(\mathbf{r_1}, \mathbf{r_2})$ is a Meyer-Meyer overlap function, $\rho(\mathbf{r})$ denotes the density of particles and $\mathbf{r_1}$ and $\mathbf{r_2}$ are vectors denoting the position and/or orientation of two particular particles. Its value equals -1 if there is any overlap between two hard-particles located at $\mathbf{r_1}$ and $\mathbf{r_2}$; otherwise its value is equal to zero. This expression has been used for a variety of cases to study entropy induced ordering in hard particle fluids. Onsager was first to show that Eq. 1.1 is essentially exact for isotropic spherocylinders when $L/D_{\rm sc} \rightarrow \infty$, where L is the length and $D_{\rm sc}$ is the diameter of the spherocylinder (Onsager 1949). As the aspect ratio of spherocylinders is increased the third and higher virial coefficient become negligible.

The second virial theory also predicts a stable smectic phase in a solution of perfectly aligned spherocylinders as well as for spherocylinders with both positional and orientational degrees of freedom (Hosino et al. 1979; Mulder 1987; van Roij et al. 1995; van der Schoot 1996). However, to quantitatively describe the suspensions at densities of the nematic-smectic phase transition it is necessary to include higher virial coefficients in the free energy expression. For perfectly aligned spherocylinders inclusion of the third and fourth virial coefficient into the free energy results in theoretical predictions for the N-S transitions which are in quantitative agreement with simulation results. The calculations that consider ordering transitions using only second virial coefficients are uncontrolled approximations, unless it can be shown that higher virial coefficients are negligible, as is the case of the Onsager treatment of I-N phase transition.

In any hard-particle fluid, due to the simplicity of interaction potential, the energy of any allowed configuration is simply proportional to nkT with n being the number density of particles. Due to this simple fact the minimum of free energy of a hard particle fluid $F = E - ST = T(\alpha - S)$ (α is a constant) is equivalent to the maximum of entropy. Furthermore the resulting phase diagram is temperature independent (athermal) because both α and S are independent of temperature. Ordering transitions in hard-particle fluids are still possible because the expression for entropy, or equivalently free energy, splits into two parts. The first integral in Eq. 1.1 is the ideal part of free energy and always attains a minimum value for the uniform probability distribution $\rho(\mathbf{r})$ = constant. Therefore this contribution to the total free energy always suppresses an ordering transition. The second integral in Eq. 1.1 represents the second virial approximation for the interaction free energy, which is proportional to the excluded volume and under certain circumstances is lower for an ordered state. Therefore the interaction part of free energy drives the system towards ordering. The actual location of the ordering transition is determined from the competition between the ideal and interaction contribution to the total free energy. In this section we briefly review the theoretical description of phase transitions that can be described using Eq. 1.1 of pure hard rods.

1.2.1 Isotropic-Nematic phase transition within the second virial approximation

The density functional of the sort shown in Eq. 1.1 was first used in a seminal paper by Onsager in 1949 (Onsager 1949). He was seeking to explain the formation of the

nematic phase in solutions of rod-like Tobacco Mossaic Virus (TMV), inorganic needles of vanadium pentoxide, and discs of bentonite. These transitions were found to occur at very low volume fraction (Bawden et al. 1936; Zocher 1925).

In the Onsager theory the system is assumed to be spatially uniform and therefore it is assumed $\rho(\mathbf{r}, \mathbf{\Omega}) = (N/V)f(\mathbf{\Omega})$ where Ω is a solid angle describing the orientation of the spherocylinder, N is the number of rods, and V is the volume of the system. Since $f(\Omega)$ indicates the probability that a rod is pointing at a solid angle Ω. It should be normalized as follows :

$$\int f(\Omega)d\Omega = 1. \tag{1.2}$$

Using this information it is possible to recast Eq. 1.1 into Onsager free energy functional for a solution of rod-like molecules :

$$F = \log\frac{N}{V} + \int f(\Omega)\log(4\pi f(\Omega))d\Omega - \frac{1}{2}\frac{N}{V}\int\int \beta(\Omega,\Omega')f(\Omega)f(\Omega')d\Omega d\Omega' \tag{1.3}$$

The $\beta(\Omega, \Omega')$ function is the volume excluded to the spherocylinder with orientation Ω' due to the presence another spherocylinder with orientation Ω. For two spherocylinders is given by

$$\beta(\Omega,\Omega') = \beta(\gamma) = -2L^2 D_{\rm sc}\sin(\gamma) - 2\pi D_{\rm sc}^2 L - \frac{4}{3}\pi D_{\rm sc}^3. \tag{1.4}$$

where γ is the relative angle between two spherocylinders. For spherocylinders with a large aspect ratio the first term in the Eq. 1.4 dominates and it can be shown that the contribution of the other terms is of the same order as the contribution of the third virial coefficient. Therefore it is often assumed that $\beta(\gamma) = -2L^2 D_{\rm sc}\sin(\gamma)$. By using this approximation and variational calculus to minimize Eq. 1.3 with the respect to the distribution function $f(\Omega)$ one obtains the following integral equation :

$$\log[4\pi f(\theta)] = \lambda - \frac{8\rho}{\pi}\int \sin(\theta)f(\theta)d\theta, \tag{1.5}$$

where $\rho = \frac{\pi}{4}L^2 D_{\rm sc}\frac{N}{V}$ and λ is a constant determined through normalization of constraint in Eq. 1.2. This integral equation cannot be solved analytically. However, it has been solved using two different numerical procedures which yield almost identical results (Herzfeld et al. 1984; Lekkerkerker et al. 1984). Once the probability distribution function is known, it is easy to calculate the nematic order parameter (S_2) using the following relation:

$$S_2 = 2\pi\int_0^\pi \left(\frac{3}{2}\cos(\theta) - \frac{1}{2}\right) f(\theta)\sin(\theta)d\theta. \tag{1.6}$$

In this equation we assume that the orientational distribution function is uniaxial and therefore $f(\Omega) = f(\theta)$ where θ is the angle between the orientation of a specific rod and the nematic director. The value of the nematic order parameter varies between 0 and 1, with $S_2 = 0$ describing a perfectly isotropic solution and $S_2 = 1$ describing a perfectly aligned nematic phase. Although the numerical solution of Eq. 1.5 yields the

most accurate results, it is also possible to proceed from Eq. 1.3 by assuming a form of the orientational distribution function such as:

$$f(\alpha, \cos(\theta)) = \frac{\alpha \cosh(\alpha \cos(\theta))}{4\pi \sinh(\alpha)}. \tag{1.7}$$

Using this ansatz, first introduced by Onsager, and evaluating the integrals for the case of hard rods Onsager obtained an expression for the free energy which is a function of dimensionless concentration ρ and orientation parameter α:

$$\begin{aligned} F(\alpha, \rho) &= \rho \log(\rho) + \sigma(\alpha)\rho + \xi(\alpha)\rho^2 \\ \sigma(\alpha) &= \log\left(\frac{\alpha \cosh(\alpha)}{4\pi \sinh(\alpha)}\right) - 1 + \frac{\arctan(e^{\alpha}) - \arctan(e^{-\alpha})}{\sinh(\alpha)} \\ \xi(\alpha) &= \frac{2I_2(\alpha)}{\sinh^2(\alpha)}. \end{aligned} \tag{1.8}$$

The advantage of assuming the probability distribution (Eq. 1.7) is the analytical expression for the free energy (Eq.1.8). The most convenient variable to formulate the Onsager theory is the dimensionless concentration

$$\rho = B_2^{iso}\frac{N}{V} = \frac{\pi}{4}L^2 D_{\rm sc}\frac{N}{V} = \frac{L}{D_{\rm sc}}\phi \tag{1.9}$$

where ϕ is the volume fraction of the rods and $B_2^{iso} = (\pi/4)L^2 D_{\rm sc}$ is the second virial coefficient for a suspension of hard rods in an isotropic solution. By performing a stability analysis of the Onsager equation, Kayser and Ravenche found that the isotropic phase becomes unstable towards orientational fluctuations when $\rho = 4$ (Kayser and Raveche 1978). It follows that within the Onsager theory the volume fraction of the hard rods at the I-N transition scales as $\phi = 4\frac{D_{\rm sc}}{L}$. Therefore, for long thin rods the volume fraction of the I-N transition is small and the virial theory, which is an expansion of the free energy in density becomes accurate at the level of the second virial coefficient. Numerical calculations of the second and third virial coefficients indicate that the Onsager theory is quantitatively correct for rods with $L/D_{\rm sc} > 100$ (Frenkel 1988).

However, the second order transition predicted by the stability analysis is preempted by a first order phase transition. Minimizing the Onsager free energy with respect to the orientational distribution function numerically and subsequently solving the co-existence equations yields the following concentration of the co-existing isotropic and nematic phases,

$$\rho_{\rm iso} = 3.289, \quad \rho_{\rm nem} = 4.192, \quad S_2 = 0.7922. \tag{1.10}$$

These results were obtained by Herzfeld et. al., Lekkerkerker et. al., and Chen (Herzfeld et al. 1984; Lekkerkerker et al. 1984; Chen 1993). The Onsager trial function (Eq. 1.7) yields the following co-existence concentrations :

$$\rho_{\rm iso} = 3.339, \quad \rho_{\rm nem} = 4.487, \quad S_2 = 0.848. \tag{1.11}$$

By comparing accurate numerical result from Eq. 1.5 with the Onsager approximation (Eq. 1.8) we observe a difference in both the coexistence concentrations at the I-N phase transition and the nematic order parameter (S_2) of the nematic phase.

1.2.2 Extension of Onsager theory to charged rods

The Onsager theory outlined in the previous section can be extended to the experimentally important case of charge stabilized rods. The first treatment of the I-N phase transition of charged rods can be found in the original paper by Onsager and was elaborated by Stroobants and coworkers (Onsager 1949; Stroobants et al. 1986). Besides the hard core repulsive interaction, charged rods have a long range repulsive interaction of the following form:

$$\frac{U_{el}(x)}{kT} = \frac{A' e^{-\kappa(x-D_{\rm sc})}}{\sin(\gamma)} \tag{1.12}$$

where x is the closest distance between two charged rods, A' is the proportionality constant obtained by solving the Poisson-Boltzman equation, κ^{-1} is the Debye screening length and γ is the angle between two rods. In the case of charged rods there are contributions to the second virial coefficient from both the hard core excluded volume interaction and the long range electrostatic repulsion interaction. These two contributions can be calculated separately. Integrating the interaction potential over a uniform orientational distribution function which describes the isotropic phase we obtain the following expression for the second virial coefficient of charged rods:

$$B_2^{\rm iso} = \frac{1}{4}\pi L^2 D_{\rm eff} = \frac{1}{4}\pi D L^2 + \frac{1}{4}\pi\kappa^{-1}L^2(\ln A' + C_E + \ln 2 - \frac{1}{2}) \tag{1.13}$$

where $D_{\rm eff} = (\ln A' + C_E + \ln 2 - 1/2)/\kappa$. It follows that the thermodynamics of charged rods in the isotropic suspension will be equivalent to the thermodynamics of thicker hard rods with the effective diameter ($D_{\rm eff}$). However, if the interaction potential is integrated over an anisotropic distribution function then the relationship given by Eq. 1.13 is no longer exact. The reason for this is that the electrostatic energy is lower for perpendicular rods then for parallel rods. Therefore the charge effectively destabilizes the nematic phase by shifting the I-N transition to higher concentrations and reducing the order parameter of the nematic phase coexisting with the isotropic phase. However, most biopolymers (including *fd* virus) are highly charged in which case it turns out that the electrostatic "twisting" effect is insignificant compared to the excluded volume interactions (Tang and Fraden 1995; Stroobants et al. 1986). Therefore from now on we approximate $D_{\rm eff}$ in the nematic phase by $D_{\rm eff}$ of the isotropic phase. This is reasonable for co-existing phases, but we expect this approximation to get progressively worse with increasing concentration.

1.2.3 Extension of Onsager theory to semi-flexible rods

Semi-flexible rods are characterized by their persistence length, which is the length along the contour of the chain after which the local tangents become uncorrelated. The effect of semi-flexibility on the isotropic-nematic phase transition has been first considered by Khokhlov and Semenov (Khokhlov and Semenov 1982). For semi-flexible rods, besides orientational and translational entropy it is also necessary to take into account the internal configurations of the semi-flexible chain. This modifies the orientational entropy term in Eq. 1.1 while the excluded volume term between rod-like segments

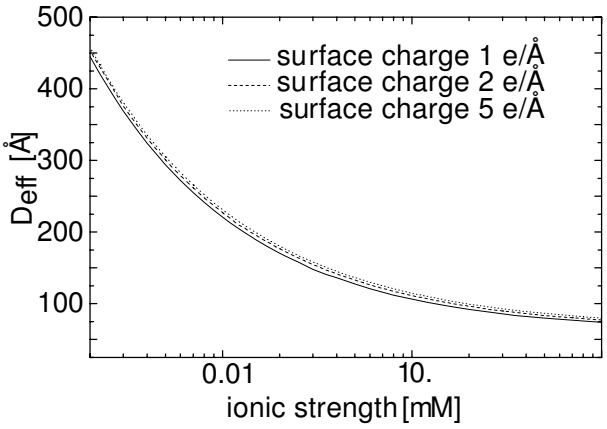

Figure 1.1: The effective diameter for a charged rod calculated from Eq. 1.13 for a range of ionic strengths. The hard rod diameter $D_{\text{bare}} = 66$Å is that of the *fd* virus. Due to the highly non-linear nature of the Poisson-Boltzman equation the value of D_{eff} barely changes as the surface charge varies from $1e^-$/Å to $10e^-$/Å. Experiments indicate that the surface charge is about $2e^-$/Å at pH=8.0 (Zimmermann et al. 1986). (Taken from Ref. (Tang and Fraden 1996))

is still treated as in the Onsager theory for rigid rods. The resulting expression for the free energy has been solved analyticaly in the limit of almost rigid rods (P$\gg$L) and very flexible rods (L$\ll$P) (Khokhlov and Semenov 1981; Khokhlov and Semenov 1982). It is possible to empirically interpolate between these two solutions and obtain a numerical approximation for the configurational entropy of rods with arbitrary persistence length as was done by Hentscke, Odijk, and Yang et. al. (Hentschke 1990; Odijk 1986; DuPre and Yang 1991). This interpolated expression can be combined with the Onsager approximation for the orientational distribution to obtain analytical results for the I-N phase transition of semi-flexible rods. These results are compared to accurate numerical solutions of the Khokhlov-Semenov free energy due to Chen (Fig. 1.2).

From Fig. 1.2a we conclude that increasing flexibility destabilizes the nematic phase by displacing the I-N transition to higher volume fractions. Increasing the flexibility also drastically reduces the concentration difference between the co-existing isotropic and nematic phases (figure not shown) and the order parameter of the nematic phase (Fig. 1.2b). The Onsager approximation (Eq. 1.7) for the ODF qualitatively agrees with the accurate numerical results due to Chen. It is important to note that the agreement between these approximations for the location of the phase transition (Fig. 1.2a) is much better then for the order parameter of the coexisting nematic phases (Fig. 1.2b). This indicates that measuring the order parameter is a more sensitive test of the a theory for I-N phase transition.

Chen compares his numerical solution to the analytical solution of Khokhlov and Semenov who also use Onsager approximation for the ODF. This comparison in the

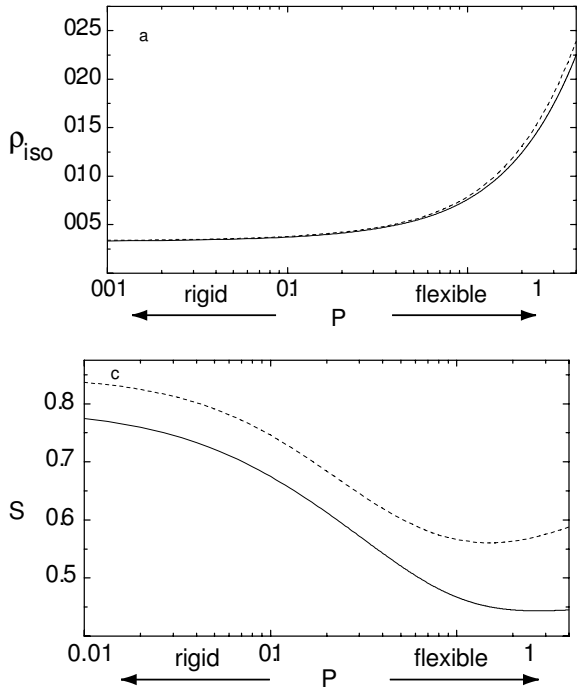

Figure 1.2: Concentration ($\rho_{\rm iso} = (4/\pi)L^2 D_{\rm sc}(N/V)$) and the order parameter (S_2) of the nematic phase co-existing with the isotropic phase as a function of the flexibility of the particle $P = L/l_p$. The full lines are the exact numerical results within the second virial approximation due to Chen (Chen 1993) while dashed lines are results obtained by using the Onsager approximation for the orientational distribution function (Eq. 1.7). In both figures the aspect ratio of the rod is fixed at 100 and the persistence length l_p varies from infinity to 25.

paper by Chen seems much better then what is shown in Fig. 1.2. The reason for this is that Khokhlov and Semenov, besides using Onsager approximation for the ODF, also approximate the excluded volume $\xi(\alpha)$ by expanding it in powers of α. These two approximations fortuitously cancel each other and the final result seemingly agrees better with the numerical solution.

1.2.4 Extension of Onsager theory to rods with finite aspect ratio using scaled particle theory

Scaled particle theory (SPT) of hard rods was developed by Cotter and coworkers (Cotter and Wacker 1978; Cotter 1979). The main advantage of the scaled particle theory is that it takes into account third and all higher virial coefficients in an approximate way. Therefore this theory should be more adequate at describing the data at higher concentration of rods or equivalently rods with lower $L/D_{\rm sc}$ ratios. We note that

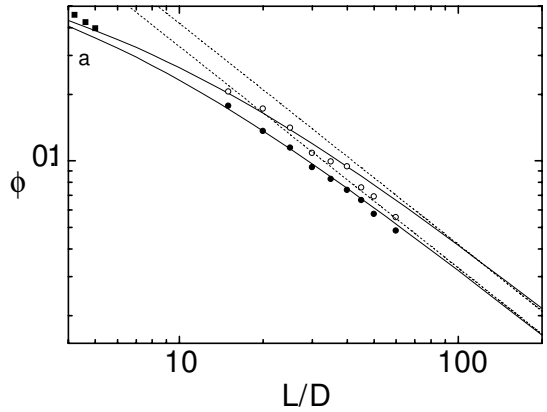

Figure 1.3: Full lines show the I-N coexistence concentrations as a function of the aspect ratio ($L/D_{\rm sc}$) as predicted by the scaled particle theory for rigid rods. The dashed line represents the I-N co-existence as predicted by a theory that only includes second virial coefficient. The circles are the results of the computer simulations (Bolhuis and Frenkel 1997). The filled squares at low $L/D_{\rm sc}$ represent results from the same work but the coexistence width was too narrow to be measured. The coexistence is plotted in terms of real volume fraction $\phi = \pi D_{\rm sc}^3/6 + LD_{\rm sc}^2\pi/4$ while the total aspect ratio including the hemispheres is $L/D_{\rm sc} + 1$.

the expression for the free energy reduces to the Onsager second virial approximation for very long rods. For spherical particles the SPT free energy reduces to the Percus-Yevick free energy for hard spheres.

The scaled particle expression accounts for higher virial coefficients in an approximate way. Comparing the SPT prediction for the I-N phase transition with the solution obtained through the second virial approximation provides a way to establish the range of $L/D_{\rm sc}$ ratios for which the second virial approximation is quantitatively valid. The results are shown in Fig. 1.3. At $L/D_{\rm sc} = 45$ the second virial approximation yields I-N co-existence concentrations that are 10% different from the scaled particle result. We conclude that for rods with $L/D_{\rm sc} > 75$ the second virial approximation quantitatively describes the I-N transitions in hard-rods. Currently available computer simulation results agree very well with the scaled particle theory (Bolhuis and Frenkel 1997; Kramer and Herzfeld 1998).

1.2.5 Nematic-Smectic phase transition within the second virial approximation

Here we review the interplay between the ideal and interaction contributions to the free energy that are responsible for the formation of the smectic phase in parallel hard rods. From the second virial approximation (Eq. 1.1) we can easily find the free energy difference between a weakly ordered smectic and a uniform nematic state (Mulder

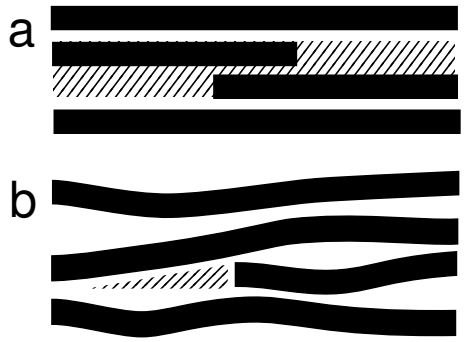

Figure 1.4: A schematic illustration of the excluded volume interaction in a dense suspension of aligned rods for the case of (a) rigid rods and (b) semi-flexible rods. (From Ref. (Tkachenko 1996)

1987):

$$\begin{aligned} \delta F &= F_{\text{layered}} - F_{\text{uniform}} = F(n + a\cos(kz)) - F(n) = \\ & n + 8n^2 j_0(k). \end{aligned} \tag{1.14}$$

The positive free energy difference $\delta F(n,k) > 0$ implies that at volume fraction n and wavevector k the nematic phase has the lowest free energy and therefore is the equilibrium phase. On the other hand, at values of n_c and k_c which satisfy the equation $\delta F(n_c, k_c) = 0$ the system becomes unstable towards smectic fluctuations since they do not cost any energy to create. We identify n_c and k_c as the critical volume fraction and wavevector of the second order nematic-smectic phase transition. It is important to note that the first term in Eq. 1.14 originates from ideal part of free energy in Eq. 1.1, while the second term in Eq. 1.14 originates from the interaction part of free energy in Eq. 1.1. We observe that the difference in the ideal part of the free energy between the layered and uniform phase is always positive and given by $\delta F \propto n$. Therefore the ideal part of free energy always suppresses the ordering transition as expected. On the other hand, the difference in the interaction part of free energy between the uniform and layered phase is given by $\delta F \propto n^2 j_o(k)$. Since this part of free energy difference scales as n^2, for high enough volume fraction of rods and for specific values of wavevector k this term is negative and large enough to drive the system towards the smectic phase. Considering the highly approximate nature of the theory, the conditions $n_c = 0.575$ and $k_c = 2\pi/1.398L$ obtained for the nematic-smectic phase transition compare favorably to the results of the computer simulations of parallel rods $n_c = 0.43$ and $k_c = 2\pi/1.27L$ (Frenkel et al. 1988). Inclusion of third virial coefficient brings the theoretical prediction for the N-S transition closer to what is observed in simulations (Mulder 1987).

The above simple model suggests a physical picture of the excluded volume effects responsible for the formations of a smectic phase first introduced by Wen and Meyer (Wen and Meyer 1987). A spatially uniform nematic phase results in a very inefficient packing of rods as shown in Fig. 1.4a. In such a state the ideal part of free

energy attains its minimum value while the interaction part does not. The reason for this is that the nematic phase is under the constraint of uniform packing, and thus the excluded volume between any two rods is eight times the volume of a single rod since rods are allowed to approach each other from any direction. One way to decrease excluded volume is to impose a smectic like periodic density modulation. Then the probability of two rods approaching each other along their axial direction will decrease while the probability of sideways approach will increase. For example, in an extreme case where the probability distribution of centers of rods consists of very sharp delta-like functions spaced at distances slightly longer than the rod length, rods are allowed to approach each other only sideways and the overlap between the ends of the rods is completely forbidden. Consequently, the excluded volume between two rods will be half the value of the excluded volume for an uniform density distribution. Because of this simple reason, the value of the interaction part of free energy decreases with increasing order in Eq 1.14. The actual volume fraction of the ordering transition and the resulting density distribution $\rho(\mathbf{r})$ is therefore determined by the competition between the ideal and interaction part of the free energy given in expression Eq. 1.1. The treatment of the nematic smectic phase transition of the second virial approximation was also extended to the case of rods with orientational freedom (van Roij et al. 1995). In this case the calculation becomes much more involved.

It is easy to extend the above argument to consider the influence of flexibility on the nematic-smectic phase transition (Tkachenko 1996; van der Schoot 1996). Experimentally it is found that the flexibility acts to stabilize the nematic phase and destabilize the smectic phase (Dogic and Fraden 1997). As was first noticed by Tkachenko, in the case of perfectly aligned rigid rod nematics the only way to fill the space created by an end of a rod is to place another rod above it as shown in Fig. 1.4a. In the case of a nematic solution of semi-flexible rods it is possible for other molecules to occupy space around the end of a particular molecule by deflecting around its end as shown in Fig. 1.4b. This results in more efficient packing of semi-flexible rods in the nematic state which in turn leads to the suppression of the nematic-smectic phase transition. This picture of the effect of flexibility on the nematic-smectic phase transition has been confirmed using computer simulations (Polson 1997).

1.2.6 Phase behavior of a binary mixture of hard particles

Recently the second virial approximation has also been extended to study ordering and demixing transitions in binary mixtures of hard rods (Koda and Kimura 1994; Cui and Cheng 1994; Sear and Jackson 1995; Sear and Mulder 1996; van Roij 1996; van Roij and Mulder 1996; van Roij 1996; van Roij 1994; van Roij et al. 1998). In many of these cases it is not obvious if terminating the free energy expansions at a second virial level is sufficient to describe the phase diagram of binary mixture. For example, it was recently shown that although Onsager theory quantitatively describes the I-N phase transitions of rods, it fails to predict even qualitative features of a binary mixture of rods with two different diameters (Purdy et al. 2004). In other cases, such as a mixture of perfectly aligned spherocylinders and hard spheres the second virial theory predicts the right qualitative features as has been verified by computer simulations for

the lamellar phase, but fails to described the columnar phase (Adams et al. 1998). Expressions of the stability matrix for a binary mixture of parallel spherocylinders and spheres are given in the following references (Koda et al. 1996; Dogic et al. 2000).

1.3 Experimental phase diagram of a suspension of *fd* virus

Theory and simulation indicate that with increasing concentration, rod-like particles will form isotropic, nematic and smectic phases (Hosino et al. 1979; Frenkel et al. 1988; Bolhuis and Frenkel 1997; Mulder 1987; Wen and Meyer 1987). The columnar phase turns out to be metastable with respect to the smectic phase for all aspect ratios and rod concentrations (Bolhuis and Frenkel 1997). So far the only experimental systems whose phase behavior agrees with theoretical predictions are colloidal suspensions of viruses *fd*, *pf1*, TMV and inorganic β-FeOOH rods (Maeda and Maeda 2003). This is due to the fact that nature makes all viruses identical to each other. This results in a colloidal suspension of very high monodispersity, much higher then what can be achieved with current synthetic methods. Recently using a combination of recombinant DNA technology and traditional chemical methods it was possible to prepare monodisperse PBLG polymers. Although these polymers are not available in large quantities they where reported to form a smectic phase (Yu et al. 1997). This is a potentially powerful technique to create novel liquid crystals. While the present review focuses on the fundamental aspects of the phase behavior of rods and rod/sphere mixture, individual viruses and virus assemblies might become technologically useful materials. In this respect, the recent work by the Belcher group seems promising (Lee et al. 2002).

In this review article we focus on the phase behavior of rod-like bacteriophage *fd* and its closely related M13. The phase behavior of another class of anisotropic colloids composed of minerals has recently been review elsewhere (Gabriel and Davidson 2003). The phase behavior of polymeric liquid crystals such as PBLG is reviewed in the following reference (Sato and Teramoto 1994). Historically, the first observation of the nematic liquid crystalline phase of *fd* was reported in the study by Lapointe and Marvin (Lapointe and Marvin 1973). Shortly thereafter a smectic phase was also reported in a little noticed paper (Booy and Fowler 1985).

We note that *fd* forms a cholesteric instead of a nematic phase. Cholesteric and nematic phases are locally identical to each other. If often takes many days after sample preparation for the *fd* solution to form a fully twisted cholesteric phase. This indicates that the free energy difference between these two structures is very small. Therefore, we expect that the Onsager theory equally well describes the isotropic-nematic and isotropic-cholesteric phase transition. In this review we use nematic and cholesteric terms interchangeably depending on the particular context. Often when confined to small droplets, such as tactoids observed at the isotropic-cholesteric coexistence, the cholesteric phase is unable to develop and the sample remains nematic.

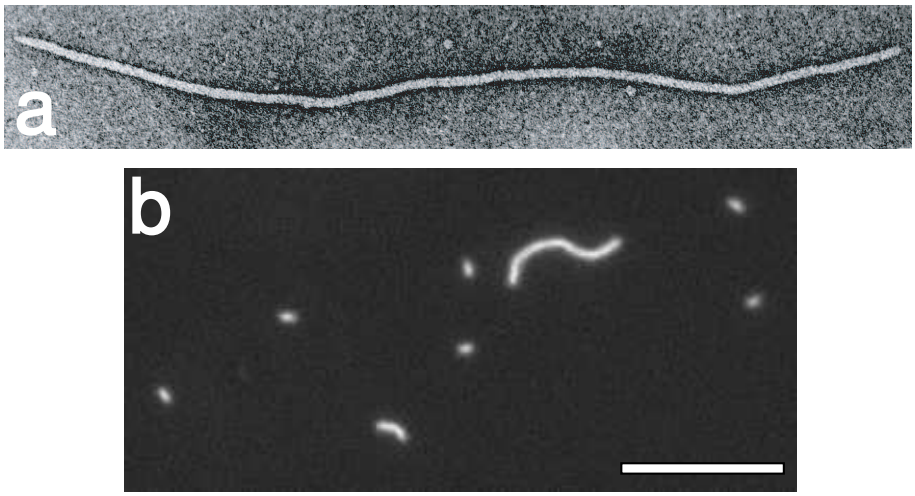

Figure 1.5: (a) Electron microscopy image of a bacteriophage *fd*. The contour length of the virus corresponds to 0.9 μm. (b) Image of a dilute isotropic solution of *fd* confined to chamber of approximately 1 μm thickness. The presence of *fd* with much larger contour length then the wild type is easily seen. *Fd* was grown in recA$^+$ strain (JM101) and labelled with Alexa 488 (Molecular Probes). The image was taken with a fluorescent microscope equipped with a cooled CCD camera (CoolSnap HQ, Roper Scientific). The scale bar indicates 10 μm.

1.3.1 Properties and preparation of filamentous bacteriophage

The structure of the bacteriophage *fd* is very simple with a self-assembled hollow cylindrical shell composed of roughly 2800 copies of a single coat protein pVIII. A single circular strand of DNA is enclosed within this hollow shell. Length of the whole virus is determined by the length of the DNA. The ends of the assembly are covered with end capping proteins which are different from the major coat protein pVIII. In addition, the two ends are different from one another which makes *fd* a polar colloid. This characteristics can be used to selectively label each end (Lee et al. 2002).

The physical characteristics of the *fd* virus are the contour length of 880 nm, bare diameter of 6.6 nm, aspect ratio $L/D_{\rm sc} \approx 130$. The semi-flexibility of the virus is characterized by the persistence length $l_p = 2.2\mu m$ which has been reported to change with temperature (Tang and Fraden 1996). The colloidal stability of the virus is preserved due to the fact that it has a very high negative surface charge at pH=8.0 (Zimmermann et al. 1986). For a more comprehensive list of most known physical constants of *fd* the reader is refereed to the following review article (Fraden 1995).

There are well established methods for growing bacteriophage *fd* and closely related M13 (Maniatis et al. 1989; Dogic and Fraden 2001). In brief, one first grows a large quantity of *E. Coli.* host. Once the host strain reaches log phase it is infected with viruses at a well defined multiplicity of infection (MOI) and the culture is grown for an additional eight hours. The bacteria is separated from the culture by centrifugation at low speed and the virus in the supernatant is concentrated by adding neutral polymer

such as poly(ethylene glycol) (PEG Mw 8000) which acts as a depleting agent. In principle it is possible to further purify the virus using a cumbersome CsCl gradient centrifugation step. In practice, we found that a two step sequence of low-speed and high-speed centrifugation produces *fd* virus of sufficient purity for most of our experiments. Once grown *fd* should be kept in a low ionic strength buffer at 4°. Under these conditions the solution should be stable for at least one year although it is difficult to prevent microbial growth over such a long time period even in the presence of sodium azide. Therefore, before use of the virus we dialyze it against fresh buffer and spin down aggregates and bacterial debris using a low speed centrifugation step. The usual yields are about 15-20 mg per liter of infected *E. Coli.* culture.

There is a tendency for all viruses to form multimeric structure with a contour length which is an integer multiple of the the length of wild type *fd*. We have found that it is important to chose the appropriate *E. Coli.* host strain in order to reduce the number of multimers. Although recA^+ strains such as JM101 grow faster and produce higher yields of virus we found that these hosts have a tendency to form dimer and multimer viruses. These can easily be identified once the viruses are labelled and visualized using fluorescence microscopy. Viruses purified from recA^+ host form smectic phase at different concentrations when compared to viruses purified form recA^- strains such as Xl1-Blue. In addition, many other structures such as the lamellar phase described in section 1.6, are not observed in a *fd* virus grown in recA^+ strains. This is presumably due to increased polydispersity of the virus.

It is difficult to asses the polydispersity of the virus. They have a pronounced tendency to break or aggregate during preparation of grids for electron microscopy. It is possible to run agarose gel electrophoresis on whole viruses which are stained with Commassie Blue protein stain (Griess et al. 1990). However, sometimes longer *fd* does not easily enter the gels. It is also possible to strip the viruses of its protein and run DNA gel electrophoresis, which is subsequently stained with Ethidium Bromide. Recently, we have prepared *fd* viruses labelled with fluorescent dye Alexa 488 (Molecular Probes) which appear very bright when viewed with fluorescence microscope. These could be used to quantify the polydispersity of the virus. When labelled at very high fraction with Alexa 488 (Molecular Probes) dye, we do not observe any aggregation over a period of a year. In contrast, if the viruses are labelled with larger and more hydrophobic dyes such as tetra-methyl-rhodamine (TAMRA) they aggregate into bundles over a period of days. With the proper use of anti-bleaching solution it is possible to continuously observe Alexa 488 labelled viruses for 5-10 minutes under full illumination with a 100 W Mercury lamp. Fig. 1.5 shows a fluorescent microscopy image of Alexa-488 labelled recA^+ *fd*. It is easy to observe a number of *fd's* with a contour length much longer then that of *fd* wt.

All the available data points to the fact that the contour length of *fd* is determined by the size of its DNA. Therefore it is possible to alter the length of the *fd* by simply adding additional DNA into *fd*'s genome using standard recombinant DNA techniques. A few decades ago *fd*'s with different contour length were genetically engineered and used to study the rotational diffusion of rod-like colloids with varying aspect ratio (Maguire et al. 1980). However, this potentially powerful method was not pursued any further. Using similar methods mutants up to 5 μm long have been

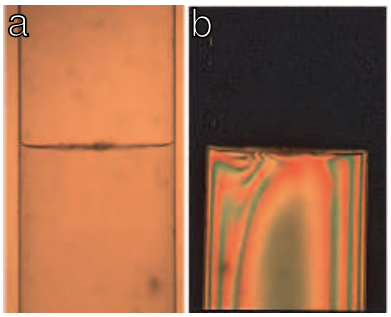

Figure 1.6: The bulk phase separation between isotropic and nematic phases observed in a TMV suspension. The image on the left is taken with white light while the image on the right is taken between crossed polarizers. Since the difference in density between the nematic and isotropic phase can be up to 30% over a period of days the nematic phase sediments to the bottom. The phase diagram for TMV suspension is shown in (Fraden et al. 1989). Identical bulk phase separation is observed in *fd* suspension. By measuring the concentration of the virus in coexisting phases it is possible to measure the phase diagram such as the one shown in Fig. 1.7

described in the biological literature (Herrmann et al. 1980). We have tried to reproduce this method, but have found that during a large scale preparation involving many generations of bacteria division, foreign DNA is easily expelled. The resulting culture quickly reverts back to wild type *fd*. We have had more success of creating mutant *fd* using the phagemid methods, as described in detail in the following reference (Sambrook et al. 1989). The resulting *fd* are sufficiently monodisperse to form a smectic phase shown in Fig. 1.16. For more details the reader is refereed to the following reference (Dogic 2003).

1.3.2 Isotropic-cholesteric phase transition in *fd* suspensions

Due to the entropic nature of the *fd* suspension, the only variable that determines the phase behavior is the density of the constituent rods. Therefore, with increasing *fd* concentration an isotropic suspension of *fd* undergoes a first order phase transition to the nematic/cholesteric phase. It follows that the density of the cholesteric phase is higher then that of the isotropic phase in a coexisting sample. The denser cholesteric phase slowly sediments to the bottom of the sample container resulting in a macroscopically phase separated sample (Fig. 1.6).

Recently we quantitatively compared the experimental results of the I-Ch transition to the predictions of the Onsager theory (Tang and Fraden 1996; Purdy and Fraden 2004b). To accomplish this it is necessary to take into account both the charge and flexibility of an *fd* virus. As explained in Sec. 1.2.2 it is possible to describe the thermodynamic behavior of a dilute suspension of charged rods using the concept of effective diameter. D_{eff} for *fd* is plotted in Fig. 1.1 for three different surface charges. Due to the non-linear nature of the Poisson-Boltzman equation, changing the surface

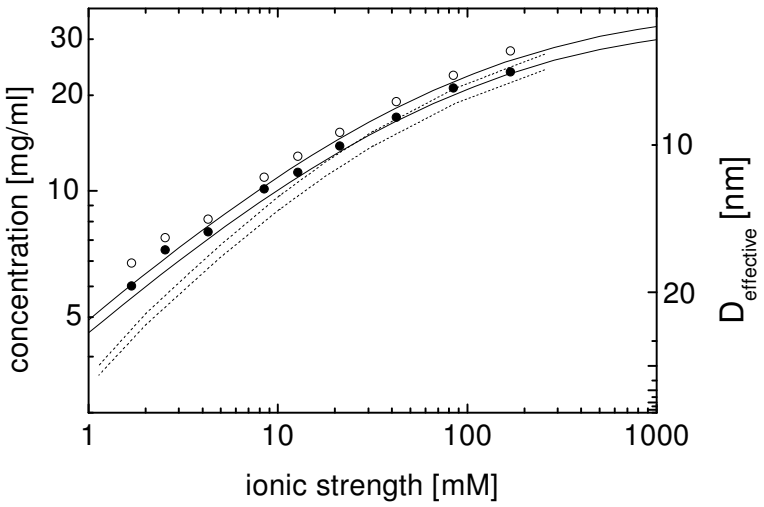

Figure 1.7: The I-Ch co-existence concentrations measured in an aqueous suspension of *fd* virus as a function of the ionic strength (Tang and Fraden 1995). The full line is the numerical solution of Chen for the I-Ch co-existence, which treats excluded volume interactions at the second virial level while the orientational distribution function is calculated numerically. The dashed line is the scaled particle solution for the I-Ch co-existence in which all virial coefficients are included in an approximate way and the orientational distribution function has an approximate form given by Eq. 1.7. The scale on the right side indicates the effective diameter for a given ionic strength. (From ref. (Tang and Fraden 1996))

charge by an order of magnitude has minimal effect on the resulting D_{eff}. The flexibility is included according to the prescription given by Khokhlov and Semenov and discussed in more detail in Sec. 1.2.3.

Figure 1.7 shows that with increasing ionic strength the location of the I-Ch phase transition shifts to higher concentrations. However, increasing ionic strength increases L/D_{eff} which in Onsager theory should decrease the volume fraction of the rods at the I-N transition. The discrepancy can easily be understood if one looks at the condition for instability of the isotropic phase: $(4/\pi)\ L^2 D_{\text{eff}}(N/V) = 4$. The concentration in Fig. 1.7 is not proportional to the effective volume fraction, but to the number density of the virus. If D_{eff} is decreased with the length of the rod remaining constant, it follows that the number density of the virus at the transition has to increase so that condition for the nematic/cholesteric instability is still satisfied. The experimental data points are compared to the numerical solution of Chen who approximates the excluded volume interaction by the second virial coefficient and treats the ODF in an accurate numerical way (Chen 1993). We have also plotted the result of a theory in which higher virial coefficients have been taken into account within the scaled particle theory while the orientational degrees of a semi-flexible polymer confined by the nematic field is approximated using approximation descried in Sec. 1.2.3.

At the first sight the agreement between the theory due to Chen and the experiment

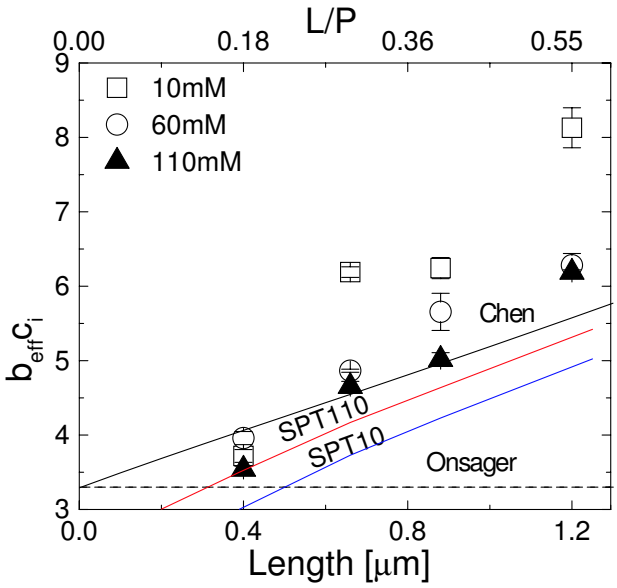

Figure 1.8: Dimensionless concentration of the isotropic phase in coexistence with the nematic phase as a function of M13 contour length at pH 8.2. The dimensionless concentration $b_{\rm eff}c_i = (\pi/4)D_{\rm eff}L^2N_i/V$. For rigid rods the Onsager theory predicts that the location of the I-N phase transition is independent of the theory.(dashed line). The solid lines SPT110 and SPT10 are results of the scaled particle theory for ionic strength of 110 and 10 mM. SPT theory agrees with experiment at high ionic strengths but fails for low ionic strength (Purdy and Fraden 2004b).

as shown in Fig. 1.7 is quite good. However, there is reason to believe that this agreement is fortuitous at low ionic strength. For example, at 1 mM ionic strength $D_{\rm eff} \approx 60$ nm which results in the aspect ratio $L/D_{\rm eff} \approx 15$. Figure 1.3 clearly shows that for these small aspect ratios third and higher virial coefficients cannot be ignored. Indeed, the results of the scaled particle theory, which include these higher coefficients predict that the I-N(Ch) transition is located at significantly lower concentration than what is found by the experiments and Chen's theory. The agreement between the scaled particle theory, the experiments and the theory of Chen is much better at high ionic strength where the effective aspect ratio is large (at 100 mM ionic strength $L/D_{\rm eff} \approx 83$) and therefore the excluded volume interactions are more accurately approximated by the second virial coefficient.

We note that the results from the scaled particle theory shown in Fig. 1.7 should also be treated with a degree of scepticism. To compare the scaled particle theory with experiments on charged rods we use the effective diameter of the rod. However the concept of $D_{\rm eff}$ introduced in Eq. 1.13 is only rigorously justified for conditions for which the second virial coefficient is quantitatively valid. There is a recent theoretical attempt to extend the scaled particle theory to charged particles (Kramer and Herzfeld

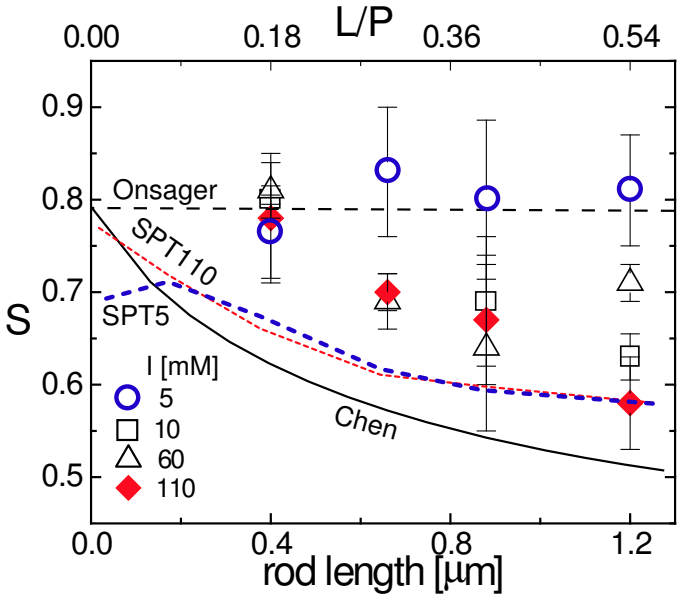

Figure 1.9: Experiments and theory showing the depndence of the order parameter of coexisting nematic phase as a function of rod length for four different ionic strengths. Dashed line represents the prediction of the Onsager theory, full lines is the theoretical calculation by Chen while the dotted lines are the prediction of the scaled particle theory for 5 mM (SPT5) and 110 mM (SPT110) ionic strength. Theoretical curves are calculated for rods with persistence length of 2.2 μm while the contour length varies between 0.4 μm and 1.2 μm. (From ref (Purdy and Fraden 2004b))

1999; Kramer and Herzfeld 2000). Unfortunately, this theory does not interpolate to Onsager theory for dilute rods, in contrast to the scaled particle theory for hard rods. We also note that the twisting factor ignored in our treatment of $D_{\rm eff}$ for *fd* is strongest at low ionic strength (Stroobants et al. 1986). This effect displaces the I-N(Ch) transition to higher densities.

The effect of the contour length of M13 virus on the I-Ch phase transitions has also been measured (Purdy and Fraden 2004b). Mutant viruses of various contour length have been prepared using molecular cloning as described in Sec. 1.3.1. Fig. 1.8 shows the location of the I-Ch phase transition as a function of contour length in terms of dimensionless concentration $b_{\rm eff}c_{\rm i}$. The Onsager theory predicts that the location of the I-Ch will occur when $b_{\rm eff}c_i \approx 4$. In these units the location of the phase transition is independent of the rod aspect ratio as indicated by the dashed line. Including finite flexibility significantly shifts the location of the I-Ch phase transition to higher concentration as is indicated by the full line. The I-Ch phase transition at high ionic strength indicated by filled triangles agrees well with these predictions. However, as the ionic strength decreases to 10 mM there is significant deviation between experiment and theory.

Another important parameter that characterizes the I-Ch phase transition is the order parameter of the nematic/cholesteric phase at coexistence. Fig. 1.9 show the behavior of the nematic order parameter as a function of both the contour length and ionic strength. The order parameter can be extracted from birefringence measurements once the birefringence per particle is measure using x-ray scattering as described in Sec. 1.3.5 and the following reference (Purdy et al. 2003). Onsager theory predicts that for rigid rods the order parameter of the coexisting nematic phase is approximately $S_2 = 0.8$. For finite flexibility the order parameter significantly decreases as is indicated by the full line (solution due to Chen) and dotted lines (solution with SPT). At high ionic strength the measurements of the order parameter almost quantitatively follow the theoretical predictions. However, at the lowest ionic strength of 5 mM the order parameter is almost independent of the ratio of contour length to persistence length and much higher then the theoretical predictions which account for flexibility. Surprisingly, the low ionic strength data agree with the Onsager model for rigid rods. The theory of electrostatic stiffening of charged polymer predicts that the persistence length of *fd* is independent of ionic strength because the bare persistence length of *fd* is very long (Purdy and Fraden 2004b).

From these data we conclude that the Onsager theory extended to account for flexibility and charge quantitatively describes the I-Ch phase transition of *fd* wt in the limit of high ionic strength. With decreasing ionic strength there is a systematic disagreement between the experimental results and theoretical predictions. In this limit the location of the isotropic-nematic phase transition is at higher rod concentration then theoretical predictions and the nematic order parameter is also higher then what is predicted. This is probably due to the approximate incorporation of the electrostatic interaction into the theoretical free energy via D_{eff}.

1.3.3 Polymer coated *fd* and its isotropic-cholesteric phase transition

It is possible to eliminate electrostatic interactions between viruses by preparing sterically stabilized *fd* suspensions. This is achieved by covalently coupling poly(ethylene gylcol) PEG to amine groups that are present on the virus surface (Dogic and Fraden 2001). Water at room temperature is a good solvent for PEG and therefore PEG coated surfaces interact through purely repulsive interactions (Kuhl et al. 1994). By measuring the increase in the index of refraction of PEG coated virus suspensions the number of attached polymer per virus can be determined. These measurements indicate that the density of the deposited polymer is at a transition from isolated "mushrooms" to a extended brush-like coverage (Grelet and Fraden 2003). It is important to mention that polymer stabilized rods still have a charged surface and the effective interaction between two viruses will be a combination of electrostatic and steric repulsion.

The polymer stabilized *fd* undergoes an isotropic to cholesteric phase transition. Fig. 1.10 shows the concentration of the coexisting isotropic phase for a suspension of bare *fd* and *fd* coated with PEG-5,000 and PEG-20,000. For *fd*-PEG-20,000 the location of the I-Ch phase transition is completely independent of the ionic strength. This

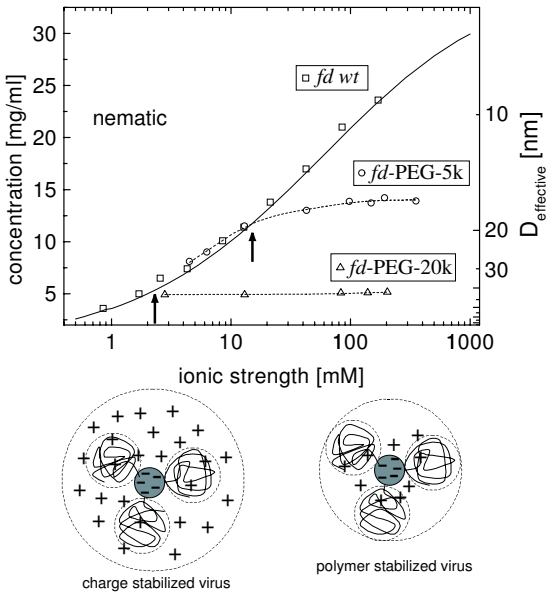

Figure 1.10: The concentration of the isotropic phase which coexists with the nematic phase as a function of ionic strength. The data is shown for pure *fd* suspension (open squares), *fd* coated with PEG-5000 (open circles) and *fd* coated with PEG-20000 (open triangles). The labels on the right size indicate the effective diameter at which the location of the I-Ch transition occurs. The dashed lines are a guide to the eye.The I-N transition of PEG-coated virus come independent of ionic strength (indicated by arrows) when the effective diameter of the virus is set by the polymer diameter and not by the range of electrostatic repulsion (After Ref. (Dogic and Fraden 2001))

indicates that the steric repulsion has a longer range then the electrostatic repulsion for the range of ionic strengths studied. However, for *fd*-PEG-5,000 it is possible to observe a transition from the sterically stabilized region to the electrostatically stabilized region by measuring the ionic strength dependence of the I-Ch transition. At high ionic strength the transition is independent of the ionic strength indicating steric repulsion. With decreasing ionic strength the concentration of the I-Ch transition decreases and agrees with the I-Ch transition of bare virus. In this regime the virus is electrostatically stabilized. From Fig. 1.10 we can deduce that the steric size of the virus-polymer complex is D_{eff}=45 nm which is approximately equal to $D_{\text{bare}}+4R_g$=35 nm. This indicates that the the density of the grafted PEG is slightly in the "extended" brush regime. Although not the subject of this chapter we note that using polymer stabilized viruses it is possible to study the phase behavior of a binary mixture of rods with different diameters (Purdy et al. 2004).

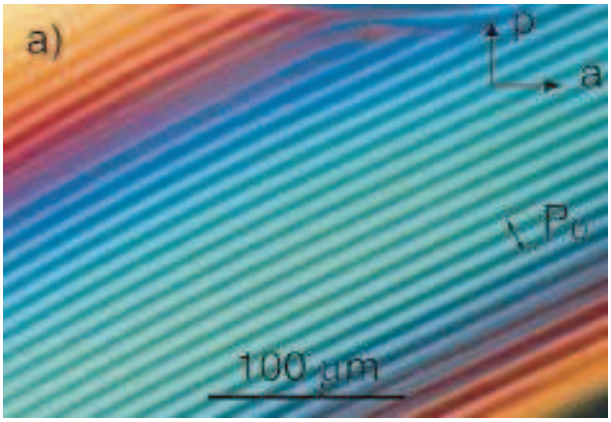

Figure 1.11: An image of a cholesteric phase of *fd* taken with polarization microscope. The location of polarizers and analyzer are indicated by arrows. The dark lines correspond to regions where rods point perpendicular to the image while bright regions correspond to regions where the rods lie in the plane. The best way to observe the cholesteric texture such as the one shown here is to fill a cylindrical x-ray capillary and focus on its midplane. (After ref. (Dogic and Fraden 2000))

1.3.4 Cholesteric phase of *fd*

The cholesteric phase is locally identical to the nematic phase. However, in a cholesteric phase the nematic director twists into a helical structure. *Fd* forms a cholesteric phase as evidenced by the typical cholesteric fingerprint texture shown in Fig. 1.11. The distance that it take for the director to rotate by 2π is called the cholesteric pitch. Experimentally it is easy to determine the value of the pitch by simply measuring the distance between either two dark or bright lines in images such as Fig. 1.11. The cholesteric pitch will also diffract light from which the magnitude of the pitch can be determined (Oldenbourg 1981).

In thermotropic liquid crystals it is conventional wisdom that chiral molecules will form a cholesteric phase while achiral molecules will form a nematic phase. However, this does not seem to be true for colloidal rods and the molecular origin of the cholesteric phase remains poorly understood. Some chiral polymers such as *fd*, PBLG and DNA form a well developed cholesteric phase (Leforestier and Livolant 1993; Livolant 1991; Van Winkle et al. 1990; DuPre and Duke 1975; Dogic and Fraden 2000). However, other viruses such as TMV and *pf1* form nematic structures under the same conditions in which the cholesteric twisting is observed in *fd* suspension. Surprisingly, the molecular structure of TMV and *pf1* is also chiral and quite similat to *fd*. The main challenge is to formulate a microscopic theory of chiral polymers and explain why some chiral molecules such as *fd* form a cholesteric phase while other ones like *pf1* and TMV form a nematic phase.

Following the initial work of Onsager, Straley was the first to propose a microscopic theory of the cholesteric phase base on excluded volume (Straley 1976). He considered

a nematic solution of rod-like molecules which have additional chiral threads similar to chiral screws. Similar to Onsager, in the Straley model the formation of the cholesteric phase is driven by pure excluded volume effects. The excluded volume between two screw-like rods is minimum not when they are parallel to each other, but when they approach each other at a specific angle at which the chiral grooves can interpenetrate. The initial work of Straley was extended to semi-flexible molecules (Odijk 1987; Pelcovits 1996). More recent work indicates that mean field approaches used by Straley fail to describe the cholesteric phase since rotations along the rods long axis effectively average out the chiral structure of the molecules (Kamien and Lubensky 1997). These latter authors further argue that it is the biaxial correlations that are responsible for the formation of the cholesteric pitch. In addition to excluded volume interactions it has been proposed that other type of chiral interactions, such as van der Waals can induce the formation of the cholesteric phase (Issaenko et al. 1999).

As already mentioned, the origin of the cholesteric phase in *fd* solution is not understood. Even when *fd* is coated with a thick layer of achiral PEG polymer, the resulting polymer stabilized rods still form a cholesteric structure (Grelet and Fraden 2003). This would imply that it is not the microscopic chiral arrangement of coat proteins that is responsible for the cholesteric structure; rather it has been suggested that the virus twist into mesoscopic helical structure. However, up to now there is no concrete experimental evidence that supports this hypothesis. Interestingly, the relative angle between two neighboring molecules is very small in a cholesteric phase. The typical size of the cholesteric pitch is roughly 20 μm while the spatial separation between two rods in such a sample would be of the order of 20 nm. This would indicate that there are about 1000 molecules along the cholesteric pitch which results in the average angle between two rods that is at most a fraction of a degree. This is much smaller then the average angle by which the rods locally fluctuate due to the width of the orientation distribution function which typically ranges from $0.6¡S_2¡0.9$.

The cholesteric pitch has been measured as a function of the virus concentration and ionic strength. At a high ionic strength of 100 mM the cholesteric pitch decreases with increasing concentration according to the power law $P \propto= c^{-\nu}$ where $\nu = 1.65$ (Dogic and Fraden 2000). As the *fd* concentration approaches the smectic phase the cholesteric pitch deviates from the above power law and it slowly unwinds. This is presumably due to pre-smectic fluctuations since similar behavior is observed in thermotropic liquid crystals (Pindak et al. 1974). Upon decreasing the ionic strength to 4 mM the value of the power exponent ν systematically decreases to 1.1. Interestingly the exponent ν measured at high ionic strength agrees with the theoretical predictions of Odijk (Odijk 1987). This result also agrees with previous measurements on PBLG (DuPre and Duke 1975). Measurements of the cholesteric pitch of DNA are inconsistent with each other (Jizuka and Yang 1978; Senechal et al. 1980). In conclusion, much still remains unanswered about the microscopic origin of the cholesteric pitch.

1.3.5 Nematic order parameter of *fd* suspensions

As discussed in the theory section (Fig. 1.2b) the effect of finite rod flexibility has a dramatic effect on the order parameter of the nematic phase. For example, the

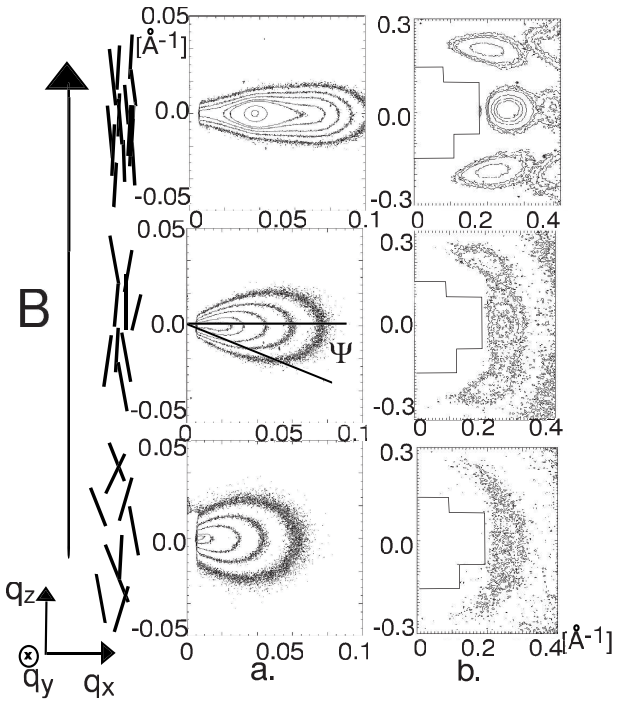

Figure 1.12: Contour plots of X-ray diffraction of a magnetically aligned *fd* suspension at concentrations of 93, 33 and 15.5 mg/ml respectively in 10 mM ionic strength buffer. In column (a) scattering at small reciprocal angle up to 0.1 $\AA^{-1}$ due to interparticle interference is shown. In column (b) the intraparticle scattering at higher angle reveal the *fd* form factor and the low angle interparticle interference is blocked by the beamstop. The orientational distribution function can be determined from the angular spread in both the intraparticle and interparticle peaks. (After ref. (Purdy et al. 2003))

Khohklov-Semenov (KS) theory predicts that the finite flexibility of *fd* reduces the nematic order parameter S_2 of the coexisting nematic phase from the rigid rod limit of 0.8 to 0.65. The fact that the I-Ch coexistence concentrations agree with the KS theory provides an indirect test of the KS theory. However, a more stringent test of this theory would be to measure the nematic order parameter.

It is possible to induce the cholesteric to nematic phase transition by placing the sample in a sufficiently strong magnetic field (Meyer 1968; Meyer 1969). This fact was used to prepare uniformly aligned monodomain nematics and subsequently measure their nematic order parameter. The applied filed is strong enough to align the sample but at the same time does not affect the orientational distribution function. The traditional techniques for determining the nematic order parameter are x-ray scattering and quantitative measurements of the birefringence. To determine the absolute value of the order parameter from the birefringence measurements it is necessary to know the birefringence per particle, which has to independently determined. Both of these tech-

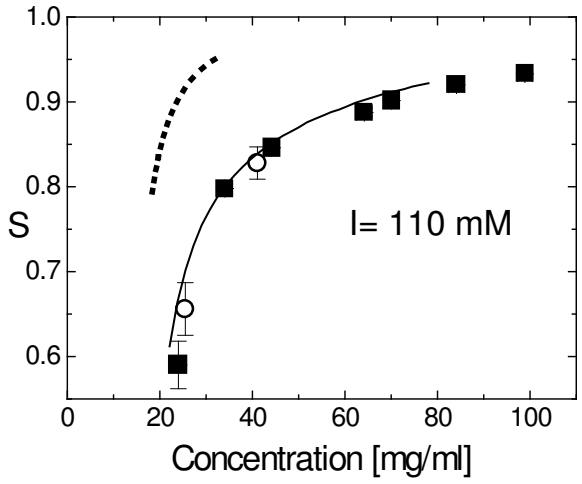

Figure 1.13: Nematic order parameter of the *fd* phase obtained from x-ray scattering pattern such as the ones shown in Fig. 1.12. Solid symbols are the order parameters values obtained from interparticle scattering while open symbols are values obtained from intraparticle scattering. Solid line shows the prediction of the scaled particle theory extended to semi-flexible charged rods as described in the theory section. Dotted line is the prediction of the Onsager theory for rigid charged rods. (After ref (Purdy et al. 2003))

niques were used to measure the nematic order parameter of an *fd* suspension (Purdy et al. 2003).

X-ray scattering patterns from colloidal nematic liquid crystals are shown in Fig. 1.12. The scattering at a small angle shows a typical butterfly pattern which is due to the interference between neighboring rods (Ao and Meyer 1991; Kamien et al. 1992; LeDoussal and Nelson 1991). This pattern is usually observed in polymer liquid crystals without much internal structure such as PBLG. The intensity along an arc of constant radius is usually assumed to be a function of the orientiational distribution function. At low angles this is an assumption that needs to be tested. The reason for this is that unlike spherical particles, the structure factor of a solution of rod-like particles does not necessarily decouple from the anisotropic form factor and it is the decoupling assumption that needs to be tested. Here we compare the order parameter obtained at low angles with that obtained from high angle to test the decoupling assumption.

In addition to interparticle scattering at low angle, a nematic *fd* solution shows a clear scattering pattern at high angles due to the single particle form factor (Fig. 1.12). At these high angles the structure function is one and interparticle interference does not contribute to the scattering. Therefore in this region the precise shape of the orientational distribution function can be rigorously determined from the scattering pattern. This method has been previously used to determine S for nematic TMV suspensions (Oldenbourg et al. 1988). But up to now the decoupling approximation has not been tested by comparing the ODF obtained from low angle interparticle

scattering and high angle intraparticle scattering.

Fig. 1.12 shows the scattering patterns due to both interparticle and intraparticle interference taken on magnetically aligned nematic monodomains of *fd*. With increasing rod concentration the width of the patterns decreases, which indicates that the order parameter increases. The concentration dependence of the order parameter is shown in Fig. 1.13. As can be seen from this figure the agreement between theory and experiment is very good at high ionic strength. We note that at a lower ionic strength of 10 mM there is a noticeable discrepancy between the theoretical curve and experimental data (data not shown) consistent with discrepancies observed for the isotropic-cholesteric coexistence (Purdy et al. 2003).

Equally important, we find that the order parameter obtained from interparticle and intraparticle scattering are always almost identical. This supports the decoupling approximation and provides validation for measurements of the order parameter from low angle interparticle scattering pattern. In addition it has been shown that the birefringence scales in the same way as the order parameter obtained from x-ray scattering. From this comparison the magnetic birefringence per single rod *fd* can be determined to be $\Delta n_{\mathrm{sat}}/c = 3.8 * 10^{-5}\mathrm{ml/mg}$ where c is the concentration of rods. We believe that the measurements of the concentration dependence of the order parameter represents the most stringent test for the validity of the KS theory to date. The breakdown of the theory at low ionic strength indicates the need to improve the treatment of electrostatic repulsion for strongly interacting particles.

Direct visualization of fluorescently labelled polymers dissolved in a nematic *fd* background is another novel method by which it is possible to measure the nematic order parameter. Fig. 1.14 shows the images of four different labelled polymers dissolved in the invisible background of unlabeled *fd* nematics. The conformation of the rods changes from coil-like to rod-like as the background fluids undergoes a isotropic-nematic phase transition. Interestingly this is true for relatively rigid rods such as neurofilaments, wormlike micelles and actin while relatively flexible DNA demixes from the background *fd* suspension. Using these images it is possible to determine the order parameter of the polymers dissolved in the background nematic. It is found that the order parameter significantly increases with increasing the length of the dissolved polymer . For more information the reader is referred to the following reference (Dogic et al. 2004b).

It might be possible to determine the nematic order parameter of the nematic suspension by directly labelling *fd* rods. Present experiments indicate that the exposure times necessary to acquire sufficient signal are too long to accurately determine the orientation of an individual *fd* virus. During the necessary exposure time individual rods undergo significant rotational diffusion which blurs the signal. Using laser as a illumination source it might be possible to reduce the exposure time to levels where the order parameter measurements are possible.

1.3.6 Smectic phase of *fd*

At high concentration *fd* forms a smectic A phase in which rods have long range orientational order and one dimensional positional order. The smectic phase in a

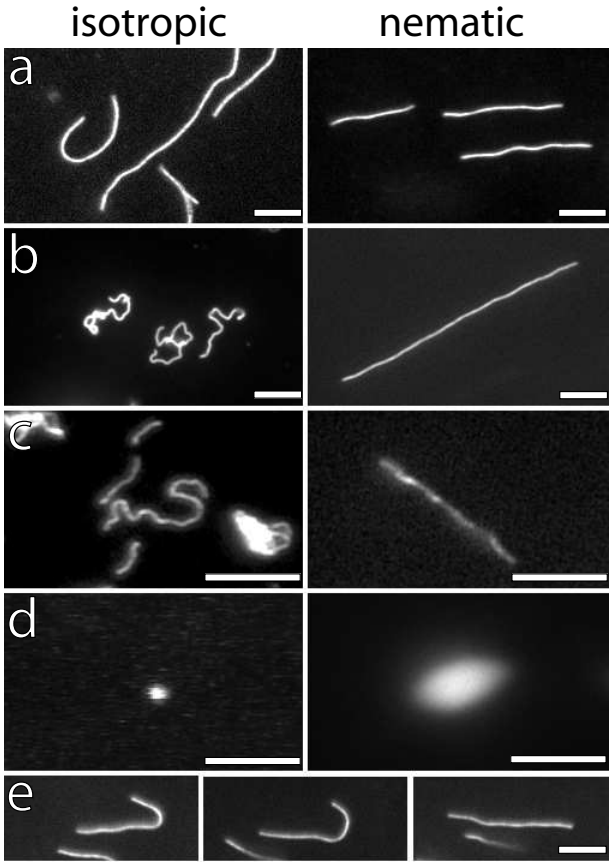

Figure 1.14: Images of the fluorescently labelled biopolymer in isotropic (left panel) and nematic (right panel) background suspension composed of *fd* virus. (a-d) are respectively images of actin ($l_p = 16\mu m$), worm-like micelles ($l_p = 0.6\mu m$), neurofilaments ($l_p = 0.2\mu m$) and DNA ($l_p = 0.05\mu m$). (e) a sequence of images illustrating an escape of an actin filaments from a hairpin defects. Scale bar is 5 μm. (After ref (Dogic et al. 2004b))

suspension of *fd* was first reported in the following reference (Booy and Fowler 1985). The smectic phase is easily recognized by the bright iridescence it exhibits when it is illuminated by white light as shown in Fig. 1.15. Due to the large contour length of *fd* it is also possible to directly observe the smectic density modulation using video enhanced optical microscopy (Fig. 1.15a). When 488 nm light is used to scatter light from a smectic phase it is possible to observe up to 5 Bragg peaks. From the relative intensity and the position of the peaks it is possible to deduce the detailed structure of the smectic phase (Dogic and Fraden 1997).

Computer simulations predict the concentration of the nematic to smectic phase transition is roughly a volume fraction of 0.5. Furthermore, it is found that the location

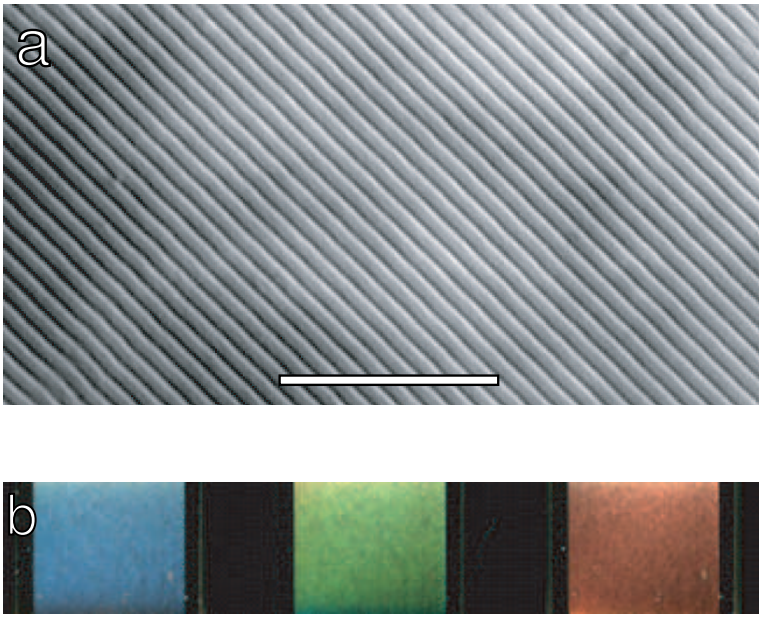

Figure 1.15: a) A DIC image of *fd* virus with varying contour length. The high contrast lines are smectic gaps. Light scattering indicates that the smectic spacing is 920 nm while the half width of the gap is 90 nm. Scale bar is 10 μm. b) Light scattering of a white light from a uniformly aligned one dimensional density modulations of the smectic phase of *fd*. By changing the angle of the incident light, the Bragg condition $d = \lambda \sin\theta/2n$ changes and the sample appears with different colors.

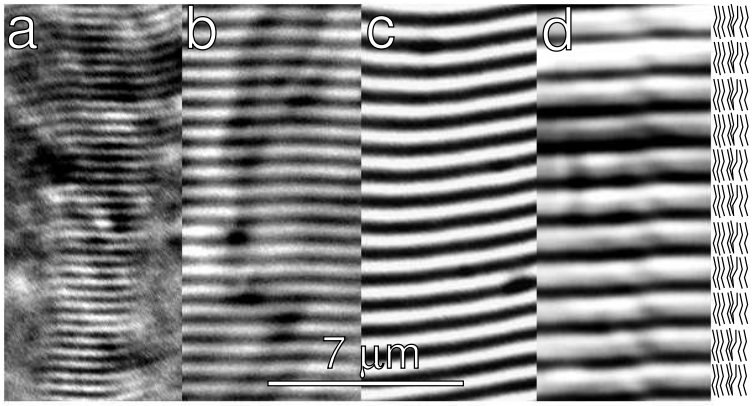

Figure 1.16: Images of the smectic phase of four different mutants of *fd* virus. The contour length varies from 0.4 μm to 1.2 μm. The mutant viruses are prepared according to standard methods of molecular cloning as described in Sec. 1.3.1. (After ref. (Dogic and Fraden 2001))

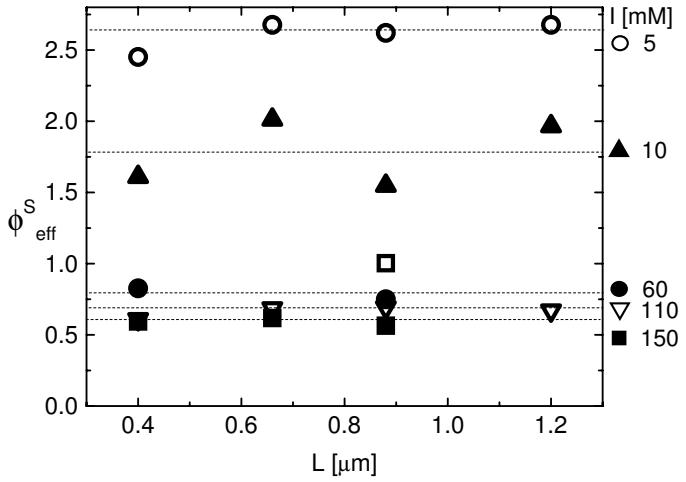

Figure 1.17: Effective volume fraction of the nematic-smectic phase transition for multiple ionic strengths and contour lengths. The data is taken at pH 8.2. The actual volume fraction of the rods ϕ^s is rescaled using the effective diameter with the following relationship $\phi^s_{\text{eff}} = \phi^s(D^2_{\text{eff}}/D^2)$, where D is the hard core diameter. (After ref. (Purdy and Fraden 2004a))

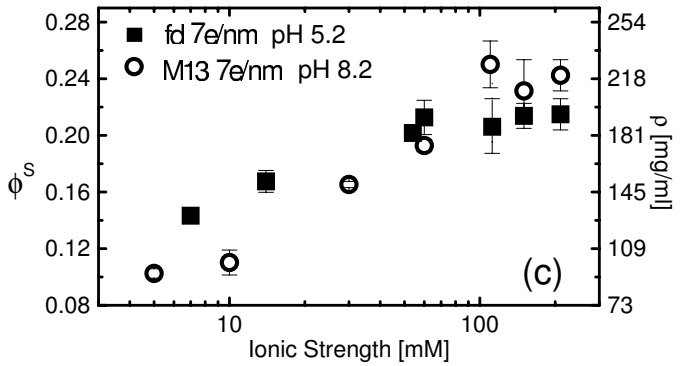

Figure 1.18: The ionic strength dependence of the nematic-smectic phase transition for a suspension of *fd* and M13. The pH of the suspension is adjusted so that the line charge density is $7^-/nm$ for both rods. (After ref. (Purdy and Fraden 2004a))

of this phase transition is independent of the rod aspect ratio (Bolhuis and Frenkel 1997). The initial studies done over a limited ionic strength indicated that the location of the nematic-smectic phase transition scales with D^2_{eff} (Dogic and Fraden 1997). As discussed in Sec. 1.3.2 the concept of D_{eff} quantitatively describes the isotropic-nematic phase transition at high ionic strength. Recently the nature of the Ch-S phase transition in *fd* has been characterized in more detail (Purdy and Fraden 2004a). This new study leads to the conclusion that the electrostatics of highly concentrated charged

rods cannot be accounted for with a simple concept such as D_{eff}.

Figure 1.17 shows the ionic strength and contour length dependence of the cholesteric-smectic phase transition. The data clearly shows that varying the contour length of the rods has no effect on the location of the nematic-smectic phase transition. This is in agreement with theoretical and simulation predictions (Tkachenko 1996; Bolhuis and Frenkel 1997). However, the data below 60 mM ionic strength does not scale with D_{eff}^2. Additionally, the effective volume fraction of the nematic-smectic phase transition at low ionic strength is much higher then the close packing of rods ($\phi = 0.92$) which leads to conclusion that D_{eff} overestimates electrostatic interactions.

The location of the nematic-smectic phase transition for suspensions of bacteriophages *fd* and M13 is shown in Fig. 1.18. The main difference between these two bacteriophages is the point mutation in the coat protein which converts a negatively charged amino acid for case of *fd* to a neutral one for the case of M13. This results in *fd* having higher charge than M13 by 30% for same conditions. The pH of the solution in Fig. 1.18 was adjusted so that that surface charge of *fd* and M13 suspension is equivalent. With increasing ionic strength the volume fraction ϕ^s of the nematic-smectic phase transition increases until it saturates at ionic strengths higher than 100 mM. There are two surprising conclusions that follow from experiments described in Fig. 1.18. First, the concentration of the nematic-smectic phase transition saturates at ionic strengths higher then 100 mM. This leads to the conclusion that in the limit were the Debye screening length becomes much smaller then the rod diameter, the phase behavior of charged rods approaches that of hard rods. Surprisingly the nematic-smectic phase transition saturates at 0.24 volume fraction which is much lower then theoretical prediction of 0.75 for semi-flexible rods (Tkachenko 1996; van der Schoot 1996; Polson 1997). Second, although the linear charge density for *fd* and M13 are equal the concentration of the N-S phase transition in the limit of high ionic strength is not the same. This indicates that the electrostatic continuum model fails and that it is necessary to take into account the molecular arrangements of the charges on the virus.

Another colloidal system where the N-S phase transition has been carefully characterized is the suspension of rigid TMV rods (Wen et al. 1989). There are significant differences when the N-S phase transition in TMV is compared to the Ch-S of *fd*. The ratio of layer spacing to rod contour length is 1.3 for the case of TMV as compared to 1.03 for the case of semi-flexible *fd*. Significant pre-transitional smectic fluctuations are also observed in TMV suspensions while no nematic-smectic pre-transitional fluctuations are observed in the case of semi-flexible *fd*. For more detailed comparison of the nematic-smectic transition between these two systems the readers is referred to the following reference (Dogic and Fraden 1997). We also note that in partially dried samples of *fd* a smectic-C phase is observed (Welsh et al. 1996; Lee et al. 2003).

We conclude the section on the phase behavior of hard rods by noting that the isotropic and nematic phase of *fd* suspension is well understood in the limit of high ionic strength. In this limit the rod charge can be quantitatively taken into account via the effective diameter. As the rod concentration increases to the smectic phase or the ionic strength decreases, the behavior of *fd* suspensions cannot be described by current theories. The experimental data indicates that there is a need to incorporate

the electrostatic interaction at a more fundamental level in these cases. This remains an area where further theoretical and experimental work is needed.

1.4 Bulk phase behavior of rod-sphere and rod-polymer mixtures

With the basic understanding of the phase behavior of a pure suspension of hard rods and hard spheres established, recent experiments have shifted toward exploring the phase behavior of more complex mixtures. As an introduction we first briefly summarize the behavior of samples where hard spheres are mixed with depleting agents that are in an isotropic phase. These can be either a suspension of polymers, or small diameter hard spheres or an isotropic solution of rod-like molecules. After summarizing the behavior of these mixtures, we turn our attention to less explored systems where it is necessary to take into account orientational and/or positional ordering of rods.

In the rest of this article we review the phase behavior of mixtures of rods with spherical polymers such as Dextran, poly(N-isopropyl-acrylamide) (NIPA) and poly(ethylene oxide) PEO and the behavior of rods with hard spheres such as charge stabilized polystyrene (PS) colloids. Much of the phenomena described is general to both rod/hard sphere mixtures and rod/polymer mixtures while there are also important differences between these two cases. In general, we use "rod/sphere" mixture to refer to a generic mixture of rods with either hard spheres or polymers while "rod/hard sphere" or "rod/polymer" refers to that specific mixture.

1.4.1 Depletion interaction between hard spheres

An important concept for understanding colloid/polymer mixtures is the depletion potential introduced by Asakura and Oosawa (AO) in the late 1950's (Asakura and Oosawa 1958). A few decades later the depletion interaction was rediscovered by Vrij (Vrij 1976). In the non-additive AO model spherical colloids with diameter D_{sp} interact with each other via the hard core excluded volume interaction, polymers behave as an ideal gas with no interaction while colloids interact with polymer through the excluded volume interaction. Consequently, there is a volume shell equval to the polymer's radius of gyration R_g, around each colloid from which the center of mass of a polymer is excluded as illustrated in Fig. 1.19. As two colloids approach each other there is an overlap of the excluded volume shells. The exclusion of the polymer between the colloid leads to an imbalance of the osmotic pressure, which in turns leads to an effective attractive force. The depletion force is proportional to $V_{\rm excl}\Pi_{\rm polymer}$ where $V_{\rm excl}$ is the excluded volume and $\Pi_{\rm polymer}$ is the osmotic pressure of the polymer solution. The range of the depletion attraction is proportional to the polymer radius of gyration (R_g) while the strength of the attraction is proportional to the polymer concentration.

An alternative explanation of the AO depletion can be gained by considering the total entropy of the sphere/polymer mixture. Bringing together two large colloids decreases the entropy of mixing of the system. However, the reduction of excluded

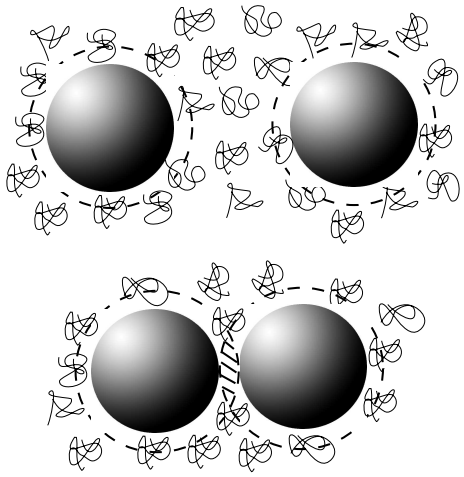

Figure 1.19: A schematic illustration of the depletion attraction in the sphere/polymer mixture. Around each colloid of diameter D_{sp} there is a shell which is inaccessible to the center of mass of a polymer. As the two colloids approach each other there is an overlap of the excluded volume shells which leads to the effective attractive potential.

volumes around large colloids results in the increase of the accessible volume to the more numerous smaller polymers, which in turn leads to an increase in the polymer component of the total entropy of the system. Since the entropy gain of the dispersed polymer is larger then the entropy loss of the clustered colloids the net result is an effective attractive potential with entropic origin. Therefore the depletion interaction is often paradoxically describedas "attraction through repulsion".

The depletion interaction is a very general phenomena that is always relevant to the phase behavior of mixtures. However, the quantitative AO theory breaks down for a number of experimentally relevant parameters. First, with increasing polymer size it is easy for the polymer and the colloid to interpenetrate each other, which leads to a significant decrease in both the range and the strength of the depletion potential (Tuinier et al. 2000). Second, the AO model assumes that the polymer behaves as an ideal gas. While it is experimentally possible to achieve this condition by changing the solvent quality, frequently it is necessary to take into account the excluded volume interaction between polymers (Hanke et al. 1999; Tuinier et al. 2003). The extreme limit of this case are two large colloids immersed in a suspension of colloids with much smaller size (Mao et al. 1995). At a low density of small colloids the interaction potential between large colloids can be approximated using the AO interaction. However, with increasing concentration of small colloids the effective intermolecular potential between large colloids deviates significantly from the AO potential and exhibits significant oscillatory behavior that is a consequence of the liquid-like structure of small colloids. The oscillatory nature of the depletion potential in a binary mixture of hard colloids was measured using a scanning laser tweezer (Crocker et al. 1999). Third, the AO depletion is quantitatively valid when the polymer is in the dilute regime. In the

semi-dilute region, the relevant length scale is determined by the polymer correlation range. Since this length scale is smaller then R_g, the range of the depletion attraction decreases with a crossover from a dilute to semi-dilute regime. Such depletion attraction was directly measured with optical tweezers using 1 μm silica spheres immersed in a DNA solution which acts as a depleting agent (Verma et al. 2000). These experiments illustrate that with a cross-over from the dilute to semi-dilute regime the range of the depletion attraction rapidly decreases.

It is possible to induce a depletion attraction with other colloidal solutions besides polymers or spheres. For example, the depletion caused by the dilute isotropic suspension of rods has been studied in detail both theoretically and experimentally. The depletion interaction between flat plates immersed in a solution of rods has been calculated and using the Derjaguin approximation the result was generalized to the interaction of spherical colloids(Mao et al. 1997). This depletion interaction was consequently obtained using the exact solution to first order in rod concentration by Marques and coworkers (Yaman et al. 1998). The exact calculation indicates that the Derjaguin approximation works well when the length of the rods is much smaller then the diameter of the spheres, but significantly overestimates the depletion potential when the rod length approaches the sphere diameter.

The depletion force between two spheres induced by the presence of a semi-dilute suspension of 0.9 μm long *fd* rods has recently been measured using a line tweezer (Lin et al. 2001). At short distances there is a significant enhancement of the depletion interaction when compared to the "exact" theory developed for spheres immersed in a solution of rigid rods (Yaman et al. 1998). This is probably due to additional depletion associated with the bending degree of freedom of semi-flexible rods (Lau et al. 2003). Interestingly, by fitting the experimental data to their model the authors were able extract the persistence length of *fd* from their data. This turns out to be 1.1 μm which significantly differs from previous measurements (Song et al. 1991). The systematic experimental study of how the depletion strength varies as a function of the ratio of sphere diameter D_{sp} to rod length (L) is so far lacking.

1.4.2 Phase diagrams of hard spheres and polymers or isotropic hard rods

Once the depletion potential between two isolated spherical colloids has been "engineered" by choosing appropriate polymer size and concentration it is of fundamental interest to understand how does the chosen potential affect the phase behavior of spherical colloids. Theory, computer simulation and experiments have shown that the parameter which most critically affects the phase behavior is the range of attractive interaction (Gast and Russel 1983; Gast et al. 1983; Gast et al. 1986; Lekkerkerker et al. 1992; Hagen and Frenkel 1994). For potentials with very short range attraction there is a direct equilibrium phase transition from a dilute colloidal gas (G) to a concentrated colloidal crystal (C). There is an additional transition from the dilute colloidal gas to a dense disordered colloidal liquid (L) as illustrated in Fig. 1.20a. However, this transition is metastable with respect to the equilibrium gas-solid phase transition. Only when the range of attraction increases is a stable gas-liquid phase

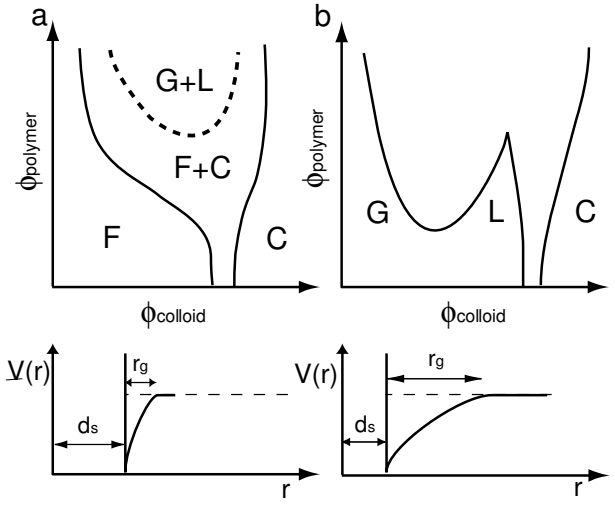

Figure 1.20: The phase diagram of a colloid/polymer mixture is found to critically depend on the range of attraction, which in turn is determined by the polymer size F:Fluid, L: Liquid, G: Gas and C: crystal. a) For short range attraction only an equilibrium gas-solid phase transition is observed. We note that a gas-liquid phase transition is present but is metastable with the respect to the equilibrium gas-solid phase transition. b) For colloids with long range attraction both gas-liquid, liquid-solid and direct gas-solid phase transitions are observed. The topology of this phase diagram closely resembles that of molecular liquids interacting with a van der Waals potential.

transition observed with associated critical and triple points. Experimentally it is found that glassy states and/or gels often preempt the occurrence of the equilibrium phase transitions. The non-equilibrium nature of these states is poorly understood and is currently under intense study(Anderson and Lekkerkerker 2002). We note that for spheres with very short ranged attractive potentials simulations predict the existence of a first order phase transition between two solids with different densities (Bolhuis and Frenkel 1994a). So far this transition has not been observed in experiments.

The initial studies of Gast and Russel of the sphere/polymer mixture used thermodynamic perturbation theory to obtain the theoretical phase diagrams. Such theories treat the sphere/polymer mixture as a single component system of spheres which have hard core repulsive interactions to which the effect of attraction is considered as a perturbation. The underlying assumption is that depletion attraction is pairwise additive and that in a sample where two phases coexist the polymer concentration is the same in both phases. Non-additivity for sphere/polymer mixtures was treated via computer simulations and it was found that the depletion attraction is pairwise additive only if the ratio $R_{\rm g}/D_{\rm sp}$ is sufficiently small (Meijer and Frenkel 1991; Meijer and Frenkel 1994). A more complete theory that takes into account the possibility of partitioning of the polymer across the phase boundary and accounts for the non-additive nature of the colloid/polymer mixture was subsequently developed by Lekkerkerker

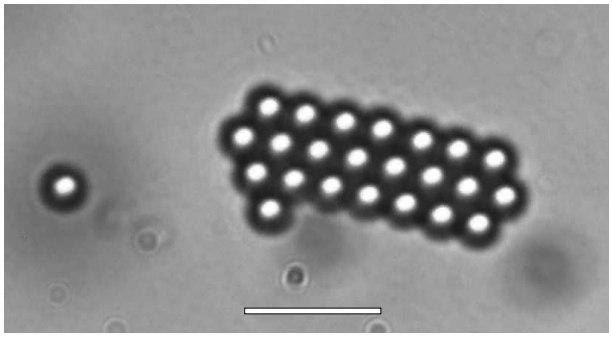

Figure 1.21: A crystalline cluster of polystyrene spheres $D_{sp} = 2\mu m$grows on the walls when *fd* rods are added. The concentration of *fd* rods is roughly 2 mg/ml. Fluctuations of the crystalline cluster are clearly visible under the microscope. Scale bar indicates 10 μm.

and coworkers (Lekkerkerker et al. 1992).

Studies of colloid/polymer mixtures show that the topology of the phase diagram depends critically on the range of attraction. This result is very general and is expected to hold for molecular liquids as well as for colloidal systems. The advantage of colloids is that the shape, range and depth of the intermolecular potential can be adjusted and experimentally measured. This makes colloids an ideal system to test the statistical mechanical theories that predict the relationship between the macroscopic phase behavior of fluids and the microscopic intermolecular potential.

The phase behavior of a binary mixture of hard spheres is very different from that of the the hard-sphere polymer mixture. On the theoretical side initial work by Lebowitz and Rowlinson showed that, within the Percus-Yevick approximation, mixtures of hard spheres are miscible for all aspect ratio and concentrations (Lebowitz and Rowlison 1964). For a long time this was considered to be the general case. Only recently, a more accurate liquid-state theory indicated that the binary mixture of spheres becomes unstable and demixes at high enough asymmetry (Biben and Hansen 1991). On the experimental side, the liquid-liquid demixing has not been observed. It seems that this transition is preempted by the liquid-crystal phase transition where the solid composed of large spheres coexists with a liquid rich in spheres with smaller diameter (Dinsmore et al. 1995; Imhof and Dhont 1995). In this way the phase behavior of binary hard spheres is reminiscent of the sphere/polymer mixture with large asymmetry (Fig. 1.20a). At even higher volume fraction it is possible to obtain well ordered binary alloys with complex crystalline structure (Bartlett et al. 1992).

As was discussed in previous section, isotropic rods are very effective depletion agents especially when the length of the rod (L) is significantly smaller then the diameter of the hard sphere D_{sp}. However, there are only limited studies about the phase behavior of a mixture of isotropic rods and colloidal spheres. In the initial work by Pecora and coworkers no demixing phase transition was observed in a mixture of rod-like poly-benzyl-glutamate (PBLG) and polystyrene spheres (Tracy et al. 1993). Early simulations predicted the phase diagram reminiscent of those found in spheres with

short range attractions (Fig. 1.20a) when the ratio D_{sp}/L is smaller then 0.3 (Bolhuis and Frenkel 1994b). For larger ratios both gas to liquid and liquid to crystal phase transitions are stable (Fig. 1.20b). These predictions have also been confirmed in theoretical work (Vliegenthart and Lekkerkerker 1999). Subsequently, the phase separation between crystals of silica spheres and an isotropic solution of boehmite (γ-AlOOH) rods coated with silica was observed (Koenderink et al. 1999). In these experiments the ratio $D_{\rm sp}$/L was kept constant at 0.3, exactly the parameter at which the gas-liquid phase transition becomes stable with the respect to the gas-crystal phase transition. Interestingly, no gas-liquid phase coexistence was reported. In these studies the authors observe formation of crystals via a two step pathway (Vliegenthart et al. 1999). In a first step the mixture forms a liquid-like aggregate that subsequently crystalizes. This point is discussed in greater detail in section 1.9 on the kinetics of phase transitions. With increasing concentration of the rods, the suspension becomes highly viscous and the sample takes too long to equilibrate. In this case it is difficult to determine the final equilibrium phase.

We have also observed demixing in a mixture of 0.9 μm long *fd* viruses and large polystyrene spheres (Fig. 1.21). It is interesting that when rods at a fixed concentration (2 mg/ml) are mixed with small polystyrene spheresw ($D_{\rm sp}$ = 1 μm) no phase separation is observed. As the sphere size is increased ($D_{\rm sp}$ = 1.5 μm) surface crystallization is observed, but not crystallization in the bulk. This is not surprising since the overlap of excluded volume between a flat wall and a sphere is twice as large as that between two spheres. Surface crystallization has previously been observed for a binary mixture of hard sphere (Dinsmore et al. 1997). For spheres with $D_{\rm sp}$ = 2 μm we observe phase separation in the bulk, but the heavy particles quickly sediment to the bottom wall and spread out on the surface. The quantitative phase diagram for the mixture of spheres and isotropic rods as a function of rod and sphere concentration and $D_{\rm sp}/L$ ratio is difficult to determine due to turbidity and sedimentation of the large spheres. A theoretical calculation explains why the phase separation in a sphere/rod mixture is so sensitive to the ratio of sphere diameter to rod length (Yaman et al. 1998) . As the rod length approaches the sphere diameter the strength of the depletion potential significantly decreases.

So far we have discussed the phase behavior of a mixture of spheres with depletants such as isotropic rods or polymer solutions. In the rest of the paper we focus on a number of surprising phenomena that are observed in rod/polymer or rod/sphere mixtures at higher rod concentration. In this case it is necessary to take into account either the orientational or positional ordering of rods, or sometimes both.

1.5 Influence of non-adsorbing polymer on the isotropic-nematic phase transition

The Onsager theory describes the entropy driven isotropic-nematic phase transition in a suspension of rods that have purely repulsive hard core interactions (Onsager 1949; Vroege and Lekkerkerker 1992). As a next step it is important to examine

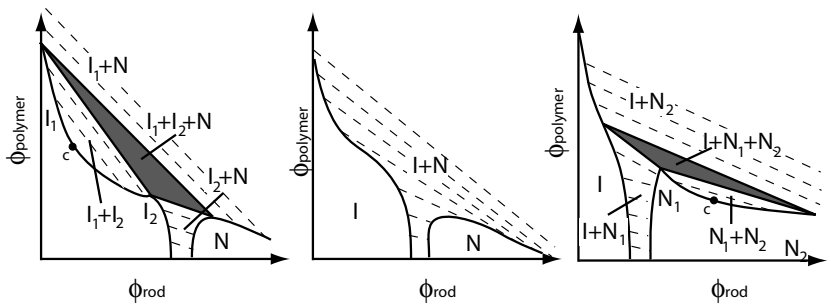

Figure 1.22: The three possible phase diagrams of a rod-polymer mixture as predicted by Lekkerkerker and Strobants. For long range attraction, in addition to I-N phase transition a stable isotropic-isotropic phase transition is predicted. Dashed lines are tie-lines between coexisting phases. For very short range attraction the isotropic-isotropic coexistence disappears but a nematic-nematic phase appears. With both isotropic-isotropic and nematic-nematic coexistence there is a triple point and an associated critical point. Because of the binary nature of the mixture the triple point spans an entire solid triangle in the phase diagram.

how the presence of attractive interactions alters the nature of the I-N phase transitions. For low molecular weight liquid crystals this issue has been reviewed extensively elsewhere (Gelbart and Barboy 1980). Experimentally, one feasible way to introduce attractions into hard-rods is by adding non-adsorbing polymer. In a similar way that the presence of polymers dramatically alters the phase behavior of hard spheres it is reasonable to expect a significant influence of polymer on the phase behavior of hard rods. In this section we focus on the bulk I-N phase transition in rod-polymer mixtures while in subsequent sections we consider the possibility of positionally ordered smectic phases. While it is tempting to connect the phase behavior of rod/polymer mixtures to that of a solution of rods with direct attractive interactions there are also some important differences between these two systems. Most importantly, the depletion interaction in the rod/polymer mixture is an effective potential. Therefore the strength of the interaction depends on the local concentration of polymer which can vary considerably in the sample especially if there are coexisting phases within the same sample.

In general, liquid state theories that describe the behavior of rod-like particles are not as developed as theories for spherical particles. While the Onsager theory accurately describes the reference state of hard rod fluids, introducing attractive interactions into such a theory is not as straightforward as for the case of hard spheres. The Onsager theory is based on a density expansion and it is therefore valid only for solutions of rods at low densities that have a fair degree of orientational disorder. Rods with depletion-like attractive interactions attain the minimum of their intermolecular potential when they are parallel to each other and their centers of mass are at a minimum separation (Fig.1.23). These are exactly configurations that need to be avoided for the Onsager theory to converge at the level of the second virial coefficient (van der Schoot and Odijk 1992). To overcome this difficulty Lekkerkerker and Strobants have

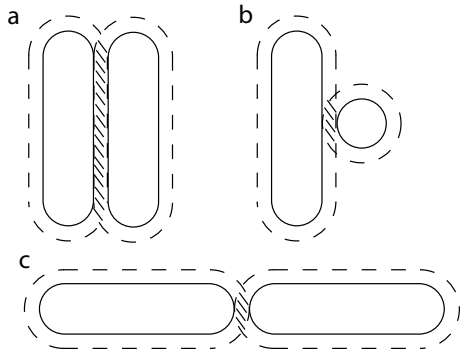

Figure 1.23: The attractive interaction induced by adding polymer to a suspension of rod-like colloids. The strength of attraction is proportional to the overlap of the excluded volume and it is strongest when the rods lie parallel to each other as illustrated in case (a) as opposed to rods lying perpendicular to each other as is shown in case (b) or end-to-end as in case (c).

calculated the phase diagram of rod/polymer mixtures using the scaled particle free energy expression of hard rods, which approximately takes into account higher virial coefficients and reduces to the Onsager theory in the appropriate limit (Lekkerkerker and Stroobants 1994; Bolhuis et al. 1997). Such an expression reproduces remarkably well the isotropic-nematic phase transitions for hard rods with finite size when compared to results of computer simulations (Kramer and Herzfeld 1998).

The topology of the phase diagrams obtained using the Scaled Particle Theory (SPT) has a striking similarity to the previously described phase diagrams of the hard sphere/polymer mixture in Section 1.4.2. For rods with long range attractions an isotropic-isotropic ($I_1 - I_2$) phase transition is observed. As a consequence there is a critical point associated with isotropic-isotropic demixing and a triple point in which two isotropic phases coexist with a nematic phase. Since the system contains two components, the triple point spans an entire triangle in the phase diagram when plotted in the rod polymer density-density plane. For a very short range attraction the system exhibits nematic-nematic phase transitions. A simpler calculation that directly extends the second virial Onsager free energy to include attractive interactions only predicts the widening of the isotropic-nematic coexistence and fails to predict either isotropic-isotropic or nematic-nematic coexistence (Warren 1994). In addition, Warren's theory abruptly breaks down and predicts coexistence between an infinitely dense nematic phase and dilute isotropic rods as soon as the second virial coefficient becomes negative. Because of this, Warren argues that the second virial theory extended to rod/polymers mixture is only valid for very weak attractions, but it is not clear at which point this approximation breaks down.

There have been a few experiments that have studied the phase diagram of rod/sphere mixtures, most notably in the cellulose/Dextran and bhoemite/polystyrene mixtures (Edgar and Gray 2002; Buitenhuis et al. 1995). In the latter work the authors observe a triple point in which two isotropic phases coexists with a nematic phase. In addition to these

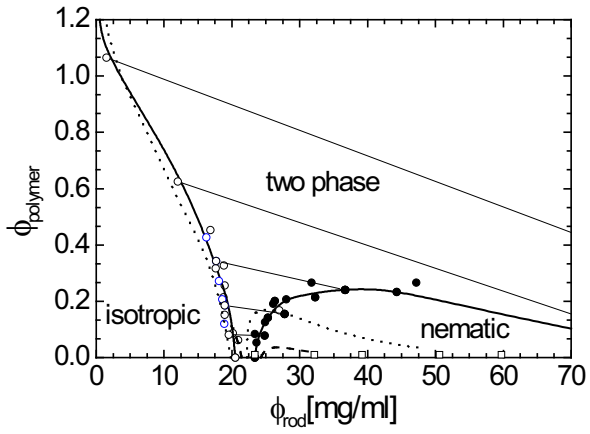

Figure 1.24: Phase diagram of an *fd* virus and Dextran, R_g=176 Åat 100 mM ionic strength. The measured points indicate the rod and polymer concentrations of the coexisting isotropic and cholesteric phases. The full line indicates the phase boundary between the two-phase isotropic-cholesteric phase coexistence and stable single phase isotropic and cholesteric phase. Tie lines are indicated by thin full lines. (After ref. (Dogic et al. 2004a))

equilibrium phases, non-equilibrium gel-like phases are also reported at fairly low rod concentration. In the former work on the cellulose/Dextran mixture, only biphasic isotopic-nematic coexistence is observed, which widens with increasing polymer concentration.

Motivated by good agreement between the Onsager theory and experimental data for the I-Ch coexistence of filamentous *fd* rods, we have recently measured the I-Ch phase transition in the presence of non-adsorbing polymer. Using fluorescein labelled Dextran it is possible to obtain macroscopically phase separated samples, measure the full phase diagram and determine the tie lines between coexisting isotropic and cholesteric phases(Dogic and Fraden 2001; Dogic et al. 2004a). An example of the typical phase diagram measured is shown in Fig. 1.24. In agreement with previous studies it is found that adding polymer widens the coexistence between the isotropic and cholesteric phase. Using the *fd*/Dextran mixture it is also possible to observe preferential partitioning of the polymer into isotropic phase, in qualitative agreement with the theoretical predictions. Unfortunately, with this system we are not able to access the parameters for which I_1-I_2-N and I-N_1-N_2 phase coexistence is predicted in work by Lekkerkerker and Stroobants.

There are a number of reasons which make quantitative comparison between the SPT theory and experiments difficult (Dogic et al. 2004a). First, the theoretical work is valid for rods that interact through hard core repulsive interaction while the *fd* viruses used in the experiments are charged stabilized. Because of the small diameter of *fd* it is not possible to add enough salt to reduce the double layer repulsive interaction to negligible levels and simultaneously preserve the colloidal stability of the system. Therefore repulsive double layer interactions have to be incorporated into the theory.

At the level of second virial coefficient it is possible to achieve this by replacing the hard core diameter D_{r} with a larger effective diameter D_{eff} which is dependent on the ionic strength as described in section 1.2.2. This procedure is rigorously valid only for rod concentrations low enough so that the Onsager second virial coefficient accurately describes the system. When comparing our data to theory we have used D_{eff} as a hard core diameter in the SPT theory although in principle this is an approximation that is not well controlled. We note that there was a recent attempt by Herzfeld and coworkers to incorporate charge into scaled particle theory (Kramer and Herzfeld 1999; Kramer and Herzfeld 2000).

Second, the SPT theory is valid for perfectly rigid rods while *fd* is a semi-flexible rod with persistence length of 2.2 μm. This flexibility is enough to significantly affect the nature of the isotropic-nematic phase transition as explained in section 1.2.3. The SPT theory has been modified to include flexibility in the same way that Khohhlov-Semenov extended Onsager theory to treat semi-flexible rods. The competition between attractive interaction and repulsive interaction can induce a bundling-unbundling transition (Kierfeld and Lipowsky 2003). Third, the R_g of the polymers used in our experiments was equal or even larger than the diameter of the rods. As mentioned in section 1.4.1 for these parameters the AO model of depletion attraction significantly overestimates both the range and the strength of the interaction. The reason for this is that the open polymer structure easily interpenetrates a slender rod. Since there is no analytical expression for depletion potential in such a case, when comparing our experimental results to the SPT theory we have used results obtained from simulation.

In spite of these caveats, in the limit of high ionic strength the agreement between experiments and theory is quite good as shown in Figure 1.24. It remains to see if this is fortuitus. However, as the ionic strength decreases the discrepancy between theory and experiment becomes significant. In conclusion, it is fair to say that an accurate liquid-state theory for rods which have attractive attraction is still lacking. In the section on the phase behavior of hard rods we argued that the measurement of the order parameter is a more stringent test of the validity of the Onsager theory when compared to the measurements of the I-N phase coexistence. In the same spirit we have attempted to measure the order parameter of the nematic phase at different polymer concentrations.

This is an important question when viewed in the context of the van der Waals theory of liquids, which for spherical particles states that the repulsive part of the intermolecular potential is mainly responsible for the liquid-like structure of fluids (Widom 1967). The attractive potential determines the density of the fluid by providing a cohesive energy that is largely independent of the exact configuration of the fluid. It remains to be seen if this van der Waals picture is also true for a liquid of attractive rods. If so, one would expect that the strength of the attraction only determines the density of the liquid of rods while its structure, as characterized by the order parameter, would depend only on the constituent rod concentration. The nematic samples of the *fd*/polymer mixtures turn out to be quite viscous and it is difficult to reproducibly obtain monodomain samples, which results in noisy measurements of the order parameter. Although noisy, our results indicate that the van der Waals picture also holds for the rod/polymer mixture. In other words, the nematic order parameter remains

independent of the polymer concentration in a rod-polymer mixture. For more details the reader is referred to the following paper (Dogic et al. 2004a).

It is of interest to consider if the phase diagram for rod/polymer mixtures is generic to other rod-like systems in which it is possible to induce attractive interactions. For example, another well studied and very effective agent for condensing charge stabilized rods are multivalent counterions. Most biopolymers such as *fd*, actin, DNA and microtubules are negatively charge-stabilized colloids under physiological pH conditions. Adding multivalent cations to such a solution induces the formation of tightly packed bundles (Tang et al. 1996; Tang et al. 1997; Bloomfield 1991). Bundle formation is usually observed at a very low concentration of rods and the effect of rod concentration has not been studied systematically. This corresponds to the upper left corner of the *fd*/Dextran phase diagram shown in Fig. 1.24. Interestingly, when we prepare a mixture of a polymer at very high concentration and *fd* we observe the formation of the bundles that look remarkably similar to the bundles observed in the mixture of *fd* and multivalent counterions.

Recently a study of a mixture of 50 nm long DNA fragments and trivalent or tetravalent spermidine and spermine condensing agent was published (Pelta et al. 1996; Sikorav et al. 1994). As opposed to other studies, the authors here use a finite concentration of DNA fragments and observe a formation of nematic(cholesteric) phase instead of bundles. In another recent study of actin filaments mixed with multivalent salts the authors report the formation of a new phase in which actin is condensed into two-dimensional rafts, which subsequently stack on top of each other at 90 degrees (Wong et al. 2003; Borukhow and Bruinsma 2001; Lee et al. 2004). Such a phase would have no analogy in rod/polymer mixtures. Clearly rod/counterion mixtures still remain poorly understood. In our view it would be of interest to compare such systems to the phase behavior of rod/polymer mixtures.

In this section we have only considered the influence of polymer on the bulk isotropic-nematic phase transition. When these studies are extended to account for the formation of the positionally ordered smectic phase a whole range of new and unexpected phenomena are observed. These will be reviewed in the next few sections.

1.6 Entropically driven microphase separation in rod/sphere mixtures

The influence of polymers on the entropy driven isotropic-nematic phase transition is qualitatively understood with a mixture being either in a single uniformly mixed phase or a macroscopically demixed phase. However it recently became apparent that there is a third possibility of a microphase separated state for a wide range of polymer and/or hard sphere sizes or concentrations. In microphase separation the system begins to phase separate into regions that are either rich in rod or sphere component. Unlike bulk demixing, the phase separating regions grow until they reach a critical size at which point they organize into a well ordered three dimensional structure. The full complexity of the phase diagram of the *fd*/polystyrene spheres (PS) mixture for one

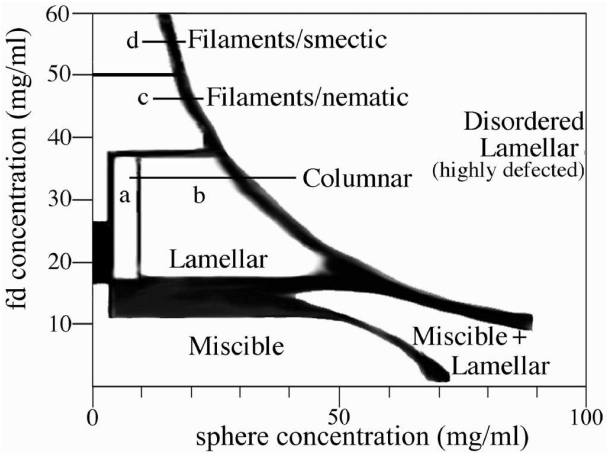

Figure 1.25: Phase diagram of a mixture of *fd* virus and polystyrene spheres ($D_{\rm sp}$=100nm) in 10 mM tris buffer. Suspension of pure *fd* forms isotropic, cholesteric(nematic) and smectic phases with increasing concentration as described in Sec. 1.3. Increasing the volume fraction of spheres induces the formation of a number of microphase separated states most notably lamellar and columnar phases. Images of these structures are shown in Fig. 1.28. The isotropic-cholesteric phase transition for pure rods is at 18 mg/ml while nematic-smectic phase transition is at 50 mg/ml. Filaments are layered structure discussed in more details in Sec. 1.9.3. (After ref. (Adams et al. 1998))

spheres size is shown in Fig. 1.25. Other phases are observed for different sized spheres.

Usually microphase separated states are found in amphiphilic molecules such as block copoloymers, lipids or surfactants (W. M. Gelbart and Roux 1994). The microphase separated state formed in rod/polymer mixtures is different in two fundamental aspects from the microphase separated states formed by amphiphilic macromolecules. First, all amphiphilic molecules and block copolymers are characterized by a covalent bond between mutually immiscible blocks. Microphase separated structures have enrmous surface area and the resulting surface energy is very high. Consequently, in the absence of the bond between immiscible blocks it is commonly assumed that such materials would bulk phase separate into two immiscible macroscopic phases. In a *fd*/polystyrene mixture the covalent bond between the immiscible components is absent, and the mixture is free to macroscopically phase separate. Therefore it is surprising that under certain conditions such a mixture forms a stable microphase separated state instead of macroscopically phase separated sample. A microphase state in a mixture implies that the surface tension between the components of the mixture is very small. In amphiphilic and copolymeric systems the phase separation is largely driven by enthalpic contributions to the free energy. In rod/sphere mixtures the interaction that dominates the phase behavior of the system are hard core excluded volume interactions. All transitions in such a system are driven by a purely entropic contribution to the free energy and it follows that the microphase separation is a state with highest entropy, not lowest energy.

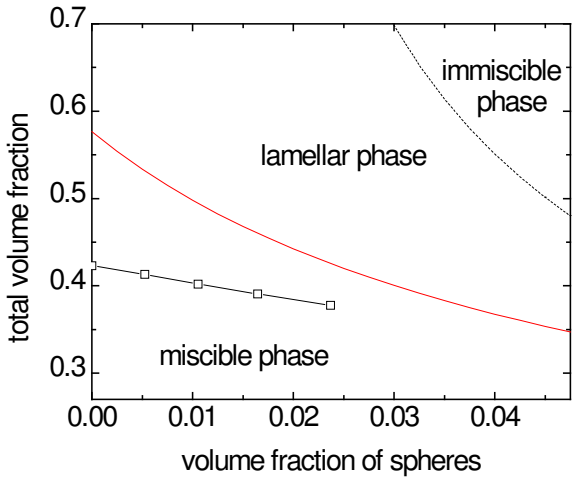

Figure 1.26: Stability boundaries for a rod-sphere mixture calculated using the theory described in Sec. 1.2.6. For this particular phase diagram the rod aspect ratio was $L/D_{\rm sc}$=20 and the diameter of spheres are equal to the diameter of rods $D_{\rm sc}/D_{\rm sp}$=1. The full line indicates the theoretical prediction for the points in the phase diagram at which the system becomes unstable towards lamellar fluctuations. The dashed line indicates the instability towards the complete demixing into two macroscopically phases. Squares indicate the nematic-lamellar phase transition obtained from Monte Carlo simulation. (After ref. (Dogic et al. 2000))

1.6.1 Lamellar phase in rod/polymer and rod/sphere mixture

In this section we review the theoretical and experimental studies of the lamellar phase, which is the simplest microphase separated state. The lamellar phase is characterized by one-dimensional long ranged order in which liquid-like layers of rods are intercalated with layers of spheres. The existence of the lamellar phase was first predicted using a density functional theory where the excluded volume interactions are treated at the level of the second virial coefficient (Koda et al. 1996). Because of the highly approximate nature of the second virial approximation the formation of the intercalated lamellar phase was also verified using Monte Carlo simulations in the same work. Both the theoretical model and the computer simulations made a number of simplifying assumptions; most importantly that the rods are perfectly aligned and that the diameter of the rods and spheres are equal. Therefore in this model the rods do not exhibit an isotropic-nematic phase transition. The same model of a mixture of spheres and perfectly aligned spherocylinders was later generalized to include sphere of arbitrary size (Dogic et al. 2000).

The theoretical prediction for the stability diagram of a typical rod/sphere mixture is shown in Fig. 1.26. The theory predicts the stable entropy driven formation of a lamellar phase when a low volume fraction of spheres is added to a nematic phase of perfectly aligned rods. At a high concentration of both rods and spheres the model predicts complete bulk phase separation, while at low sphere/rod concentrations the

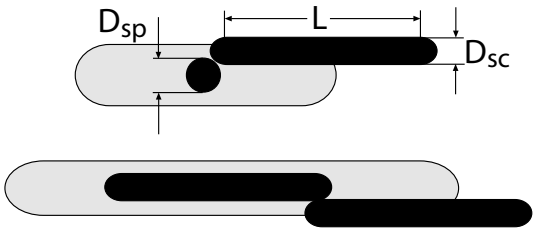

Figure 1.27: Volume excluded to the center of mass of a spherocylinder due to the presence of another sphere or spherocylinder is indicated by light shaded region. The large excluded volume between spherocylinder and a sphere is the reason for the enhanced formation of the lamellar phase. (After ref. (Dogic et al. 2000))

mixture is miscible. More importantly, it is found that the rod/sphere mixture forms the layered lamellar phase at a lower volume fraction when compared to the formation of layered smectic phase in suspension of pure hard rods. Therefore the spheres do not only passively partition into the smectic gaps, but actively shift the boundaries of the nematic-lamellar phase transition and significantly stabilize the lamellar phase. Recent simulations have considered rod/sphere mixtures in which the rods have full orientational degrees of freedom(Lago et al. 2004). The existence of a stable lamellar phase was confirmed in this more realistic model. It was also found that the spheres actively stabilize the lamellar phase with respect to nematic phase in agreement with theory and simulations on mixture of spheres and perfectly aligned rods.

A simple intuitive picture for the formation and enhanced stability of the lamellar phase emerges from the consideration of the total excluded volume in a mixture. The entropy driven transition to an ordered structure is always driven by a decrease in the total excluded volume of the system. Therefore we would expect that the excluded volume of the lamellar phase is smaller then the excluded volume of the uniform rod/sphere mixture. It is useful to compare this quantity in two extreme cases of a spatially uniform mixture and a perfectly ordered one dimensional lamellar phase. Fig. 1.27 illustrates the volume that is excluded to the spherocylinder due to the presence of either another sphere or spherocylinder. For spherocylinders with large asymmetry the excluded volume of a sphere is about half that of another spherocylinder. In a mixture in which the concentration of spherocylinders is spatially uniform replacing a single spherocylinder with two sphere leaves the total excluded volume unchanged. However, this procedure significantly decreases the total volume fraction of the particles. Therefore in a rod/sphere mixture we have packing problems similar to those encountered in a suspension of pure spherocylinders, but at a lower total volume fraction. By forming a layered lamellar phase the mixture can significantly reduce the total excluded volume because the periodic one dimensional density order associated with lamellar order significantly reduces the probability of very unfavorable sphere-spherocylinder contacts. For quantitative details that emerge from the analysis of the second virial theory the reader is referred to the following reference (Dogic et al. 2000).

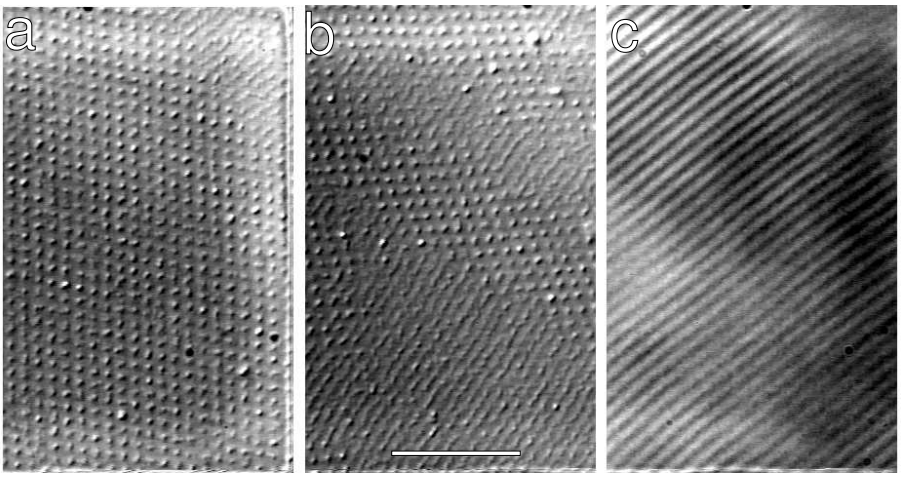

Figure 1.28: DIC images of microphase separated phases observed in a mixture of *fd* and polystyrene spheres ($D_{\rm sp}$=0.1 μm). The phase diagram of this particular mixture is shown in Fig. 1.25. a) At sphere concentrations below 1% a stable columnar phase is observed. (see Fig. 1.29) b) At intermediate concentrations the spaces between columns gradually fill in and the sample continuously transforms into the lamellar phase. c) At high sphere concentrations a single phase lamellar phase is formed with a layer spacing of 1.1 μm. Scale bar indicates 10 μm.

An alternative way to consider the enhanced stability of the lamellar phase in the rod/sphere mixture is to focus on the effect of spherocylinder ends. In section 1.2.5 we discussed the formation of the smectic phase as a consequence of unfavorable packing that occurs around the ends of rod-like molecules. Adding spherical particles to the nematic phase of rods increases the effective concentration of the "ends" without significantly changing the total volume of the solution. The only way that the system can accommodate these extra "ends" is to undergo a transition to an entropy stabilized microphase separated state.

Subsequent to the prediction by Koda and coworkers a layered lamellar phase was experimentally observed in a mixture of *fd* virus and polystyrene spheres (Koda et al. 1996; Adams et al. 1998). Under the experimental conditions, *fd* virus and polystyrene spheres approximate the behavior of hard rods and spheres, respectively. An optical micrograph of a typical lamellar phase is shown in Fig. 1.28c. The layer periodicity of the lamellar phase is 1.1 μm while that of a smectic phase of pure *fd* suspension is 0.9 μm. The evidence obtained from samples where the spheres are fluorescently labelled and from electron microscopy on freeze-fractured samples indicates that the structure of the lamellar phase is that of intercalated layers of spheres and rods. It is important to note that the experimental parameters were that the diameter of the sphere ($D_{\rm sp}$ = 0.1 μm) is roughly 10 times smaller than the rod length (L = 1 μm) and ten times larger than the rod diameter ($D_{\rm sc} \propto$ 10 nm). These parameters are very different from the parameters used in the simulation by Koda and coworkers.

The experimental results also show that spheres significantly stabilize the formation of the lamellar phase. As can be seen from the phase diagram shown in Fig. 1.25 the suspension of pure *fd* forms a layered smectic phase at 50 mg/ml. Adding spheres at a volume fraction of 2% induces the formation of the layered lamellar phase at 20 mg/ml. In addition to the above described case, the lamellar phase is consistently observed for a wide variety of polystyrene sphere sizes ranging from 0.02 μm to 0.2 μm. After filling the sample chamber we find that the layers will form within few minutes and over the next few days the defects slowly anneal and the overall order improves. We have had samples that have remained layered for a period of few years before drying up. This provides a strong indication that the lamellar phase is an equilibrium state and not a kinetically trapped structure.

Besides *fd*/PS mixtures the lamellar phase has also been observed in mixtures of *fd* virus and with a wide variety of polymers such as polyethylene oxide (PEO), Dextran and poly(N-isopropyl-acrylamide) (NIPA). This is perhaps not too surprising since in the second virial theory the effect of the sphere-sphere excluded volume has negligible effects on the overall topology of the phase diagram. It is the polymer-spherocylinder excluded volume that drives the phase transition. The effect of the polymer size has not been systematically studied so far.

The second virial theory also indicates that it should be possible to obtain a lamellar phase in a binary mixture of rods with sufficiently different contour length (Koda and Kimura 1994). Due to a paucity of well defined monodisperese hard rod systems the lamellar phase has to our knowledge been only observed in mixtures of *fd* and either colloidal spheres or polymer. We believe as better defined rod systems become available it will be shown that the lamellar phase is a generic structure found in all rod-sphere mixtures. We do note that the lamellar-like structure have been observed in a study of polydisperse TMV and the spherical protein Bovine Serum Albumin (BSA) (Adams and Fraden 1998).

While both lamellar and smectic phases have the same quasi one dimensional long range order, the main difference between these phases is the spacing of the layers. Theory predicts that the lamellar layer spacing will swell with increasing volume fraction of spheres (Koda et al. 1996; Dogic and Fraden 2001). Therefore it should be possible to go from the smectic to lamellar phase without ever crossing a phase boundary. However, it is also possible to envision a first order transition between coexisting smectic and lamellar phases. In such a sample there would be a coexistence between two layered phases with different layer spacing. On the experimental side both the continuous swelling of the smectic phase and the coexistence between a smectic phase with periodicity of 0.9 μm and a lamellar phase with 1.1 μm periodicity have been observed. These are described in greater detail in Sec. 1.9.3 and Sec. 1.9.4.

1.6.2 Columnar phase and chain-like structures in mixtures of *fd* and hard spheres

In addition to the lamellar phase, other more complex structures are observed in mixtures of *fd* rods and hard spheres. In particular, for mixture of *fd* and 0.1 μm PS spheres a columnar structure is observed. The phase diagram (Fig. 1.28) shows that

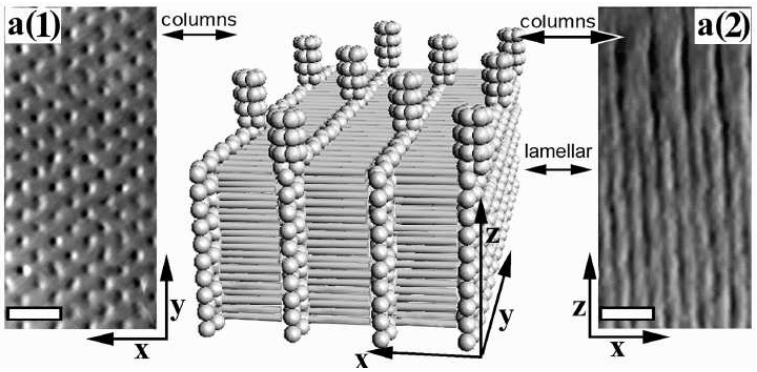

Figure 1.29: A three dimensional reconstruction using DIC optical microscopy of a sample in which the lamellar phase at the bottom is coexisting with the columnar phase at the top. The mixture is composed of 0.1 μm PS spheres and *fd* liquid crystals. Middle figure is a schematic illustration the arrangements of the rods and spheres in this particular sample. The rods in the top columnar phase are not drawn for clarity, but they form a nematic phase that fills the space between columns. (a1) Image of the XY cross-section of the top columnar phase. (a2) Image of the ZX cross section. The column spacing in the top columnar phase is twice the spacing of the bottom lamellar phase. Scale bars are 3 μm. (After ref. (Adams et al. 1998))

such a phase is formed when nematic rods are mixed with a low volume fraction of spheres. In a columnar phase 0.1 μm spheres coalesce together until they reach a critical diameter of 0.3 μm. Subsequently these clusters assemble into one-dimensional columnar structures which are oriented perpendicular to the nematic director. Furthermore these columns form a two dimensional lattice (Figs. 1.28a and 1.29) which can have varying lattice parameters. Unlike the lamellar phase, which occurs for both PS/*fd* and polymer/*fd* mixtures the columnar phase has so far only been observed in a PS/*fd* mixture.

With increasing sphere volume fraction the columnar phase will continuously transform into a lamellar phase as illustrated in Fig. 1.28b. A 3D reconstruction of such a coexisting sample is shown in Fig. 1.29. In addition to 0.1 μm spheres, columnar phases have also been observed for sphere sizes ranging from 0.06 to 0.12 μm in diameter. The theoretical understanding of the stability of the columnar phase is currently lacking. In particular, it is not known what determines the spacing of the spherical columns in the direction perpendicular to the nematic director. Furthermore, it seems that 0.3 μm is a "magical" size of the column because mixtures of rods with spheres of diameters ranging from 0.06 μm to 0.12 μm assemble into the columnar phase where individual columns always have the final diameter of 0.3 μm. Individual spheres are observed to diffuse between columns indicating that these are equilibrium and not kinetically trapped structure. The robustness of the diameter of the self-assembled columns suggest the examination of 0.3 μm spheres in a nematic background of *fd* rods.

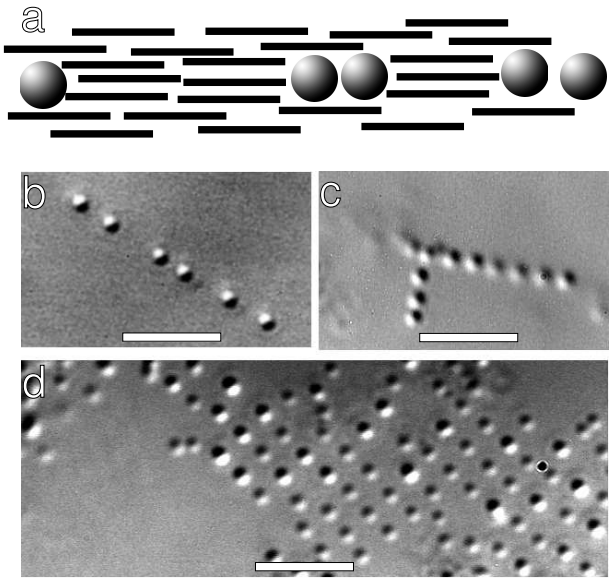

Figure 1.30: Arrangement of 0.3 μm and 0.4 μm polystyrene spheres dispersed in a *fd* nematic liquid crystal. (b) At high rod concentration just below the nematic-smectic phase transition 0.3 μm spheres form an elongated chain. The chain has an open structure in which spheres can be separated by a distance which is a multiple of the contour length of *fd* (c) With decreasing concentration of the rods we observe that the chains can assume configurations in which they come together at 90 degrees. (d) At a concentration of *fd* just above the I-N phase transition the spheres arrange themselves into cubic-like crystals. Scale bar indicates 5 μm

Unlike mixtures of *fd* and smaller spheres, large 0.3 μm spheres do not move easily through the nematic background and the sample is easily arrested in a metastable state. When a low volume fraction of 0.3 μm spheres are mixed with highly concentrated and well aligned rods which are close to the nematic-smectic phase transition chain-like structures form (Fig. 1.30b). These chains usually have an open structure where spacing between individual spheres can be several microns. However, this spacing is always a multiple of the *fd* contour length. The open chain structure is highly metastable and therefore we conclude there is a large energetic barrier preventing spheres from hopping. Often it is possible to observe open chains even days after the original sample was prepared although there is a slow tendency for spheres to eventually form closed chains where adjacent sphere are in contact. This indicates that closed chain structures have lower free energy then open chains.

With decreasing concentration of the background *fd* the nematic order decreases. When 0.3 μm spheres are suspended in such weakly aligned nematics they arrange themselves into bcc crystalline-like structures (Fig. 1.30d). At intermediate concentrations of background *fd* we sometimes observe chains that have 90 degree turns

(Fig. 1.30c). Curiously, when we increase the size of the sphere to 0.4 μm we no longer observe the formation of open chains, but only closed chains. Therefore the depletion stabilization is maximum for 0.3 μm spheres.

The formation of open and closed one-dimensional chains can be qualitatively understood if we look at a schematic illustration of a suspension of spheres in a nematic background (Fig. 1.30a). The diameter of the sphere (300 nm) is much larger then the diameter of the *fd* rod (7 nm), therefore a sphere acts as a wall which locally induces the formation of the smectic phase. The second sphere can easily be placed right next to the existing sphere or one rod length away along the nematic director because of the locally induced smectic correlations. This reasoning was used to theoretically explain the formation of the open-chain structures (van der Schoot 2000; van der Schoot 2002). For the sphere to hop between these two positions there has to be a fluctuation where all the rods move away. This is energetically very unfavorable and it is rarely observed in experiments. We suspect that as the sphere size increases beyond 0.3 μm it significantly distorts the local director. In this case the elastic free energy of the nematic leads to long range interactions which drive rearrangement of the spheres (Poulin et al. 1997). While the formation of chains is partially understood, the formation of bcc-like structures remains a mystery. One can only speculate that the chain-like structures are intimately connected to the formation of the lamellar phase while bbc-like structures are related to the formation of the columnar phase observed in a mixture of *fd* and spheres with smaller diameter. It would be of great interest to explore the behavior of the *fd*/sphere mixture as a function of the contour length of *fd*. We are curious to learn if the columnar phase observed for *fd* with other contour lengths. We encourage simulation and theoretical examination of the microphase separated structures described in Fig. 1.29 and 1.30. The simulations will be challenging as the dynamics are slow and large number of particles are necessary. However, simulating a unit cell of the lamellar or columnar phase should be readily feasible.

1.7 Self-assembled colloidal membranes and twisted ribbons

In the previous two sections we described the formation of lamellar and columnar phases, which occur when a low volume fraction of spherical particles are added to a background nematic phase of *fd* virus. The behavior of the rod/polymer mixture at different conditions, where a low volume fraction of rods is added to a high background concentration of isotropic polymers proves to be equally rich in surprising phenomena. The full phase diagram of a *fd*/Dextran mixture is shown in the inset of Fig. 1.31. In Sec. 1.5 we focused on the part of this phase diagram where bulk I-N phase separation is observed. Here we extend that work to take into account the positionally ordered smectic phase. At very high concentrations the *fd*/polymer mixture becomes essentially immiscible and phase separates into a polymer-rich isotropic phase and essentially pure suspension of highly concentrated rods. According to the rules of thermodynamics the osmotic pressure in these two coexisting phases will be equal.

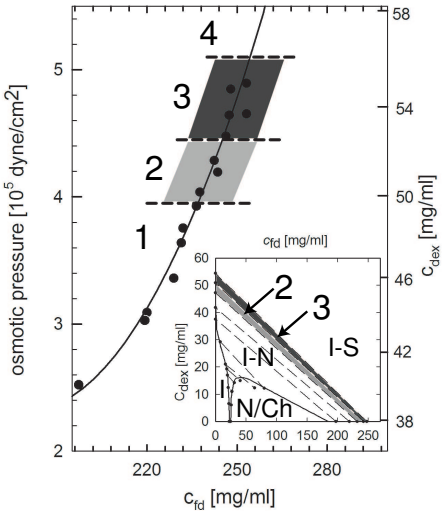

Figure 1.31: The coexistence concentrations of a highly concentrated immiscible *fd*/Dextran (M. W. 150,000) mixture. The Dextran concentration and corresponding osmotic pressure are indicated on the vertical axis while the *fd* concentration is plotted horizontally. Since the mixture is immiscible for these high concentrations the osmotic pressure of the isotropic Dextran solution is equal to the rod osmotic pressure. The complete phase diagram of a Dextran/*fd* mixture is shown in the inset of the figure. Tie lines along which the mixture phases separates into coexisting phases are indicated with dashed lines. The *fd*/Dextran mixture is dissolved in 190 mM NaCl, 10 mM tris at pH=8.15. To obtain coexistence concentrations the sample was centrifuged at 4000g for 15 minutes.(After ref. (Dogic 2003))

From previously published data, the relationship between Dextran concentration and osmotic pressure is known and thus the osmotic pressure of a suspension of rods can be deduced(Nordmeier 1993). In the *fd*/Dextran mixture the polymer osmotic pressure is analogous to temperature in molecular systems. With decreasing osmotic pressure (polymer concentration) the coexisting rods melt into the nematic phase while with increasing polymer pressure the rods freeze into the smectic phase. In the phase diagram shown in Fig. 1.31 there is possibility a triple point where isotropic, nematic and smectic phases coexist. However, this point has not been determined due to appearance of novel structures that will be described in the following sections.

In region 3 of the phase diagram we observe condensation of rods into quasi two-dimensional colloidal membranes. These membranes consist of a single layer of essentially parallel rods (Dogic and Fraden 2001; Dogic 2003). An image of a mature membrane that has been equilibrating for a few weeks is shown in Fig. 1.32. In Fig. 1.32a the rods point into the image plane and consequently the membrane is optically isotropic and shows no birefringence when observed with polarization microscopy. The interface between rods and background isotropic polymer solution shows significant fluctuations that are associated with the membrane line tension. In Fig. 1.32b,

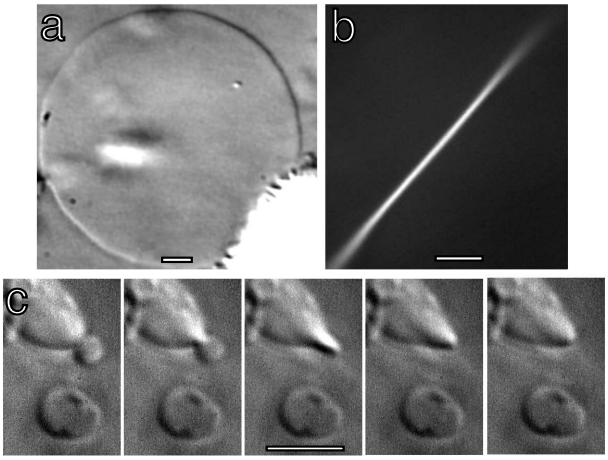

Figure 1.32: Formation of colloidal membranes in mixtures of *fd* and Dextran (M.W. 500,000) in 20 mM tris and 100 mM NaCl buffer a) DIC image of a colloidal membrane viewed edge-on in which the rods lie perpendicular to the image plane. b) Image of a membrane in which *fd* rods lie in the image plane taken with polarization microscopy. c) A sequence of images taken 1/30th of a second apart illustrating the lateral growth and coalescence of a membrane. The membranes coalesce only when they approach edge on with the rods in each membrane oriented parallel to each other. Scale bars indicate 5 μm. (After ref. (Dogic 2003; Dogic and Fraden 2001))

the rods lie in the image plane and the thickness of the membrane is approximately equal to the contour length of a *fd* virus. In this view, the membrane exhibits visible fluctuations that are associated with its bending rigidity. In principle, both the bending rigidity and the line tension could be measured by analyzing the fluctuations of a sequence of images similar to those shown in Fig. 1.32. Because of their similarity to membranes formed by amphiphilic molecules such as lipids or block copolymers, we name these two dimensional structures *colloidal membranes*.

Besides forming planar membranes, *fd*/polymer mixture can also assemble into twisted ribbons (Fig. 1.33). In general we observe that ribbons form at lower polymer concentration, while with increasing polymer concentration the flat membranes become more prevalent. The schematic illustration of the arrangement of rods in a twisted ribbon is shown in Fig. 1.33b. Images taken with a polarization microscope indicated alternating bright and dark regions along an individual ribbon. The bright birefringent regions correspond to an area where the rods lie in the plane of the image and dark regions indicate where the rods lie perpendicular to the image plane. It is possible for the ribbons to form branches as shown in Fig. 1.33. The difference in energy between twisted ribbons and flat membranes must be very low as it is often possible to observe both planar membranes and twisted ribbons within the same sample.

A sequence of images showing a transformation of a twisted ribbon into a flat membrane is shown in Fig. 1.34. In this particular case we have applied a flow field,

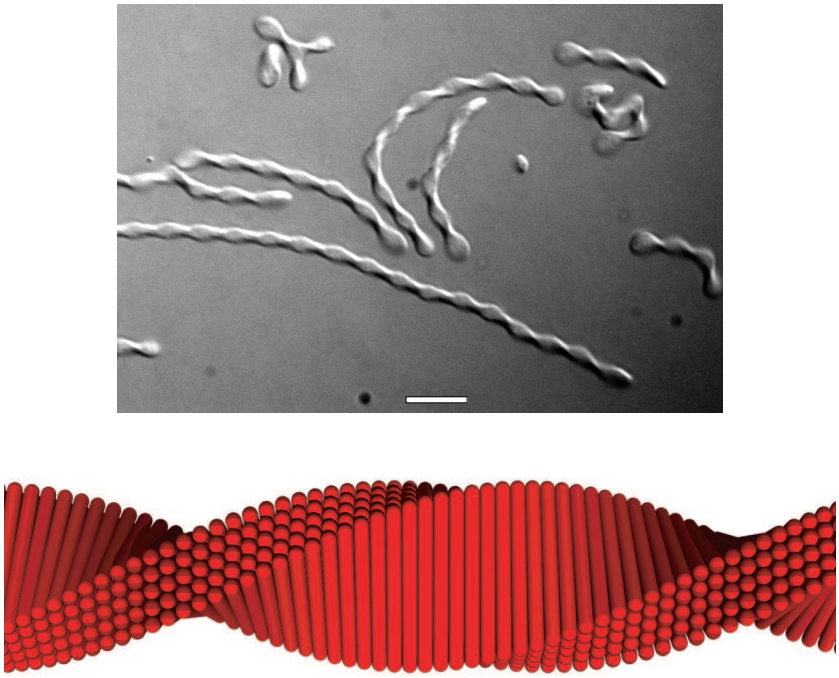

Figure 1.33: a) A DIC image of a suspension of self-assembled ribbons in a mixture of *fd* and Dextran (M.W. 500,000) in 20 mM tris and 100 mM NaCl buffer. Scale bar indicates 5 μm. b) A schematic illustration of the configuration of the rods within a single ribbon

which can simultaneously untwist the ribbon and stretch it to many times its initial length. After the flow is stopped some of the ribbons remain under tension because they are fixed at both of their ends. Subsequently, over a period of minutes these ribbons under tension will break and relax towards their equilibrium state. In the same sample some structures will relax back to a twisted ribbon and remain in that state for many hours. However, in this particular case, after an initial fast relaxation to the state shown in Fig. 1.34c the twisted ribbon continued to slowly untwist until it became a flat two dimensional membrane shown in Fig. 1.34e.

One possible reason for the stability of twisted ribbons is the chiral nature of *fd* itself. As discussed previously, a bulk solution of *fd* at intermediate concentrations forms a twisted cholesteric structure instead of nematic phase. This indicates that *fd* rods prefer to be slightly twisted with respect to each other. A flat membrane such as the one shown in Fig.1.32 is geometrically incompatible with twist. However, when rods form an elongated strip it is possible for them to twist with respect to each other. Therefore we expect two contributions to the total energy which determines the shape of a twisted ribbon or two-dimensional membrane. The formation of a flat membrane is favored by line tension since this creates a structure with minimum area

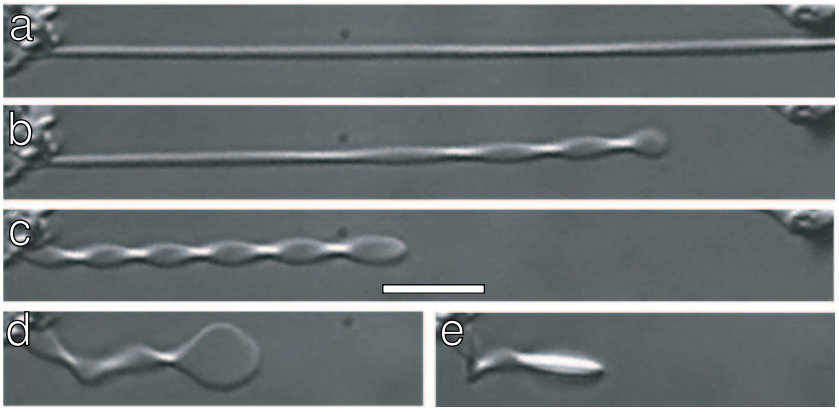

Figure 1.34: A sequence of images illustrating the collapse of a stretched, untwisted ribbon into a two-dimensional membrane. The ribbons are stretched by applying a shear flow. In this process by chance both of the ends of the ribbon are fixed. After a while the tension induces the fast collapse of a stretched ribbon into a twisted ribbon which subsequently slowly untwists into a flat membrane. The images are taken roughly a few seconds apart. Scale bar indicates 5 μm.

to circumference ratio, while the formation of twisted ribbon is favored by the chiral contribution to the free energy. It should be possible to experimentally measure the line tension by analyzing the fluctuations of the membrane. Preliminary experiments indicate that it is also possible to apply torque to birefringent ribbons and either overtwist or untwist ribbons using optical tweezers. We hope that from these experiments the chiral contribution to the free energy can be determined. These measurements should shed more light on the stability of twisted ribbons and colloidal membranes.

It is important to determine wether the colloidal membranes are a kinetically trapped metastable state, or if they represent a true equilibrium structure in region 3 of the phase diagram shown in Fig. 1.31. Their pronounced tendency to grow, albeit very slowly, indicates that they are indeed equilibrium structures. In some samples that are a few months old we observed membranes that are millimeters in size. It is also possible to observe a process of coalescence of two membranes as shown in a sequence of images in Fig. 1.32c. In order for the coalescence to take place the rods in both membranes have to be aligned along the same direction. We note that the membranes do not stack up on top of each other unless the polymer concentration is significantly higher. There are additional observations with regards to the kinetics of the underlying isotropic-smectic phase transition that suggest that membranes are stable structures for a specific range of *fd* and polymer concentrations. These are discussed in more detail in Sec. 1.9.2.

The formation of colloidal membranes seems a poorly explored, yet very generic phenomena frequently observed in rod-like particles with attractive interactions. It is observed when *fd* is mixed with a wide variety of polymers such as Dextran, PEO (Dogic and Fraden 2001), poly(N-isopropylacrylamide) (NIPA) (Alsayed et al.

2004), and ferrofluids (Lin 2004). In addition to the *fd* system, membranes are also observed in mixtures of TMV with BSA and PEO (Adams et al. 1998) and in pure suspensions of inorganinc rod-like colloids made of β-FeOOH (Maeda and Maeda 2003). The latter particles have no polymer added to it, but it is very likely that they have direct attractive forces of van der Waals origin. Since the intermolecular interaction between these components are well known it would be of great interest to measure the bending rigidity of the membrane and see how it depends on molecular parameters, such as rod length, or polymer osmotic pressure.

One possible explanation for the stability of colloidal membranes are the entropic forces associated with confining the fluctuations of the membrane when a stack of membranes forms. If these fluctuations are associated with wavelengths much larger then the thickness of the membrane they can be described within continuum theory. A stack of fluctuating membranes confined by two walls will show strong effective repulsive interactions first described by Helfrich (Helfrich 1973; Lipowsky 1995). The competition between the Helfrich repulsion and long range attractive interactions due to van der Waals can give rise to phase transitions from bound to unbound membranes (Lipowsky 1995). Because of the large thickness of the membrane, the bending rigidity is very large for colloidal membranes. Consequently, one does not expect strong repulsive interactions associated with long wavelength fluctuations, which can lead to stability of the colloidal membranes. However, in addition to long wavelength fluctuations the surface of the membrane is roughened at length scales comparable to the thickness of the membrane by the relative displacement of molecules with respect to each other. These fluctuation modes are often called protrusions (Goetz et al. 1999). The origin of a short range repulsion often observed between lipid membranes has been attributed to these protrusion fluctuations (Israelechvili 1991; Wennerstrom and Israelachvilli 1992). In lipid membranes these forces have a very short range of a few angstroms, but in colloidal membranes due to the extreme anisotropy of the constituent rods they could easily reach 100 nm. It seems plausible that these protrusion fluctuation can lead to thermodynamic stability of colloidal membranes.

1.7.1 Monte Carlo Simulation of Colloidal Membranes

To examine this issue in more detail we have preformed a Monte Carlo simulation on a simplified system. Instead of simulating the full rod/polymer mixture we have focused on a one-component system of perfectly parallel rods, which interact with each other via direct attractive interactions. The attraction potential is designed so that it mimics the depletion potential between two rods (Fig. 1.23). If spherocylinders are pointing along the z direction, in the x-y direction the strength of the attractive potential is proportional to the overlap area between two disks whose diameter is equal to $D_{\mathrm{sc}}+D_{\mathrm{sp}}$. The strength of the potential also depends on the relative displacement of the center of mass of each spherocylinder along the z direction. The depletion potential is at a maximum value when the relative displacement along the z direction of two spherocylinders is zero. The overlap along the z direction is equal to $L+D_{\mathrm{sc}}-|z_1-z_2|$ if this quantity is larger then zero. Subsequently, this dimension is multiplied with the overlap area in the x-y direction and the whole value of the excluded volume is

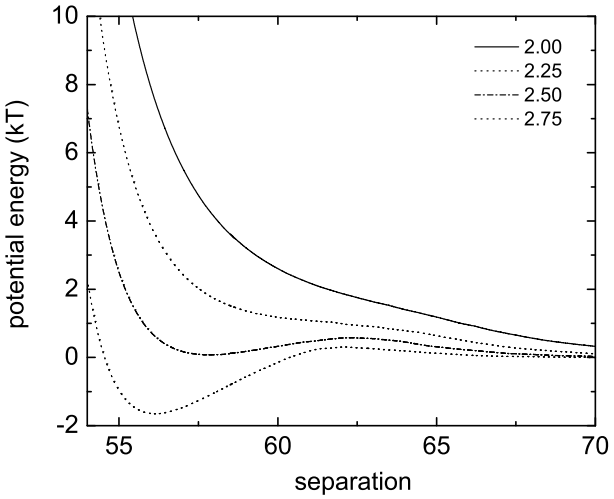

Figure 1.35: Effective potential between two membranes obtained from Monte Carlo simulation. The aspect ratio of rods is 25 (L=50,$D_{\rm sc}$=2), while the range of interaction is 0.75 $D_{\rm sc}$ = 1.5. To obtain the strength of the intermolecular attraction the overlap volume is multiplied by a constant Π, which is this particular case is -0.002. The potential was obtained for four different temperatures ($\beta = 1/kT$), which are indicated in the upper right corner. There were 144 rods within each membrane. The order within each membrane is that of a two-dimensional crystal. However, we expect that a similar intermembrane potential will be found for liquid-like membranes.

multiplied by an overall constant, which characterizes the strength of the potential.

Initially we place the rods so that they form a single crystalline membrane and find that at low temperatures the rods never escape the membrane and the membrane remains stable for the whole duration of the simulation. At high temperature rods evaporate from the membrane and the membrane eventually disintegrates. For temperatures where the membrane remains stable, we measure the effective intermolecular potential between two membranes. The probability that the membranes are separated by the distance h is determined. Once this probability is known it is easy to extract the effective potential between two membranes $U_{\rm eff} = -kT \ln \rho(z)$. To sufficiently sample all energetically unfavorable separations we use the technique of multiple histograms as described by Frenkel and Smith (Frenkel and Smith 1996).

Effective potentials obtained from this simulation are shown in Fig. 1.35. At high temperatures the effective interaction is completely repulsive between two membranes. If mapped onto an athermal rod/polmer mixture, high temperature corresponds to low polymer concentration or equivalently low osmotic pressure. In this region we expect that isolated colloidal membranes will be the equilibrium structures. As the temperature is gradually reduced, the effective potential changes from repulsive to attractive. In a certain temperature range (β=2.50) there is both a local minimum, which favors bound membranes and a global minimum energy which favors membranes

that are infinitely far apart. This would indicate that the swelling transition of a bound membrane pair is a first order phase transition. At low temperatures there is a deep attractive minimum. We would therefore expect that under these conditions individual colloidal membranes would not be stable, but would stack up on top of each other making smectic filaments. This structure is indeed observed in experiments in region 4 of the phase diagram shown in Fig. 1.31. These experiments are discussed in more detail in section 1.9. Our simulations also suggest that a smectic phase composed of highly anisotropic attractive rods will swell with increasing temperature before they melt into the nematic phase. This is in fact observed in a novel thermotropic mixture of *fd* and NIPA polymer (Alsayed et al. 2004). The behavior of this particular system is discussed in more detail in section 1.9.4.

It is perhaps not entirely surprising that for highly anisotropic rods the long range order along the rod axis will melt at a different temperature when compared to the order within each layer (colloidal membrane). In our simple example of perfectly aligned rods it is always possible to decrease the strength of attraction between layers (membranes) by increasing the length of the spherocylinder by two and decreasing the strength of depletion interaction by two. While this decreases the strength of interaction between the layers, the interaction of rods within each layers remains unchanged. Therefore we believe that the stability of the colloidal membranes is the result of the high aspect ratio of our system. This argument is true as long as the average protrusion fluctuations are smaller then the range of attractive potential. To establish a closer connection with experiments, our simulations will have to be repeated on a more realistic system where the rods are flexible and charged and are allowed both translational and rotational degrees of freedom.

1.7.2 Crystalline membranes

Two-dimensional membranes described in the previous section were formed in a mixture of *fd* and polymers with relatively high molecular weight. Their fluidity and ease by which they are deformed by an external field, such as shear flow, strongly suggests that the rods within each membrane have a liquid-like structure. By decreasing the polymer size it is possible to obtain two-dimensional membranes with hexagonal shape (Fig. 1.36). The shape of these membranes indicates that *fd* rods within each membrane assume a crystal-like configuration, but this would have to be confirmed with x-ray experiments. Changing polymer concentration modifies the appearance of the crystalline membranes dramatically. At high polymer concentration the polymer membrane boundary is relatively sharp. The induction time for crystal nucleation as evidenced by the turbidity of the sample is relatively short. Consequently many nuclei are formed relatively quickly. Each membrane has a specific nucleation site protruding into the third dimension. It seems plausible that multimeric *fd* always present at low volume fraction forms the initial nucleation site.

At lower polymer concentration the induction time can take up to an hour and the polymer membrane boundary is more fluid like. Since there are relatively few nuclei, crystals grow to a size of 30-40 μm over a period of few days. Unlike crystals at higher polymer concentrations, when viewed from the side they exhibit fluctuations

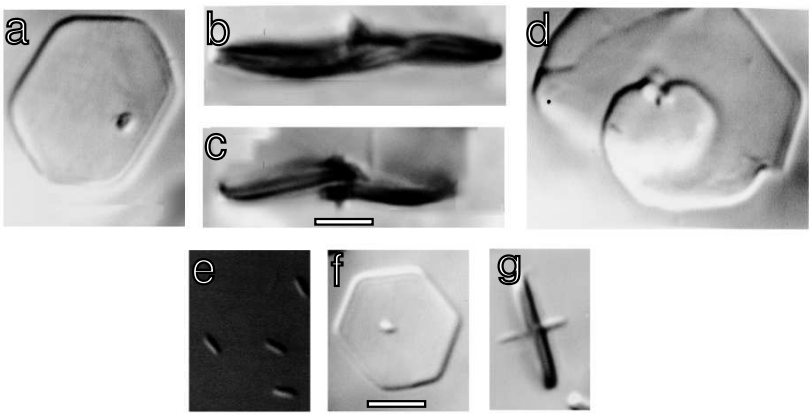

Figure 1.36: Two dimensional crystalline membranes observed in a mixture of *fd* and the low molecular weight polymer PEO (Mw 8000). (a-d) These images are taken at a relatively low polymer concentration. Under these conditions it is possible to observe crystalline membranes that have screwlike dislocations. Images (b) and (c) are sidewise images of the same membrane focused at different z positions. (e) Images of nuclei and (f,g) membranes taken at high polymer concentration. On average the size of the membranes at these conditions is much smaller that for those shown in images (a) to (d). The scale bar indicates 5 μm. (After ref. (Dogic and Fraden 2001))

visible with an optical microscope. A large number of these membranes have screw-like dislocations which can easily be identified when viewing a membrane sideways (Fig. 1.36b and c).

The concentration of rods within the membrane is so high ($\approx$ 250 mg/ml) that the polymer is probably completely excluded. There is complete phase separation into immiscible phases and the osmotic pressure of the isotropic polymer solution is identical to the pressure of the rods within the membrane. The polymers with a small radius of gyration such as PEG, Mw 8000, (R_g=4 nm) are able to induce a much higher osmotic pressure in the membrane when compared to larger polymers for which liquid membranes are observed (Dextran Mw 150,000 R_g=11nm). It follows that with increasing osmotic pressure, the rods within the membrane undergo a two dimensional liquid to crystal phase transition analogous to crystallization observed in two-dimensional disks (Bates and Frenkel 2000). We have not yet obtained conditions for which it is possible to continuously change experimental parameters so that the liquid-like membranes transform into crystalline ones. However, this remains intriguing because of the possible existence of the hexatic phase at intermediate concentrations between the liquid and crystal phases (Halperin and Nelson 1978).

1.8 Surface induced smectic ordering in rod/polymer mixtures

So far we have been only concerned with the behavior of rod-like particles in bulk phases. However, we also observe unexpected phenomena at the interfaces between two phases which will be summarized in this section. From studies of materials at the molecular scale it is well known that surfaces play an important role in the kinetics of bulk phase transition. Most materials, such as ice exhibit surface pre-melting in which a thin layer of melted liquid forms at the gas-solid interface. This occurs at temperatures below the bulk liquid-solid phase transition (Dash et al. 1995; Lied et al. 1994). In contrast, the phenomena of surface freezing, where a thin layer of ordered phase spontaneously appears at the liquid-gas interface above the temperature of bulk liquid to crystal phase transition is observed in very few materials, most notably alkanes, thermotropic liquid crystals and surfactant polymers (Wu et al. 1993; Ocko et al. 1986; Lang 1999). It has been noted that the nucleation of the bulk phase transition is closely related to the behavior of the sample at the interface. The observation that it is difficult to prepare superheated crystals is explained by the presence of the surface pre-melted layer which acts as a heterogeneous nucleation site (van der Veen 1999; Cahn 1986). For materials which exhibit surface freezing the opposite effect is true. Thus it is difficult to supercool the liquid phase below the equilibrium crystallization transition (Sloutskin et al. 2001; Sear 2002).

While most surface freezing transitions have been studied in molecular systems, we recently observed a similar phenomena in a colloidal *fd*/Dextran mixture. If the mixture described in Fig. 1.31 is prepared below the bulk isotropic-smectic coexistence (region 2 of phase diagram shown in Fig. 1.31) surface induced formation of the smectic phase is observed. An image of an isotropic-nematic surface completely covered with the surface smectic phase is shown in Fig. 1.37e. Below the image plane is a dense nematic suspension while above the image plane is an isotropic Dextran solution. The layered smectic-like structure is observed only within a thin layer confined to the isotropic-nematic interface. From optical images it is difficult to measure the exact thickness of this layer, but we can estimate that it is at most a few hundred nanometers thick. If a bulk phase separated sample which exhibits surface freezing is mixed by vigorous shaking, small nematic tactoids will form. The interface of these tactoids will be covered with surface induced smectic phase as is illustrated in Fig. 1.39b. As the tactoids coalesce the smectic phase always remains confined to the narrow layer next to the interface. This provides strong support that smectic structures in Fig. 1.37e are entirely induced by the isotropic-nematic surface.

In molecular systems which exhibit surface freezing it is usually found that with increasing temperature the thickness of the surface frozen layer continuously decreases. Surprisingly, we find that with decreasing osmotic pressure of the mixture the surface induced smectic phase swells to the point where isolated layers are observed. Therefore the surface induced smectic phase behaves very differently from the bulk phase. While the bulk smectic phase of pure rods melts into a nematic phase the surface induced smectic phase continuously swells. It is found that isolated layers exhibit

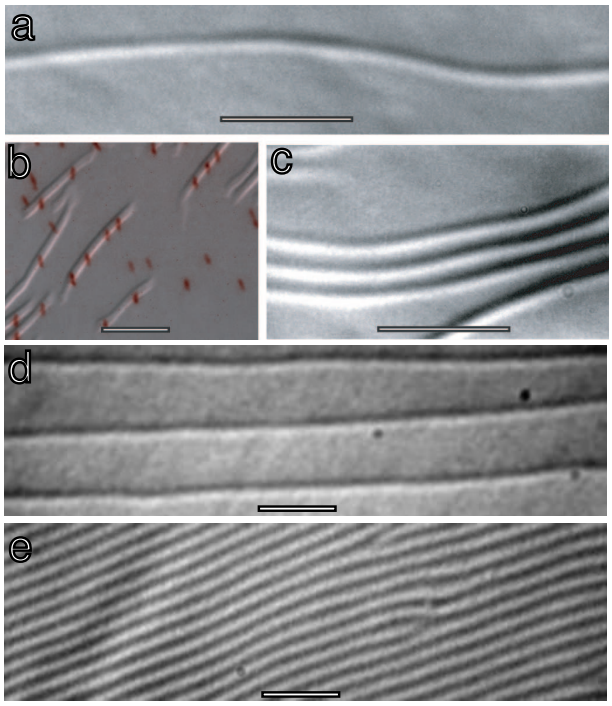

Figure 1.37: DIC optical micrographs of the surface induced smectic phase. The image lies in the plane of the isotropic-nematic interface with the denser nematic phase being below the image plane and the lighter polymer-rich isotropic phase above the image plane. (a) With decreasing polymer concentration the surface induced smectic phase swells until individual layers are observed. In (b) a low volume fraction of rods are labelled with the fluorescent dye Alexa 488 and appear as black lines. Overlaying the fluorescent image with a DIC image indicates that the surface induced phase has smectic C configuration. Scale bars is 5 μm.

large fluctuations and the rods within a layer are always aligned along the director of the background nematic field. Therefore it is possible to think of the background nematic as a confining field. The tight coupling between the surface smectic layers and the fluctuating nematic background can lead to enhanced fluctuations similar to those encountered when the semi-flexible polymer is suspended in the fluctuating nematic background (Dogic et al. 2004b). Quantitative analysis of the fluctuations of the surface induced smectic phase has not yet been preformed.

On a surface partially covered with smectic layers, the layers can be either bundled together (Fig. 1.37c) or spaced far apart from each other (Fig. 1.37d). These configurations indicate the presence of both attractive interactions, which cause bundle formation and repulsive interactions, which cause layer swelling. Because of their size, the smectic layers diffuse very slowly on the surface and it is very difficult to determine the equilibrium configuration. Often even weeks after the samples are prepared the structures continue to evolve. At present it is not yet clear what are the main physical

forces responsible for the effective potential between swollen surface smectic layers. Recently we have been able to manipulate individual layers on the surface and are hoping to experimentally measure the forces between individual smectic layers.

The reason for the formation of the surface induced smectic phase can perhaps be construed from theoretical studies of the isotropic-nematic interface in a hard-rod suspension. After some controversy, it is now well established that the density profile across the isotropic-nematic interface for Onsager rods is monotonically increasing (Chen and Noolandi 1992; Shundyak and van Roij 2001). However, if more complex mixtures of thin and thick rods are prepared in the neighborhood of its triple point it is found that the interface profile can be highly non-monotonic (Shundyak and van Roij 2002). The presence of the surface induced smectic phase would be a natural consequence of a non-monotonic density across the isotropic-nematic interface. Since the only parameter that determines the phase behavior of hard rods is their concentration and if their density is higher at the interface with the polymer-rich isotropic phase it would follow that the smectic phase would first form at the interface. At present little is known theoretically or experimentally about quantitative aspects of the density profiles across interfaces in the rod-polymer mixtures.

Besides *fd*/Dextran mixtures a surface induced smectic phase was also observed in mixtures of *fd* and PEO. Experimentally we find that the range of stability of the surface induced smectic phase is very sensitive to the size of the polymer. For a mixture of *fd* and Dextran (Mw 150,000) it is possible to observe the surface induced smectic at rod concentrations 3.5 % below the bulk isotropic-smectic phase transition, while this number decreases to 1.5 % for a mixture of *fd* and larger Dextran (Mw 500,000). For mixtures of *fd* and Dextran (Mw 2,000,000) we have not observed any surface induced freezing.

Much remains to be understood about the surface induced smectic structures. For example, the fluorescence images (Fig. 1.37b) and polarization microscopy indicate that the rods within each layer actually have a smectic-C like configuration. This again is in stark contrast to the bulk phase behavior.

1.9 Kinetics of liquid crystalline phase transitions

While the subject of how a crystal nucleus grows out of a dense liquid composed of spherical particles has been studied in great detail (Debenedetti 1996) less is known about how a smectic or nematic phase will nucleate from isotropic rods. What is the shape of the critical nucleus of nematic rods forming from a metastable isotropic solution? What determines the height of the nucleation barrier of the nematic droplet? These questions remain mostly unanswered and the kinetics of phase transitions in rod-like particles remains essentially unexplored. When the possibility of both positional and orientational order is taken into account the complexity of kinetic pathways increases even further. Here we summarize our recent experimental work on the kinetics of the phase transitions in liquid crystals. We first briefly review the behavior of pure rods and then focus in more detail on the behavior of rod/polymer mixtures.

It is important to mention that because of the slow time-scales and large length-

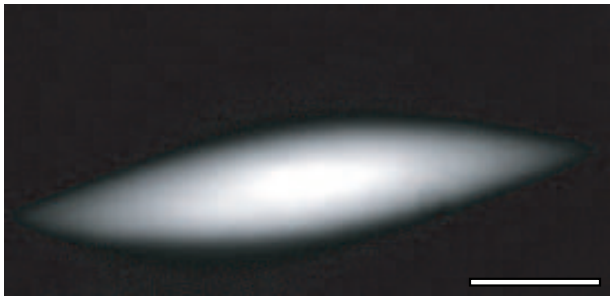

Figure 1.38: A optical micrograph of an anisotropic nematic tactoid suspended in the background isotropic liquid. The scale bar indicates 5 μ.

scales involved, colloids are in many ways an ideal system to study fundamental questions with regard to kinetics of phase transitions. The time and length scales involved make the system amiable to determining the real space structure using optical microscopy. For example, in a recent study using optical microscopy, it was possible to directly visualize critical nuclei of a colloidal crystal growing from a metastable liquid (Gasser et al. 2001). Experiments such as these make it possible to test the fundamental concepts of classical nucleation theory.

1.9.1 Kinetics of the isotropic-nematic and nematic-smectic phase transition in hard rod suspensions

While the phases formed by colloidal liquid crystals are structurally identical to those found in low molecular weight, single component, thermotropic liquid crystals it seems that the kinetics of phase transitions in rod-like colloids can be very different from their thermotropic counterparts.

If a sample is prepared in the isotropic-cholesteric coexistence region it will spontaneously form nematic droplets in the isotropic background (Fig. 1.38). The shape of the droplet is determined by three factors : (1) surface tension, which acts to minimize the surface area of the droplet, (2) boundary conditions for the orientation of the rods at the I-N interface, and (3) elastic energy, which is minimized when the rods are parallel. For the virus, the boundary conditions are that the rods align parallel to the I-N interface. Minimizing the surface tension creates a spherical droplet, but the high curvature leads to a large elastic energy. The equilibrium shape is an elongated droplet, which lowers the elastic energy at the cost of raising the surface energy. The shape of these droplets was analyzed in a recent theoretical work (Prinsen and van der Schoot 2003). Understanding the shape of nematic tactoids is the first step towards understanding the nucleation of the nematic phase out of a metastable isotropic solution. It remains an open question as to what is the actually shape of the critical tactoids and what is the height of the barrier for the nucleation of the nematic phase of hard rods from the isotropic phase.

Solutions of TMV, which closely approximate a suspension of hard rods with infi-

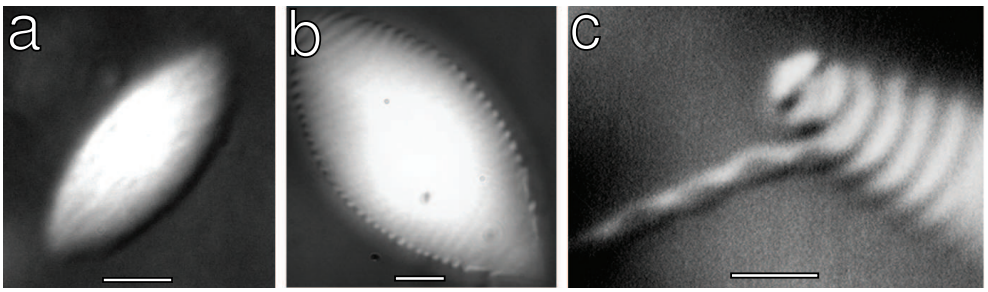

Figure 1.39: Multiple steps by which the colloidal membranes are created from a metastable isotropic suspension in a *fd*/Dextran mixture. (a) In a first step within minutes of preparing the homogeneous mixture, a metastable nematic tactoid forms from the isotropic suspension. (b) As a second step the isotropic-nematic interface is almost immediately covered with the surface induced smectic phase. (c) Finally, in a third step after a period of days, colloidal ribbons such as those discussed in section 1.7 are formed. This sample is prepared in region 2 of the phase diagram shown in Fig. 1.31. Scale bars indicate 3 μm.

nite rigidity, exhibit a nematic-smectic transition which is either second order or a very weakly first order phase transition (Wang et al. 1994). In contrast to these experimental findings, the latest computer simulations of the nematic-smectic phase transition in hard rods indicates a first order phase transition with about a 2% discontinuity between coexisting nematic and smectic concentrations (Polson 1997). On the other hand, the cholesteric-smectic phase transition in semi-flexible *fd* virus is found to be strongly first order and no pre-transitional fluctuations have been observed (Dogic and Fraden 1997). It was speculated that the finite flexibility of *fd* virus changes the order of the nematic phase transition, which was confirmed using theoretically (Tkachenko 1996).

1.9.2 Kinetics of the Isotropic-Smectic phase transition

By adding enough dextran to a solution of *fd* it is possible to widen the isotropic-nematic coexistence to the point where direct isotropic-smectic coexistence is obtained. Taking advantage of the size of *fd* viruses it is possible to directly visualize the formation of smectic layers using optical microscopy as they nucleate from the metastable isotropic phase. It is not at all obvious how the kinetics of this phase transition proceeds.

We have studied the kinetics of the isotropic-smectic phase transition in a immiscible *fd*/Dextran mixture whose phase diagram is shown in Fig. 1.31. At low polymer concentrations, below 49 mg/ml in region 1, coexistence between an immiscible polymer-rich isotropic phase and a rod-rich nematic phase is observed. The shape of the nematic droplets formed in the background isotropic phase is very similar to anisotropic tactoids formed at isotropic-nematic coexistence in pure virus suspensions. In region 2 the smectic phase wets the isotropic-nematic interface as discussed in section 1.8.

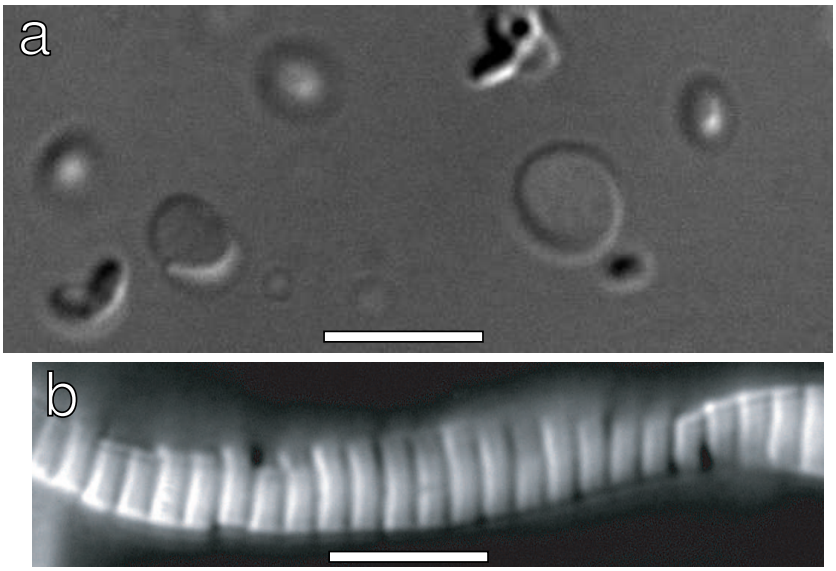

Figure 1.40: (a) At higher concentrations of polymer in region 3 of the phase diagram shown in Fig. 1.31 we observe the nucleation of colloidal membranes directly out of metastable isotropic solution. (b) With further increasing polymer concentration in region 4 bulk smectic filaments are formed. Scale bar indicates 3 μm.

In region 3 of the phase diagram there is evidence that isolated colloidal membranes discussed in section 1.7 form an equilibrium structure. Depending on the precise location within region 3 we have observed two different kinetic pathways by which these membranes form from a metastable isotropic suspension. At lower polymer concentration the structures observed during the multiple step kinetics for the formation of the membranes are shown in Fig. 1.39. In a first, fast step we observe a very quick formation of a metastable nematic tactoid (Fig. 1.39). Instantaneously, the isotropic-nematic interface of the tactoids is covered with the surface induced smectic phase. In the second, slow step that takes a few days, the surface induced smectic phase acts as a nucleation site for the formation of the twisted ribbons. These ribbons grow from the interface and can reach many hundreds of microns in length. The fact that the *fd*/Dextran mixture is essentially immiscible indicates that the ribbons grow due to the diffusion of rods from the metastable nematic phase through the surface induced smectic phase into the more stable ribbons-like structures.

If the polymer concentration is increased within region 3 of Fig. 1.31 membranes directly nucleate from the isotropic solution as illustrated in Fig. 1.40a. The membranes remain stable in this region as they laterally coalesce (Fig. 1.32) and can reach sizes of many tens of microns in diameter. These structures were discussed at length in section 1.7. Finally, at higher polymer concentration in region 4 the membranes stack up on top of each other and form elongated filaments, which internally have a smectic-like structure (Fig. 1.40b) (Frenkel and Schilling 2002). This transition from

isolated membranes to smectic filaments is predicted by the simulation of parallel spherocylinders with direct attractive interaction described in more detail in section 1.7. It is important to mention that the the boundaries between different structures are not very well defined and it is often possible to observed multiple structures within the same sample.

As discussed in section 1.8, the bulk isotropic-smectic phase transition is superseded by the surface induced formation of the smectic phase at the isotropic-nematic interface. For a long time it was thought that the state of order at the interface regulates the kinetics of the bulk phase transition. The kinetics pathway illustrated in Fig. 1.39 provides direct visual evidence for the importance of the surface smectic layer to the overall kinetic pathway of the formation of the smectic phase.

Another factor that can significantly affect the kinetics of the phase transition is the presence of a metastable phase boundary (Sirota and Herhold 1999; ten Wolde and Frenkel 1997; Olmsted et al. 1998). For example, colloids with short range attractions have an equilibrium phase diagram as shown in Fig. 1.20b where a gas-liquid phase transition is metastable with respect to the gas-crystal phase transition. Recent simulations suggest a remarkable enhancement of the nucleation rate of a crystal when the sample is prepared in the vicinity of the critical point associated with the metastable gas-liquid phase transition (ten Wolde and Frenkel 1997). The reason is because the crystals nucleus is formed in two steps for these particular conditions. In a first step, a dense liquid droplet associated with the metastable gas-liquid phase separation is formed and in a subsequent step a crystal nucleates within this dense droplet. This significantly reduces the nucleation barrier when compared to nucleation of a crystal directly from a dilute gas phase. In a similar way the presence of the metastable nematic phase is important for the nucleation of the smectic phase or colloidal membranes. Figure 1.39 shows that for slightly supersaturated rod/polymer mixtures a metastable nematic tactoid nucleates in a first, fast step. Subsequently, isolated colloidal membranes are formed after two additional intermediate stages - the surface smectic (Fig. 1.39b) and the twisted ribbon (Fig. 1.39c).

1.9.3 Filamentous structures associated with nematic-smectic phase transitions

In certain regions of the rod/sphere phase diagram the whole sample forms a single lamellar phase (Fig. 1.28). However, upon changing the concentration of either component of the rod/sphere mixture it is also possible to obtain co-existence between the lamellar phase and either a nematic, or a smectic phase with a wavelength different from the lamellar phase. In contrast to nematic tactoids in the isotropic background, the droplets associated with lamellar-nematic or smectic-nematic coexistence assume a shape of elongated filaments with a cylindrical cross section. Often these filaments can be many millimeters long (Fig. 1.41a). They are observed in both rod/sphere and rod/polymer mixtures when the total rod concentration is close to the nematic-smectic phase transition. In contrast, when polymers are added to a nematic phase of *fd* rods at low concentrations close to I-N phase transition they will phase separate into isotropic, polymer rich tactoids in the background nematic phase. These inverted tac-

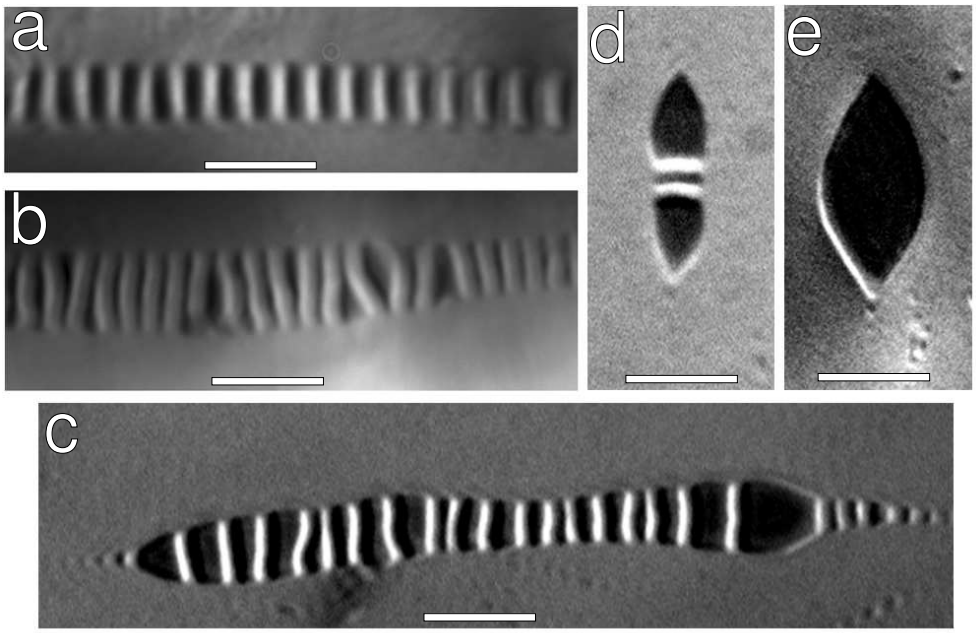

Figure 1.41: Coexistence between the lamellar phase and the background nematic phase observed in a mixture of *fd* and Dextran (M.W. 500,000). The virus/polymer mixture is prepared in a tris buffer pH=8.0 at 100 mM ionic strength. The sequence of images illustrate the transformation of layered lamellar filaments into isotropic, polymer rich tactoids that occurs when polymer is added to the mixture. Scale bar indicates 5 μm.

toids (Fig. 1.39e) have the same shape as nematic tactoids in an isotropic background (Fig. 1.38).

It is of interest to examine how the cylindrical smectic filaments transform into polymer rich tactoids with increasing dilution. If a sample containing smectic filaments, such as ones shown in Fig. 1.41a, is diluted with buffer solution the layers within a filament will swell as illustrated in Fig. 1.41b. Upon continued dilution the layers swell further and filaments decrease in length so it is possible to observe their ends (Fig. 1.41c). Finally, at the lowest concentration, individual polymer rich tactoids are observed in the nematic background. These tactoids are often deformed by a few isolated monolayers. While filaments observed in Fig. 1.41 are obtained by adding a low volume fraction of polymer or spheres to a very dense nematic phase that is close to the nematic-smectic phase transition it is also possible to obtain very similar filamentous structures by adding a high concentration of polymer to dilute isotropic rods. In this case, one obtains smectic filaments which coexist with an isotropic background suspension. The formation of such filaments was theoretically studied by Frenkel and Schilling (Frenkel and Schilling 2002).

The observation of nematic-lamellar phase co-existence might seem contradictory

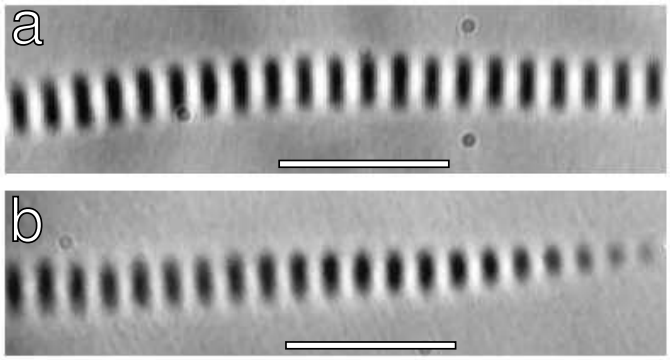

Figure 1.42: Coexistence between the lamellar phase and the background nematic phase observed in a mixture of polystyrene spheres ($D_{\rm sp} = 0.1\mu$m) and *fd* virus at 5 mM ionic strength (10 mM tris, pH=8.15). Unlike layered filaments formed in *fd*/Dextran mixtures the spacing of these filaments is always 1.1 μm. They can be many millimeters long, but occasionally it is possible to observe a tapered end of a filament as illustrated in image (b). Scale bar is 5 μm.

to the generic-phase diagram of the rod/polymer mixture shown in Fig. 1.31. In this phase diagram there are no indications of the lamellar phase or tie-lines between the nematic and lamellar phase. In order to obtain bulk coexistence necessary to measure the phase diagram we had to centrifuge the samples in region 3 and 4. Due to the density difference between the lamellar layers and dextran solution is seems plausible that the centrifugation procedure induces the lamellar to smectic phase transition. It seems likely that as the volume fraction of rods within region 3 is increased we actually go from isolated membranes to swollen lamellar phase to smectic phase. However, this is merely a speculation at this point. We do feel that the phase diagram presented in Fig. 1.31 is not final and that the location of the lamellar phase in the rod/polymer mixture should be carefully examined in future work.

While Fig. 1.41 illustrates the behavior observed in *fd*/poylmer mixtures, identical filaments are also observed in mixtures of *fd* and polystyrene spheres with $D_{\rm sp} = 0.1\mu m$. There are however, two important differences between these two cases. First, in the polymer/*fd* mixture it is possible to prepare samples with different layer spacing and with decreasing osmotic pressure these layers continuously swell (Fig. 1.44). In contrast, *fd*/PS mixture exhibit only lamellar phases with constant 1.1 μm spacing. This might be because there is a direct phase transition from isotropic phase to lamellar phase in the rod/PS mixture. Therefore, the swelling transition might be preempted by the melting of rods into the isotropic phase. Second, in the *fd*/PS mixture it is also possible to obtain coexistence between a smectic phase with 0.9 μm and a lamellar phase with 1.1 μm periodicity. This indicates a first order phase transition between a smectic and lamellar phase. So far we have not observed a similar discontinuous transition between two layered structure with different periodicity in the *fd*/polymer mixture. In fact, the work summarized in the next section indicates that swelling of

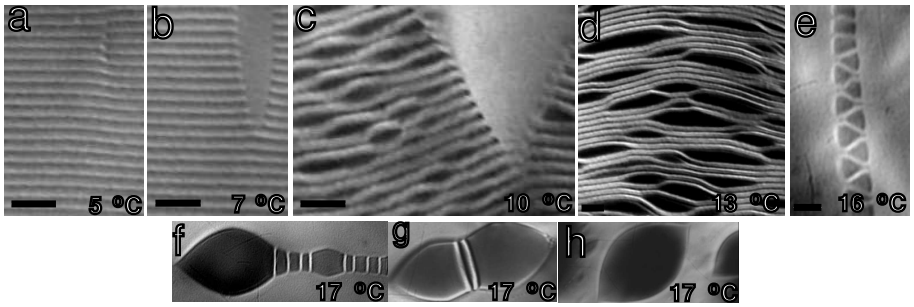

Figure 1.43: Melting of the lamellar phase observed in a *fd*/NIPA mixtures (50 mg/ml *fd* and 7.5 mg/ml NIPA). At low temperatures the mixture forms a uniform lamellar phase with periodicity of 1.3 /*mu*m. Images a to f indicate the process by which the microphase separated lamellar phase melts into bulk isotropic-nematic coexistence. Scale bar indicates 5 μm. (After ref. (Alsayed et al. 2004))

the lamellar phase in *fd*/polymer is continuous.

1.9.4 Multiple pathways observed in melting of the lamellar phase

Up to now we have only discussed the behavior of entropic suspensions of rods, or rod-polymer mixtures. Athermal, excluded volume interactions govern the phase behavior of such systems and the only parameter that determines the phase diagram are the concentrations of the constituent components. In athermal systems it is possible to melt the structure using shear flow and subsequently study the process of nucleation and growth of ordered structures, such as the smectic phase or colloidal crystals (Dogic 2003; Gasser et al. 2001). However, to study the reverse process of melting would require changing the colloidal concentration *in situ*, which is a challenging experimental task.

To overcome this difficulty and have an easily tunable experimental parameter with which it is possible to control the phase behavior of colloidal systems we have recently designed a novel thermotropic-lyotropic *fd*/polymer mixture (Alsayed et al. 2004). Instead of athermal polymers such as Dextran or PEO, we used the thermo-sensitive polymer poly(N-isopropylacrylamide) (NIPA). The solubility of NIPA in water is highly temperature dependent and below its Θ temperature of 31 °C it assumes a swollen coil, while above this temperature it is water insoluble and assumes a collapsed globule from (Wu and Wang 1998). A small increase in temperature results in increasing monomer-monomer attraction, which in turn decreases the osmotic pressure of the polymer solution. When this polymer solution is in coexistence with an immiscible suspension of hard rods, aqueous solvent flows from the low osmotic pressure polymer-rich phase into the higher osmotic pressure rod-rich phase. This subsequently dilutes the rods and leads to a temperature induced phase transition in a suspension of hard rods.

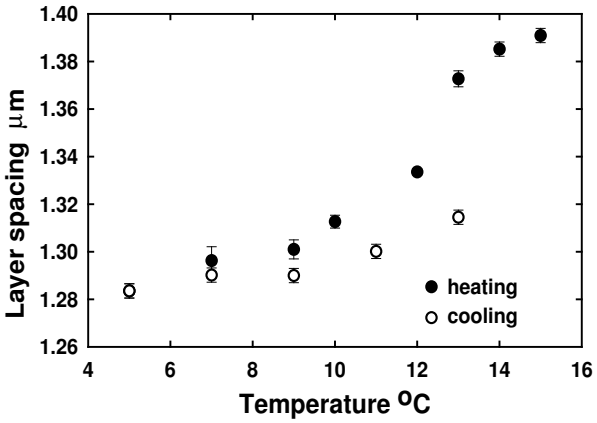

Figure 1.44: Plot of the lamellar periodicity as a function of temperature obtained from a light scattering experiment. Upon heating it is possible to swell the sample to 1.40 μm while upon cooling we only observe formation of lamellar phase of 1.31 μm, indicating the presence of large hysteresis. The images illustrating the appearance of the lamellar phase at each temperature in the heating cycle are shown in Fig. 1.43. (After ref. (Alsayed et al. 2004))

At low temperatures the *fd*/NIPA mixture forms a microscopically phase separated lamellar phase similar to those discussed in section 1.6.1. With increasing temperature dislocations act as a nucleation site for the formation of the nematic tactoids (Fig. 1.43b). Interestingly, the nematic tactoids in the smectic background have a shape very similar to those encountered at isotropic-nematic coexistence. As discussed in section 1.6.1 the nematic phase is highly immiscible with spherical particles and therefore the formation of the nematic tactoids is accompanied with the expulsion of the polymer into lamellar layers which results in the swelling of the layers (Fig. 1.43c). With further increase in temperature most of the sample melts into the nematic phase, which coexists with highly swollen lamellar filaments (Fig. 1.43d). These lamellar filaments transform into isotropic droplets (Fig. 1.43e-g) in a similar way to filaments observed in *fd*/Dextran mixtures and described in section 1.9.3.

The process of lamellar melting can also be followed with light scattering to obtain the lamellar layer spacing averaged over a large sample volume (Fig. 1.44). The scattering pattern shows a single sharp ring, and with increasing temperature it simultaneously moves to lower angles and broadens significantly. This indicates that the lamellar phase continuously swells. Above a temperature of 15 °C only large forward scattering is observed. Interestingly, when cooling the sample down from high temperatures lamellar spacing is only observed at temperatures below 13 °C. This indicates that the lamellar melting is a strongly first order phase transition with large hysteresis and a large nucleation barrier.

It is worth looking back on the simulation results for the effective intermolecular potential between colloidal membranes obtained from the computer simulation of

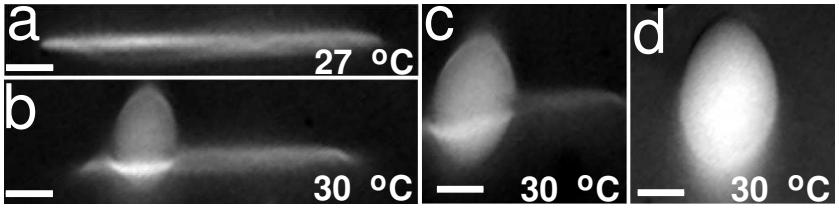

Figure 1.45: Isolated colloidal membranes observed when low volume fraction or *fd* rods are dissolved in the background NIPA polymer (7.5 mg/ml *fd* and 37 mg/ml NIPA). Below 25 °C there is a coexistence between isolated membranes and multiple layers stacked up on top of each other. At 26 °C multiple layers melt into nematic tactoids while single layer membranes remain stable up to 30°C. At this temperatures small three dimensional tactoids nucleate within two-dimensional membrane. It can be concluded Scale bar indicates 5 μm. (After ref. (Alsayed et al. 2004))

perfectly aligned spherocylinders with a depletion attraction potential. These simulations indicate that the position of the minimum between two layers continuously increases with increasing temperature until the layers become unbound 1.35. This is in qualitative agreement with experiments shown in Fig. 1.44.

The behavior of the *fd*/NIPA mixture in a different region of the phase diagram, where a low volume fraction of *fd* is dissolved in the background polymer, exhibits a coexistence between multilayer lamellar droplets and isolated colloidal membranes, such as ones shown in Fig. 1.45a. With increasing temperature the multilayer droplets melt around 26 °C. However, single isolated layers remain stable up to temperatures of 30 °C. Once a nematic tactoid nucleates within the membrane the rest of the membrane is quickly transformed into the nematic phase. This observation suggests that there is a topological nucleation barrier for melting of the two-dimensional membrane into a three dimensional nematic tactoid. In order for the tactoid to form there has to be a collective protrusion of the rods into third dimension. By examining the behavior of isolated membranes in Fig. 1.45 and stacks of membranes in Fig. 1.44 is possible to conclude that there are not only nucleation barriers to freezing into the lamellar phase, but also for melting of the lamellar phase. This is in stark contrast to three-dimensional crystals, which are very difficult to superheat above their melting temperature (Dash 1999).

The structures observed during the process of lamellar melting are in many ways very similar to structures observed in athermal *fd*/polymer mixtures described in the previous two sections. The advantage of the *fd*/NIPA mixtures is that it is possible to continuously cycle between these structures by simply changing the temperature. However, there are a few differences worth mentioning between this study and the previous studies on the isotropic-smectic coexistence. The NIPA polymers used in these experiments have large radius of gyration (R_g = 70nm) compared to Dextran (M. W. 150,000, R_g = 20nm) used for studies of isotropic-smectic phase transition. For this large polymer we do not observe the phenomena of surface freezing. In addition, *fd* mixtures with large polymers have a pronounced tendency to form a lamellar phase,

while smaller polymers such as Dextran 150,000 phase separate directly into isotropic-smectic coexistence (Fig. 1.39).

1.10 Conclusions and open questions

In this chapter we have summarized the phase behavior of colloidal rods and mixtures of rod-like and sphere-like colloids whose interactions are dominated by short ranged repulsive interactions. We have first reviewed the Onsager theory of the isotropic-nematic phase transition which treats the excluded volume interactions at a second virial level. The Onsager theory can be generalized to include positionally ordered smectic phases. The predictions of these very simple theories and confirmed by computer simulations are that rods form isotropic, nematic and smectic phases with increasing concentration. This agrees well with the experimentally measured phase diagram of monodisperse virus particles. The measurements of the order parameter represent the most stringent test of the Onsager theory extended to semi-flexible charged rods. For this particular experiment, the agreement with theory is quantitative at high ionic strength. These experiment firmly establish *fd* rods as ideal hard rod systems.

While the phase behavior of hard rods is well understood, extending the theory to account for long range repulsive interactions due to surface charge results in significant quantitative differences with experiment. These effects become significant at either low ionic strength or high rod concentration. Another extension of the Onsager theory has been to include attractive interactions. Introducing such interactions results in a rapid breakdown of second virial approximation. So far there are no satisfactory theoretical solutions to these problem.

A major part of this review is devoted to description of numerous novel structures observed in rod/sphere mixtures. While the behavior of the bulk suspension of pure rods is at least qualitatively understood, the observation of lamellar phases, colloidal membranes, surface-induced smectic phases and twisted ribbons are mostly lacking theoretical description. We believe that these structure are generic to the phase behavior of rod/sphere mixtures and will be observed in other model rod-like systems as they are developed in the future.

In many ways the phase behavior of rod/sphere mixtures encompasses the behavior of both thermotropic liquid crystals and amphiphilic molecules. The classic model systems of soft condensed matter physics, such as thermotropic liquid crystals or ampiphilic molecules are reasonably well understood. On the one hand, thermotropic liquid crystals with increasing temperature melt from layered smectic phases into nematics and finally into the orientationally disordered isotropic phase. There are only scattered reports of a smectic phase that can be successfully swollen by the addition of isotropic solvent (Rieker 1995). On the other hand, the amphiphilic systems such as lipid membranes, form a layered smectic phase at high concentration. With dilution these systems will swell to a large degree until they form isolated vesicles. The latter systems will almost never melt into nematic phase. With increasing dilution of rod/sphere mixtures we observe both swelling of the smectic layers to the point where

isolated membranes are observed and their subsequent melting into a nematic phase. The competition between these two processes results in a myriad of novel colloidal structures, which are outlined in the present review. The relative stability of these structures will have to be carefully examined in future work.

1.11 Acknowledgments

This review article summarizes recent experiments on the liquid crystalline phase behavior of rod-like viruses and virus/sphere mixtures carried out in our laboratories. Important contributions to this research have been by Kirstin Purdy, Marie Adams, Eric Grelet and Phil Huang at Brandeis University, Ahmed Alsayed and Arjun Yodh at University of Pennsylvania and Edward Barry at Rowland Institute at Harvard. Zvonimir Dogic is supported by a Junior Fellowship from Rowland Institute at Harvard while Seth Fraden is supported by an NSF-DMR grant. Additional information and movies are available at the following websites http://www.elsie.brandeis.edu and http://www.rowland.harvard.edu/rjf/dogic/index.php.

Bibliography

Adams, M., Dogic, Z., Keller, S. L., and Fraden, S., 1998, *Nature* **393**, 349.

Adams, M. and Fraden, S., 1998, *Biophys. J.* **74**, 669.

Alsayed, A. M., Dogic, Z., and Yodh, A. G., 2004, *Phys. Rev. Lett.* **93**, 057801.

Anderson, V. J. and Lekkerkerker, H. N. W., 2002, *Nature* **416**, 811.

Ao, X. L. and Meyer, R. B., 1991, *Physics A* **176**, 63.

Asakura, S. and Oosawa, F., 1958, *J. Polym. Sci.* **33**, 183.

Bartlett, P., Ottewill, R. H., and Pusey, P. N., 1992, *Phys. Rev. Lett.* **68**, 3801.

Bates, M. A. and Frenkel, D., 2000, *Phys. Rev. E* **61**, 5223.

Bawden, C. F., Pirie, N. W., Bernal, J. D., and Fankuchen, I., 1936, *Nature* **138**, 1051.

Biben, T. and Hansen, J. P., 1991, *Phys. Rev. Lett.* **66**, 2215.

Bloomfield, V. A., 1991, *Bioploymers* **31**, 1471.

Bolhuis, P. and Frenkel, D., 1994a, *Phys. Rev. Lett.* **72**, 2211.

Bolhuis, P. G. and Frenkel, D., 1994b, *J. Chem. Phys.* **101**, 9869.

Bolhuis, P. G. and Frenkel, D., 1997, *J. Chem. Phys.* **106**, 668.

Bolhuis, P. G., Stroobants, A., Frenkel, D., and Lekkerkerker, H. N. W., 1997, *J. Chem Phys* **107**, 1551.

Booy, F. P. and Fowler, A. G., 1985, *Int. K. Biol. Macromol.* **7**, 327.

Borukhow, I. and Bruinsma, R. F., 2001, *Phys. Rev. Lett.* **87**, 158101.

Buitenhuis, J., L. N. Donselaar, P. A. B., Stroobants, A., and Lekkerkerker, H. N., 1995, *J. Colloid Interface Sci.* **175**(46-56).

Cahn, R. W., 1986, *Nature* **323**, 668.

Chen, Z. Y., 1993, *Macromolecules* **26**, 3419.

Chen, Z. Y. and Noolandi, J., 1992, *Phys. Rev. E.* **45**, 2389.

Cotter, M. A., 1979, in *The Molecular Physics of Liquid Crystals*, edited by G. R. Luckhurst and G. W. Gray, pp. 169–189. Academic Press, London.

Cotter, M. A. and Wacker, D. C., 1978, *Phys. Rev. A* **18**, 2669.

Crocker, J. C., Matteo, J. A., Dinsmore, A. D., and Yodh, A. G., 1999, *Phys. Rev. Lett.* **82**, 4352.

Cui, S. and Cheng, Z. Y., 1994, *Phys. Rev. E.* **50**, 3747.

Dash, J. G., 1999, *Rev. Mod. Phys.* **71**, 1737.

Dash, J. G., Fu, H. Y., and Wettlaufer, J. S., 1995, *Rep. Prog. Phys.* **58**, 115.

Debenedetti, P. G., 1996, *Metastable liquids : Concepts and Principles*. Princeton University Press.

Dinsmore, A. D., Warren, P. B., Poon, W. C. K., and Yodh, A. G., 1997, *Europhys. Lett.* **40**, 337.

Dinsmore, A. D., Yodh, A. G., and Pine, D. J., 1995, *Phys. Rev. E* **52**, 4045.

Dogic, Z., 2003, *Phys. Rev. Lett.* **91**, 165701.

Dogic, Z. and Fraden, S., 1997, *Phys. Rev. Lett.* **78**, 2417.

Dogic, Z. and Fraden, S., 2000, *Langmuir* **16**, 7820.

Dogic, Z. and Fraden, S., 2001, *Phil. Trans. R. Soc. Lond. A.* **359**, 997.

Dogic, Z., Frenkel, D., and Fraden, S., 2000, *Phys. Rev. E* **62**, 3925.

Dogic, Z., Purdy, K. R., Grelet, E., Adams, M., and Fraden, S., 2004a, *Phys. Rev. E* **69**, 051702.

Dogic, Z., Zhang, J., Lau, A. W. C., Aranda-Espinoza, H., Dalhaimer, P., Disher, D. E., Janmey, P. A., Kamien, R. D., Lubensky, T. C., and Yodh, A. G., 2004b, *Phys. Rev. Lett.* **92**, 125503.

DuPre, D. B. and Duke, R. W., 1975, *J. Chem. Phys.* **63**, 143.

DuPre, D. P. and Yang, S., 1991, *J. Chem. Phys.* **94**, 7466.

Edgar, C. D. and Gray, D. G., 2002, *Macromolecules* **35**, 7400.

Forsyth, Jr., P. A., Marcelja, S., Mitchell, D. J., and Ninham, B. W., 1978, *Adv. in Coll. and Int. Sci.* **9**, 37.

Fraden, S., 1995, in *Observation, Prediction, and Simulation of Phase Transitions in Complex Fluids*, edited by M. Baus, L. F. Rull, and J. P. Ryckaert, pp. 113–164. Kluwer Academic Publishers.

Fraden, S., Hurd, A. J., Meyer, R. B., Cahoon, M., and Caspar, D. L. D., 1985, *J. de Physique* **C3**, 85.

Fraden, S., Maret, G., and Caspar, D. L. D., 1993, *Phys. Rev. E* **48**, 2816.

Fraden, S., Maret, G., Caspar, D. L. D., and Meyer, R. B., 1989, *Phys. Rev. Lett.* **63**, 2068.

Frenkel, D., 1988, *J. Phys. Chem.* **92**, 3280.

Frenkel, D., Lekkerkerker, H., and Stroobants, A., 1988, *Nature* **332**, 822.

Frenkel, D. and Schilling, T., 2002, *Phys. Rev. E* **66**, 041606.

Frenkel, D. and Smith, B., 1996, *Understanding Molecular Simulation*. Academic Press.

Gabriel, J. C. P. and Davidson, P., 2003, *Coll. Chem. I Topics in Curr. Chem,* **226**, 119.

Gasser, U., Weeks, E. R., Schofield, A., Pusey, P. N., and Weitz, D. A., 2001, *Science* **292**, 258.

Gast, A. P., Hall, C. K., and Russel, W. B., 1983, *Farday. Discuss. Chem. Soc.* **76**, 189.

Gast, A. P. and Russel, C. K. H. W. B., 1983, *J. Colloid Interface Sci.* **96**, 251.

Gast, A. P., Russel, W. B., and Hall, C. K., 1986, *J. Colloid Interface Sci.* **109**, 161.

Gelbart, W. M. and Barboy, B., 1980, *Acc. Chem. Res.* **13**, 290.

Goetz, R., Gompper, G., and Lipowsky, R., 1999, *Phys. Rev. Lett.* **82**, 221.

Grelet, E. and Fraden, S., 2003, *Phys. Rev. Lett.* **90**, 198302.

Griess, G. A., Moreno, E. T., Herrmann, R., and Serwer, P., 1990, *Biopolymers* **29**, 1277.

Hagen, M. H. J. and Frenkel, D., 1994, *J. Chem. Phys.* **101**, 4093.

Halperin, B. I. and Nelson, D. R., 1978, *Phys. Rev. Lett.* **41**, 121.

Hanke, A., Eisenriegler, E., and Dietrich, S., 1999, *Phys. Rev. E.* **59**, 6853.

Hansen, J. P. and McDonald, I. R., 1986, *Theory of Simple Liquids*. Academic Press, London:, second edn.

Helfrich, W., 1973, *Z. Naturforsh. C* **28**, 693.

Hentschke, R., 1990, *Macromolecules* **23**, 1192.

Herrmann, R., Neugebauer, K., Pirkl, E., Zentgraf, H., and Schaller, H., 1980, *Molec. gen. Genet.* **177**, 231.

Herzfeld, J., Berger, A. E., and Wingate, J. W., 1984, *Macromolecules* **17**, 1718.

Hosino, M., Nakano, H., and Kimura, H., 1979, *J. Phys. Soc. Jpn.* **46**, 1709.

Hurd, A. J., Fraden, S., Lonberg, F., and Meyer, R. B., 1985, *J. de Physique* **46**, 905.

Imhof, A. and Dhont, J. K. G., 1995, *Phys. Rev. Lett.* **75**, 1662.

Israelechvili, J., 1991, *Intermolecular and Surafce Forces*. Academic Press, London, 2nd edn.

Issaenko, S. A., Harris, A. B., and Lubensky, T. C., 1999, *Phys. Rev. E.* **60**, 578.

Jizuka, E. and Yang, J. T., 1978, in *Liquid Crystals and Ordered Fluids*, edited by J. Johnson. Plenum Press.

Kamien, A. B. H. R. D. and Lubensky, T. C., 1997, *Phys. Rev. Lett.* **78**, 1476.

Kamien, R. D., Doussal, P. L., and Nelson, D. R., 1992, *Phys. Rev. A* **45**, 8728.

Kayser, Jr., R. F. and Raveche, H. J., 1978, *Phys. Rev. A* **17**, 2067.

Khokhlov, A. R. and Semenov, A. N., 1981, *Physica* **108a**, 546.

Khokhlov, A. R. and Semenov, A. N., 1982, *Physica* **112a**, 605.

Kierfeld, J. and Lipowsky, R., 2003, *Europhys. Lett.* **62**, 285.

Koda, T. and Kimura, H., 1994, *J. Phys. Soc. Jpn.* **63**, 984.

Koda, T., Numajiri, M., and Ikeda, S., 1996, *J. Phys. Soc. Jpn.* **65**, 3551.

Koenderink, G. H., Vliegenthat, G. A., Kluijtmans, S. G. J., van Blaaderen, A., Philipse, A. P., and Lekkerkerker, H. N. W., 1999, *Langmuir* **15**, 4693.

Kramer, E. M. and Herzfeld, J., 1998, *Phys. Rev. E* **58**, 5934.

Kramer, E. M. and Herzfeld, J., 1999, *J. Chem. Phys.* **110**, 8825.

Kramer, E. M. and Herzfeld, J., 2000, *J. Chem. Phys.* **61**, 6872.

Kreibig, U. and Wetter, C., 1980, *Z. Naturforsch.* **35c**, 750.

Kuhl, T. L., Leckband, D. E., Lasic, D. D., and Isrealachvili, J. N., 1994, *Biophys. J.* **66**, 1479.

Lago, S., Cuetos, A., Martinez, B., and Rull, L. F., 2004, *J. Mol. Recognition* **17**, 417.

Lang, P., 1999, *J. Phys. Chem. B* **103**, 5100.

Lapointe, J. and Marvin, D. A., 1973, *Mol. Cryst. Liquid Cryst.* **19**, 269.

Lau, A. W. C., Lin, K. H., and Yodh, A. G., 2003, *Phys. Rev. E* **66**, 020401.

Lebowitz, J. L. and Rowlison, J. S., 1964, *J. Chem. Phys.* **41**, 133.

LeDoussal, P. and Nelson, D. R., 1991, *Europhys. Lett.* **15**, 161.

Lee, K., Borukhov, I., Gelbart, W. M., Liu, A. J., and Stevens, M. J., 2004, *Phys. Rev. Lett.* **93**, 128101.

Lee, S. W., Mao, C. B., Flynn, C. E., and Belcher, A. M., 2002, *Science* **296**, 892.

Lee, S. W., Wood, B. M., and Belcher, A. M., 2003, *Langmuir* **19**, 1592.

Leforestier, A. and Livolant, F., 1993, *Biophys. J.* **65**, 56.

Lekkerkerker, H. N. W., Coulon, P., der Haegen, V., and Deblieck, R., 1984, *J. Chem. Phys.* **80**, 3427.

Lekkerkerker, H. N. W., Poon, W. C.-K., Pusey, P. N., Stroobants, A., and Warren, P. B., 1992, *Europhys. Lett.* **20**, 559.

Lekkerkerker, H. N. W. and Stroobants, A., 1994, *Nuovo Cimento D* **16**, 949.

Lied, A., Dosch, H., and Bilgram, J. H., 1994, *Phys. Rev. Lett.* **72**, 3554.

Lin, K. H., 2004, unpublished results.

Lin, K. H., Crocker, J. C., Zeri, A. C., and Yodh, A. G., 2001, *Phys. Rev. Lett.* **87**, 088301.

Lipowsky, R., 1995, in *Generic interactions of flexible membranes.*, edited by R. Lipowsky and E. Sackmann, pp. 521–602. Elsevier.

Livolant, F., 1991, *Physics A* **176**, 117.

Maeda, H. and Maeda, Y., 2003, *Phys. Rev. Lett.* **90**, 018303.

Maguire, J. F., McTague, J. P., and Rondalez, F., 1980, *Phys. Rev. Lett.* **45**(23), 1891.

Maniatis, T., Sambrook, J., and Fritsch, E. F., 1989, *Molecular Cloning*. Cold Spring Harbor University Press.

Mao, Y., Cates, M. E., and Lekkerkerker, H. N. W., 1995, *Physica A* **222**, 10.

Mao, Y., Cates, M. E., and Lekkerkerker, H. N. W., 1997, *J. Chem. Phys.* **106**, 3721.

Meijer, E. J. and Frenkel, D., 1991, *Phys. Rev. Lett.* **67**, 1110.

Meijer, E. J. and Frenkel, D., 1994, *J. Chem. Phys.* **100**, 6873.

Meyer, R. B., 1968, *Appl. Phys. Lett.* **12**, 281.

Meyer, R. B., 1969, *Appl. Phys. Lett.* **14**, 208.

Meyer, R. B., 1990, in *Dynamics and Patterns in Complex Fluids*, edited by A. Onuki and K. Kawasaki, p. 62. Springer-Verlag.

Mulder, B., 1987, *Phys. Rev. A* **35**, 3095.

Nordmeier, E., 1993, *J. Phys. Chem.* **97**, 5770.

Ocko, B. M., Braslau, A., Pershan, P. S., Als-Nielsen, J., and Deutch, M., 1986, *Phys. Rev. Lett.* **57**, 94.

Odijk, T., 1986, *Macromolecules* **19**, 2313.

Odijk, T., 1987, *J. Phys. Chem.* **91**, 6060.

Oldenbourg, R., 1981, *Elastiche and quasielastiche Lichtstreuung an magnetisch ausgerichteten polyelektrolytischen Stäbchen*, Ph.D. thesis, Universitat Konstänz.

Oldenbourg, R., Wen, X., Meyer, R. B., and Caspar, D. L. D., 1988, *Phys. Rev. Lett.* **61**, 1851.

Olmsted, P. D., Poon, W. C. K., McLeish, T. C. B., Terrill, N. J., and Ryan, A. J., 1998, *Phys. Rev. Lett.* **81**, 373.

Onsager, L., 1949, *Ann. NY Acad. Sci.* **51**, 627.

Pelcovits, R. A., 1996, *Liq.Cryst.* **21**, 361.

Pelta, J., Durand, D., Doucet, J., and Livolant, F., 1996, *Biophys. J.* **71**, 48.

Pindak, R. S., Huang, C. C., and Ho, J. T., 1974, *Phys. Rev. Lett* **32**(2), 43.

Polson, J. M., 1997, *Phys. Rev. E* **56**, R6260.

Poon, W. C. K. and Pusey, P. N., 1995, in *Observation, Prediction, and Simulation of Phase Transitions in Complex Fluids*, edited by M. Baus, L. F. Rull, and J. P. Ryckaert, pp. 3–51. Kluwer Academic Publishers.

Poulin, P., Stark, H., Lubensky, T. C., and Weitz, D. A., 1997, *Science* **275**, 1770.

Prinsen, P. and van der Schoot, P., 2003, *Phys. Rev. E* **68**, 021701.

Purdy, K. R., Dogic, Z., Fraden, S., Ruhm, A., Lurio, L., and Mochrie, S. G. J., 2003, *Phys. Rev. E* **67**, 031708.

Purdy, K. R. and Fraden, S., 2004a, *The influence of charge and flexibility on smectic phase formation in filamentou svirus suspensions*, cond-mat/0406700.

Purdy, K. R. and Fraden, S., 2004b, *Phys. Rev. E* **70**, 061703.

Purdy, K. R., Varga, S., Galindo, A., Jackson, G., and Fraden., S., 2004, *Nematic phase transitions in mixtures of thin and thick colloidal rods*, cond-mat/0406175.

Rieker, T. P., 1995, *Liq. Crys.* **19**, 497.

Sambrook, J., Fritsch, E. F., and Maniatis, T., 1989, in *Molecular Cloning: A Laboratory Manual*, chap. 4. Cold Spring Harbor Laboratory Press, second edn.

Sato, T. and Teramoto, A., 1994, *Acta. Polymer.* **45**, 399.

Sear, R. P., 2002, *Langmuir* **18**, 7571.

Sear, R. P. and Jackson, G., 1995, *J. Chem. Phys.* **102**, 2622.

Sear, R. P. and Mulder, B. M., 1996, *J. Chem. Phys.* **105**, 7727.

Senechal, E., Maret, G., and Dransfeld, K., 1980, *Int. J. Biol. Macromol.* **2**, 256.

Shundyak, K. and van Roij, R., 2001, *J. of Phys.* **13**, 4789.

Shundyak, K. and van Roij, R., 2002, *Phys. Rev. Lett.* **88**, 205501.

Sikorav, J. L., J.Pelta, and Livolant, F., 1994, *Biophys. J.* **67**, 1387.

Sirota, E. B. and Herhold, A. B., 1999, *Science* **283**, 529.

Sloutskin, E., Sirota, E. B., Kraack, H., Ocko, B. M., and Deutsch, M., 2001, *Phys. Rev. E* **64**, 031708.

Song, L., Kim, U., Wilcoxon, J., and Schurr, J. M., 1991, *Biopolymers* **31**, 547.

Stephen, M. J. and Straley, J. R., 1974, *Rev. Mod. Phys.* **46**, 617.

Straley, J. P., 1976, *Phys. Rev. A* **14**, 1835.

Stroobants, A., Lekkerkerker, H. N. W., and Odijk, T., 1986, *Macromolecules* **19**, 2232.

Tang, J. and Fraden, S., 1993, *Phys. Rev. Lett.* **71**, 3509.

Tang, J. and Fraden, S., 1995, *Liquid Crystals* **19**, 459.

Tang, J. and Fraden, S., 1996, *Biopolymers* **39**, 13.

Tang, J. X., Ito, T., Traub, P., and Janmey, P. A., 1997, *Biochemistry* **36**, 12600.

Tang, J. X., Wong, S., Tran, P. T., and Janmey, P. A., 1996, *Ber. Bunsenges. Phys. Chem.* **100**, 796.

ten Wolde, P. R. and Frenkel, D., 1997, *Science* **277**, 1975.

Tkachenko, A. V., 1996, *Phys. Rev. Lett.* **77**, 4218.

Tracy, M. A., Garcia, J. L., and Pecora, R., 1993, *Macromolecules* **26**, 1862.

Tuinier, R., Aart, D. G. A. L., Wensink, H. H., and Lekkerkerker, H. N. W., 2003, *Phys. Chem.* **5**, 3707.

Tuinier, R., Vliegenthart, G. A., and Lekkerkerker, H. N. W., 2000, *J. Chem. Phys.* **113**, 10768.

van der Schoot, P., 1996, *J. Phys. II France* **6**, 1557.

van der Schoot, P., 2000, *J. Chem. Phys.* **112**, 9132.

van der Schoot, P., 2002, *J. Chem. Phys.* **117**, 3538.

van der Schoot, P. and Odijk, T., 1992, *J. Chem. Phys.* **97**, 515.

van der Veen, J. F., 1999, *Surf. Sci.* **433-435**, 1.

van Roij, R., 1994, *J. de Physique II* **4**, 1763.

van Roij, R., 1996, *Simple Theories of Complex Fluids*. Universiteit Utrecht.

van Roij, R., Bolhuis, P., Mulder, B., and Frenkel, D., 1995, *Phys. Rev. E* **52**, R1277.

van Roij, R. and Mulder, B., 1996, *J. Chem. Phys.* **105**, 11237.

van Roij, R., Mulder, B., and Dijkstra, M., 1998, *Physics A* **261**, 374.

Van Winkle, D. H., Davidson, M. W., Chen, W. X., and Rill, R. L., 1990, *Macromolecules* **23**, 4140.

Verma, R., Crocker, J. C., Lubensky, T. C., and Yodh, A. G., 2000, *Macromolecules* **33**, 177.

Vliegenthart, G. A. and Lekkerkerker, H. N. W., 1999, *J. Chem. Phys.* **111**, 4154.

Vliegenthart, G. A., van Blaaderen, A., and Lekkerkerker, H. N. W., 1999, *Faraday Discuss.* **112**, 173.

Vrij, A., 1976, *Pure and Appl. Chem* **48**, 471.

Vroege, G. J. and Lekkerkerker, H. N. W., 1992, *Repts. on Prog. Phys.* **8**, 1241.

W. M. Gelbart, A. B.-S. and Roux, D. (eds.), 1994, *Micelles, Membranes, Microemulsions and Monolayers*. Springer.

Wang, J. H., Lonberg, F., Ao, X., and Meyer, R. B., 1994, in *Ordering in Macromolecular Systems*, edited by A. Teramoto, M. Kobayashi, and T. Norisuje. Springer-Verlag.

Warren, P. B., 1994, *J. Phys. I (France)* **4**, 237.

Welsh, L. C., Symmons, M. F., Perham, C. N. R. N., Marseglia, E. A., and Marvin, D. A., 1996, *Macromolecules* **29**, 7075.

Wen, X. and Meyer, R. B., 1987, *Phys. Rev. Lett.* **59**, 1325.

Wen, X., Meyer, R. B., and Caspar, D. L. D., 1989, *Phys. Rev. Lett.* **63**, 2760.

Wennerstrom, H. and Israelachvilli, J. N., 1992, *J. Phys. Chem.* **96**, 520.

Wetter, C., 1985, *Biologie in unserer Zeit* **3**, 81.

Widom, B., 1967, *Science* **157**, 375.

Wong, G. C. L., Lin, A., Tang, J. X., Li, Y., Janmey, P. A., and Safinya, C. R., 2003, *Phys. Rev. Lett.* **91**, 018103.

Wu, C. and Wang, X., 1998, *Phys. Rev. Lett.* **80**, 4092.

Wu, X. Z., Sirota, E. B., Sinha, S. K., Ocko, B. M., and Deutsch, M., 1993, *Phys. Rev. Lett.* **70**, 958.

Yaman, K., Jeppesen, C., and Marques, C. M., 1998, *Europhys. Lett.* **42**, 221.

Yu, S. M., Conticello, V., Zhang, G., Kayser, C., Fournier, M., Mason, T., and Tirrell, D., 1997, *Nature* **389**, 167.

Zimmermann, K., Hagedorn, J., Heuck, C. C., Hinrichsen, M., and Ludwig, J., 1986, *J. Biol. Chem.* **261**, 1653.

Zocher, H., 1925, *Z. Anorg. Allg. Chem.* **147**, 91.